Westinghouse Non-Proprietary Class 3

WCAP-15813-NP
Revision 0

August 2003

Structural Integrity Evaluation of Reactor Vessel Upper Head Penetrations to Support Continued Operation: Millstone Unit 2

Westinghouse Non-Proprietary Class 3

WCAP-15813-NP
Revision 0

Structural Integrity Evaluation of Reactor Vessel Upper Head Penetrations to Support Continued Operation: Millstone Unit 2

D. Tang

August 2003

Reviewer: _____
C. Ng
Piping Analysis & Fracture Mechanics

Approved: _____
S. A. Swamy, Manager
Piping Analysis & Fracture Mechanics

This coincides with Rev. 1 of Prop Version.

Westinghouse Electric Company LLC
P.O. Box 355
Pittsburgh, PA 15230-0355

TABLE OF CONTENTS

LIST OF TABLES

LIST OF FIGURES

LIST OF FIGURES (Cont.)

LIST OF FIGURES (Cont.)

1 INTRODUCTION

In September of 1991, a leak was discovered in the Reactor Vessel Control Rod Drive Mechanism (CRDM) head penetration region of an operating plant. This has led to the question of whether such a leak could occur at the Millstone Unit 2 Control Element Drive Mechanism (CEDM), In-Core Instrumentation (ICI), or head vent nozzle penetrations. Note that the designation CRDM (Westinghouse and French designs) and CEDM (Combustion Engineering Design) are synonymous. The geometry of interest is shown in Figure 1-1. Throughout this report, the penetration rows have been identified by their angle of intersection with the head. The location of head penetrations for Millstone Unit 2 is shown in Figure 1-2 and the angles for each penetration are identified in Table 1-1.

The CEDM leak resulted from cracking in Alloy 600 base metal, which occurred in the outermost penetrations of a number of operating plants as discussed in Section 2. This outermost CEDM location, as well as a number of intermediate CEDM locations, the ICI nozzles, and the head vent were chosen for fracture mechanics analyses to support continued safe operation of Millstone Unit 2 if such cracking were to be found. The dimensions of the CEDM penetrations are all identical, with a 3.850 inch Outside Diameter (OD) and a wall thickness of 0.566 inch [10A, 10C]. The ICI penetrations have an OD of 5.563 inch and wall thickness of 0.469 inch [10A, 10C]. The head vent OD is 1.050 inch and the wall thickness is 0.154 inch [10A, 10C]. All of these dimensions are summarized in Table 6-2.

The basis of the fracture analysis was a detailed three-dimensional elastic-plastic finite element analysis of several penetration locations, as described in detail in Section 5. The fracture analysis was carried out using crack growth rates recommended by the EPRI Materials Reliability Program (MRP). These rates are consistent with service experience. The results are presented in the form of flaw tolerance charts for both surface and through wall flaws. If indications are found, the charts will determine the allowable service life of safe operation. The service life calculated in the flaw tolerance charts are all in Effective Full Power Years (EFPY).

The flaw tolerance handbook WCAP-15813 Revision 1 is updated to reflect the following development in the Primary Water Stress Corrosion Cracking of Alloy 600:

1. New crack growth rates for evaluation Primary Water Stress Corrosion Cracking in CRDM penetration nozzle provided in MRP-55 Rev. 1 (Reference 4H).

2. MRP-55 Rev. 1 recommends the use of a factor of 2.0 for OD flaws above the attachment weld to account for uncertainty in the chemical environment of the penetration nozzle annulus. This factor was not included for OD flaws above the attachment weld in the original WCAP report.

3. Based on recent experiences with vessel head inspections of a number of power plants NRC has been requesting hoop distribution below the attachment weld if 100% of the penetration nozzle is not feasible. These hoop stress distributions will be included in the updated flaw tolerance handbook and can be used to support the submittal of relaxation request from the NRC Issued Order EA-03-009 for less than 100% inspection coverage of the penetration nozzle.

Table 1-1 Millstone Unit 2 Head Penetration Nozzles, with the Intersection Angles Identified								
Nozzle No.	Type	Angle (Degrees)	Nozzle No.	Type	Angle (Degrees)	Nozzle No.	Type	Angle (Degrees)
1	CEDM	0.0	27	CEDM	29.1	53	CEDM	37.1
2	CEDM	11.0	28	CEDM	29.1	54	CEDM	37.1
3	CEDM	11.0	29	CEDM	29.1	55	CEDM	37.1
4	CEDM	11.0	30	CEDM	29.1	56	CEDM	37.1
5	CEDM	11.0	31	CEDM	29.1	57	CEDM	37.1
6	CEDM	11.0	32	CEDM	29.1	58	CEDM	42.5
7	CEDM	11.0	33	CEDM	29.1	59	CEDM	42.5
8	CEDM	11.0	34	CEDM	35.6	60	CEDM	42.5
9	CEDM	11.0	35	CEDM	35.6	61	CEDM	42.5
10	CEDM	22.4	36	CEDM	35.6	62	CEDM	42.5
11	CEDM	22.4	37	CEDM	35.6	63	CEDM	42.5
12	CEDM	22.4	38	CEDM	35.6	64	CEDM	42.5
13	CEDM	22.4	39	CEDM	35.6	65	CEDM	42.5
14	CEDM	23.9	40	CEDM	35.6	66	CEDM	42.5
15	CEDM	23.9	41	CEDM	35.6	67	CEDM	42.5
16	CEDM	23.9	42	CEDM	38.5	68	CEDM	42.5
17	CEDM	23.9	43	CEDM	38.5	69	CEDM	42.5
18	CEDM	25.3	44	CEDM	38.5	70	ICI	54.8
19	CEDM	25.3	45	CEDM	38.5	71	ICI	54.8
20	CEDM	25.3	46	CEDM	38.5	72	ICI	54.8
21	CEDM	25.3	47	CEDM	38.5	73	ICI	54.8
22	CEDM	25.3	48	CEDM	38.5	74	ICI	54.8
23	CEDM	25.3	49	CEDM	38.5	75	ICI	54.8
24	CEDM	25.3	50	CEDM	37.1	76	ICI	54.8
25	CEDM	25.3	51	CEDM	37.1	77	ICI	54.8
26	CEDM	29.1	52	CEDM	37.1			

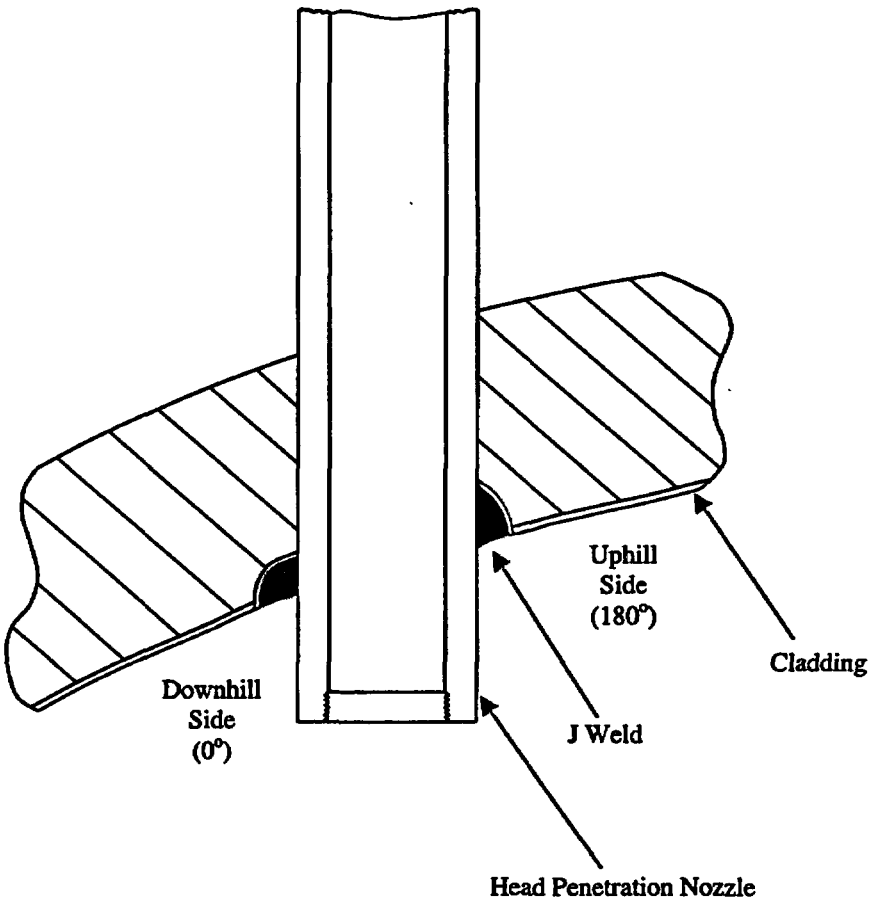

Figure 1-1 Reactor Vessel Control Element Drive Mechanism (CEDM) Penetration

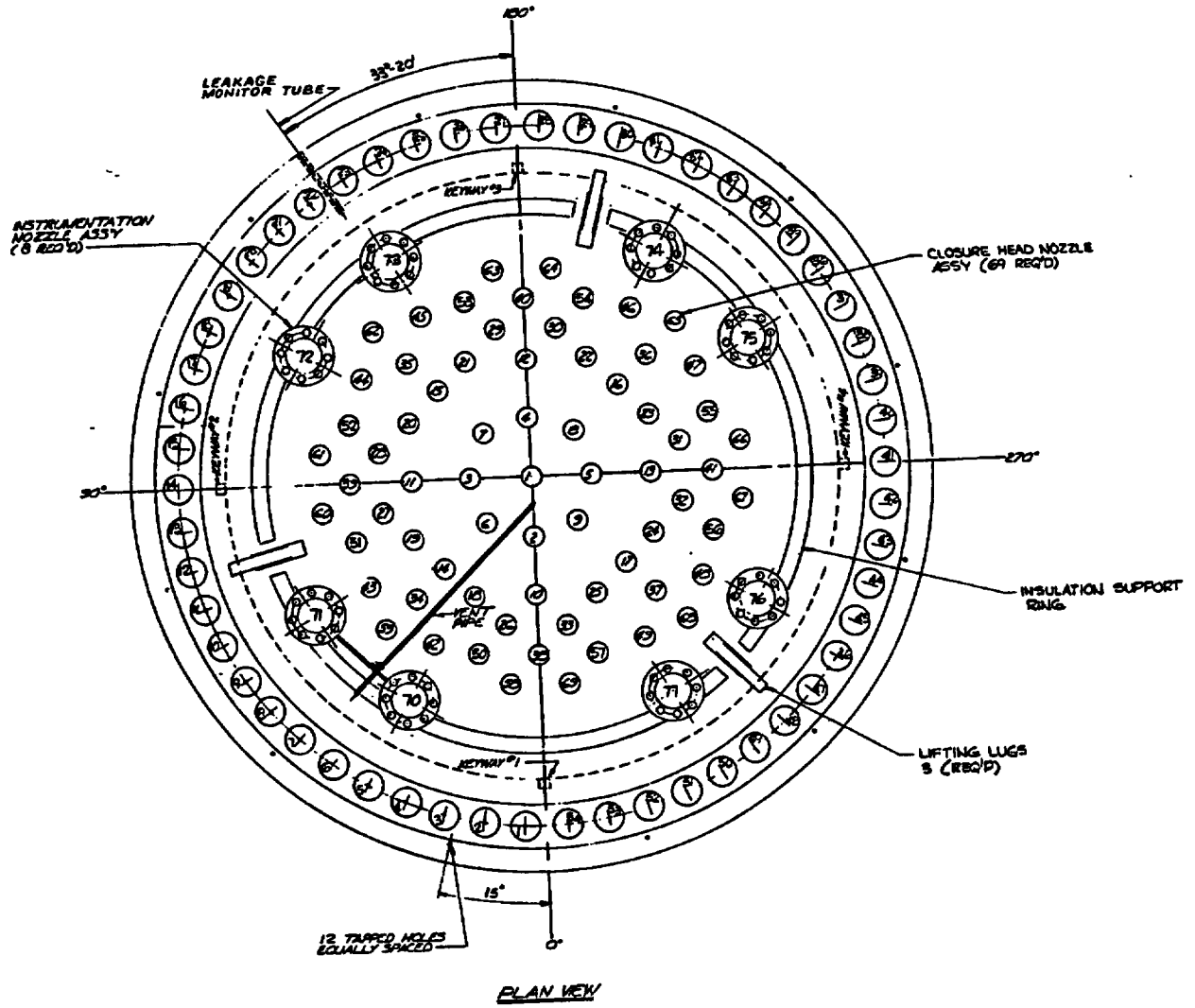

Figure 1-2 Location of Head Penetrations for Millstone Unit 2

2 HISTORY OF CRACKING IN HEAD PENETRATION NOZZLES

In September of 1991, leakage was reported from the reactor vessel CRDM head penetration region of a French plant, Bugey Unit 3. Bugey 3 is a 920 megawatt three-loop Pressurized Water Reactor (PWR) plant which had just completed its tenth fuel cycle. The leak occurred during a post ten year hydrotest conducted at a pressure of approximately 3000 psi (204 bar) and a temperature of 194°F (90°C). The leak was detected by metal microphones, which are located on the top and bottom heads. The leak rate was estimated to be approximately 0.7 liter/hour. The location of the leak was subsequently established on a peripheral penetration with an active control rod (H-14), as seen in Figure 2-1.

The control rod drive mechanism and thermal sleeve were removed from this location to allow further examination. A study of the head penetration revealed the presence of longitudinal cracks near the head penetration attachment weld. Penetrant and ultrasonic testing confirmed the cracks. The cracked penetration was fabricated from Alloy 600 bar stock (SB-166), and has an outside diameter of 4 inches (10.16 cm) and an inside diameter of 2.75 inches (7.0 cm).

As a result of this finding, all of the control rod drive mechanisms and thermal sleeves at Bugey 3 were removed for inspection of the head penetrations. Only two penetrations were found to have cracks, as shown in Figure 2-1.

An inspection of a sample of penetrations at three additional plants were planned and conducted during the winter of 1991-92. These plants were Bugey 4, Fessenheim 1, and Paluel 3. The three outermost rows of penetrations at each of these plants were examined, and further cracking was found in two of the three plants.

At Bugey 4, eight of the 64 penetrations examined were found to contain axial cracks, while only one of the 26 penetrations examined at Fessenheim 1 was cracked. The locations of all the cracked penetrations are shown in Figure 2-1. At the time, none of the 17 CRDM penetrations inspected at Paluel 3 showed indications of cracking, however subsequent inspections of the French plants have confirmed at least one crack in each operating plant.

Thus far, the cracking in reactor vessel heads not designed by Babcock and Wilcox (B&W) has been consistent in both its location and extent. All cracks discovered by nondestructive examination have been oriented axially, and have been located in the bottom portion of the penetration in the vicinity of the partial penetration attachment weld to the vessel head as shown schematically in Figure 1-1.

[

]^{a,c,e}

[

]^{a,c,e}

Non-destructive examinations of the leaking CRDM nozzles showed that most of the cracks were axially oriented, originating on the outside surface of the nozzles below the J-groove weld and propagating primarily in the nozzle base material to an elevation above the top of the J-groove weld. Leakage could then pass through the annulus to the top of the head where it was detected by visual inspection. In some cases the cracks initiated in the weld metal or propagated into the weld metal, and in a few cases the cracks propagated through the nozzle wall thickness to the inside surface.

[

]^{a,c,e}

[

]^{a,c,e}

The cracking has now been confirmed to be primary water stress corrosion cracking. Relatively high residual stresses are produced in the outermost CRDM penetrations due to the welding process. Other important factors which affect this process are temperature and time, with higher temperatures and longer times being more detrimental. The inspection findings for U.S. plants are shown in Figure 2-2. From this figure, it is interesting to note that low percentage of CE-fabricated vessels have been found cracked (only 9 of 1332 penetrations UT and/or ET inspected in CE-fabricated vessels have shown cracking whereas 117 of 628 penetrations in non-CE-fabricated vessels experienced cracking or leakage). In addition, no cracks in head vent have been found.

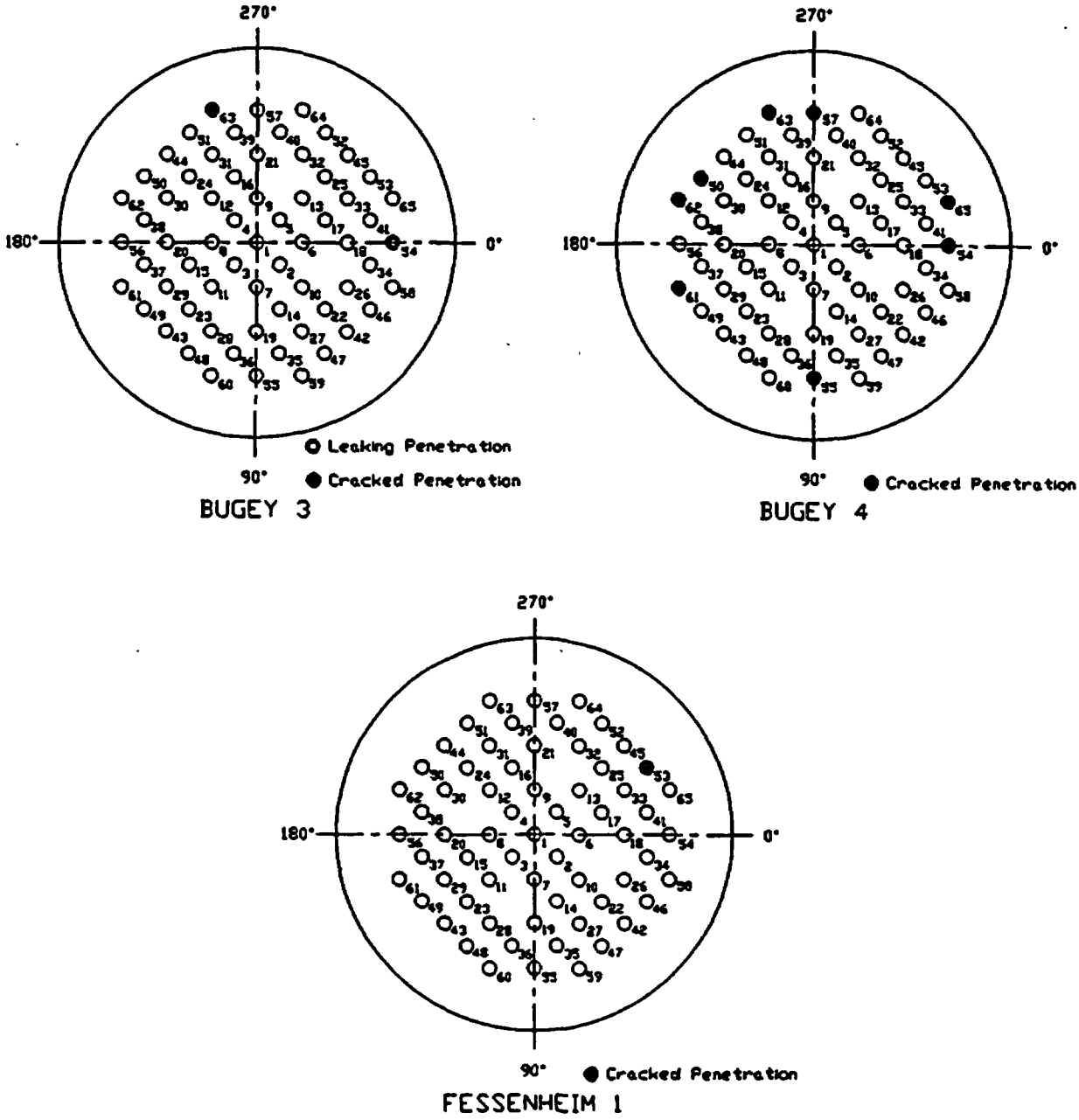

Figure 2-1 EDF Plant R/V Closure Head CEDM Penetrations – Penetrations with Cracking

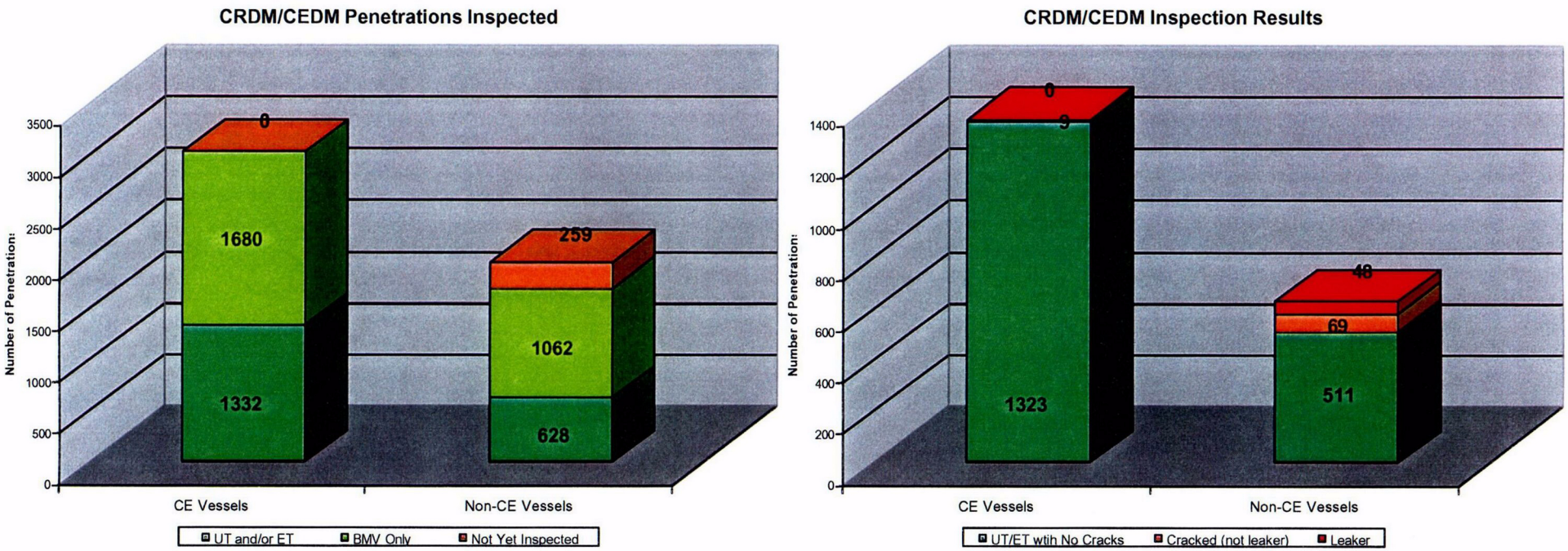

Figure 2-2 Inspection Results for U.S. CRDM/CEDM Penetration Nozzle (Spring 2003)

3 OVERALL TECHNICAL APPROACH

The primary goal of this work is to provide technical justification for the continued safe operation of Millstone Unit 2 in the event that cracking is discovered during inservice inspections of the Alloy 600 reactor vessel head penetrations.

3.1 PENETRATION NOZZLE STRESS ANALYSIS

Three-dimensional elastic-plastic finite element stress analyses applicable to Millstone Unit 2 was performed to determine the stresses in the head penetration region [6A, 6B, 6C]. These analyses have considered the pressure loads associated with steady state operation, as well as the residual stresses that are produced by the fabrication process.

[

]^{a,c,e}

3.2 FLAW TOLERANCE APPROACH

A flaw tolerance approach has been developed to allow continued safe operation until an appropriate time for repair, or the end of plant life. The approach is based on the prediction of future growth of detected flaws, to ensure that such flaws would remain stable.

If an indication is discovered during in-service inspection, its size can be compared with the flaw size considered as allowable for continued service. This "allowable" flaw size is determined from the actual loading (including mechanical and residual loads) on the head penetration for Millstone Unit 2. Acceptance criteria are discussed in Section 6.5.

The time for the observed crack to reach the allowable crack size determines the length of time the plant can remain online before repair, if required. For the crack growth calculation, a best estimate is needed and no additional margins are necessary.

The results of the evaluation are presented in terms of simple flaw tolerance charts. The charts graphically show the time required to reach the allowable length or depth, which represents additional service life before repair. This result is a function of the loading on the particular head penetration as well as the circumferential location of the crack in the penetration nozzle.

Schematic drawings of the head penetration flaw tolerance charts are presented as Figures 3-1 and 3-2. These two types of charts can be used to provide estimates of the remaining service life before a leak would develop from an observed crack. For example, if a part-through flaw was discovered, the user would first refer to Figure 3-1, to determine the time (t_P) which would be remaining before the crack would penetrate the wall or reach the allowable depth (t_a) (e.g. a/t = 0.75). Once the crack penetrates the wall, the time (t_B) required to reach an allowable crack length would be determined from Figure 3-2. The total time remaining would then be the simple sum:

$$\text{Time remaining} = t_P + t_B$$

Another way to determine the allowable time of operation with a part-through flaw would be to use Figure 3-2 directly, in effect assuming the part-through flaw is a through-wall flaw. This approach would be more conservative than that above, and the time remaining would then be:

$$\text{Time remaining} = t_B$$

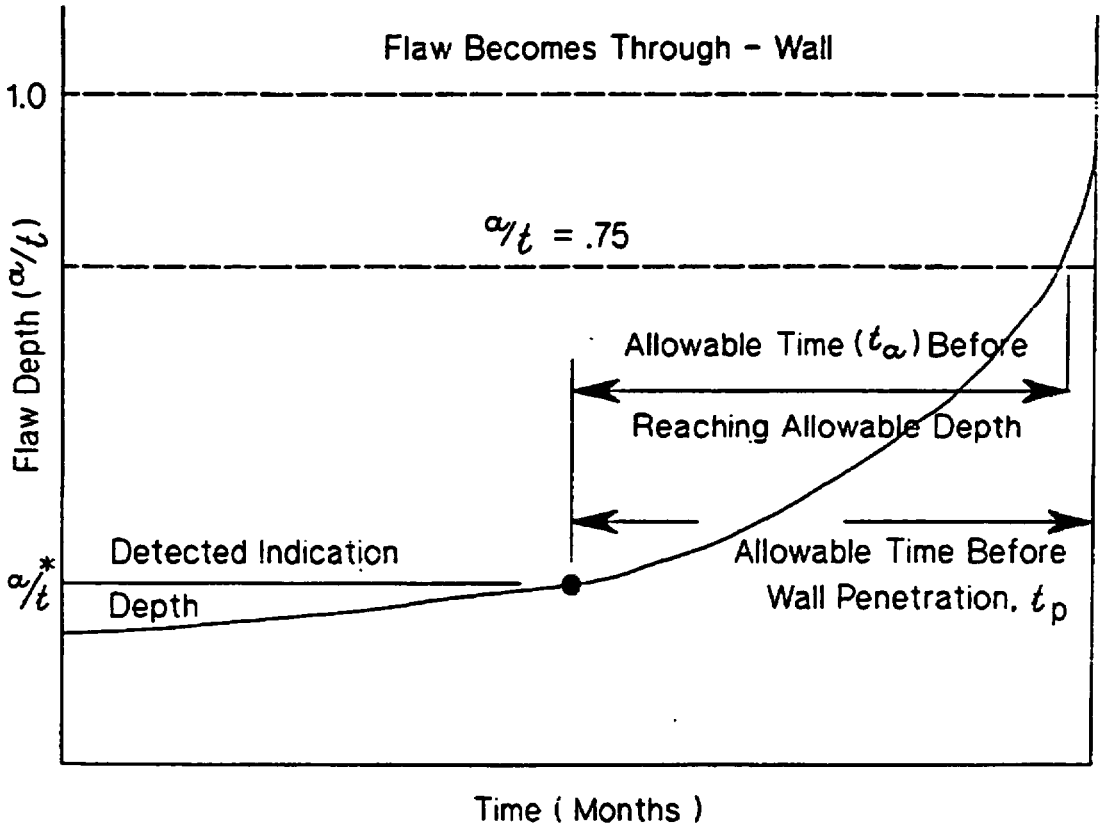

Figure 3-1 Schematic of a Head Penetration Flaw Growth Chart for Part Through Flaws

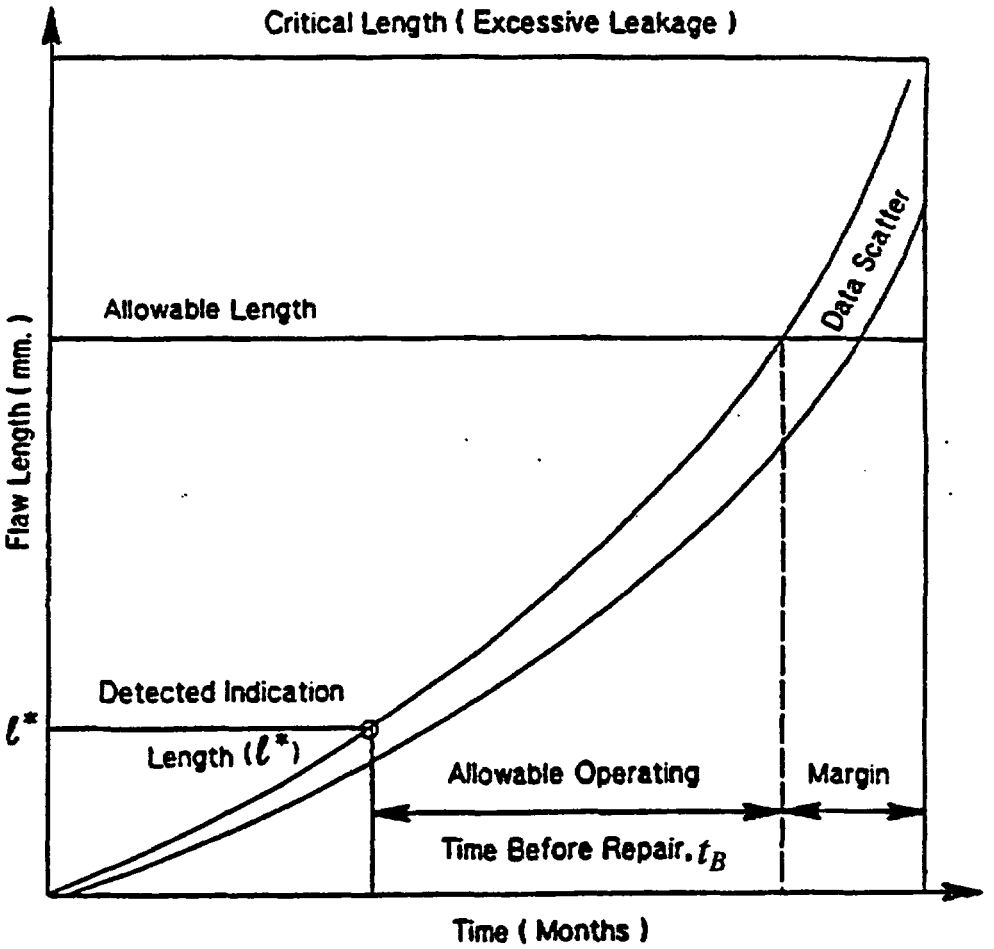

Figure 3-2 Schematic of a Head Penetration Flaw Tolerance Chart for Through-Wall Flaws

4 MATERIAL PROPERTIES, FABRICATION HISTORY AND CRACK GROWTH PREDICTION

4.1 MATERIALS AND FABRICATION

The reactor vessel for Millstone Unit 2 was manufactured by Combustion Engineering with the head penetration nozzles from material produced by Huntington Alloys in the USA. The carbon content and mechanical properties of the Alloy 600 material used to fabricate the Millstone Unit 2 vessel are provided in Table 4-1. The material CMTRs were used to obtain the chemistry and mechanical properties for the vessel head penetrations. The CMTRs for the material do not indicate the heat treatment of the material. However, Westinghouse records indicate that the materials were annealed for one hour at a temperature of 1700° - 1800°F, followed by a water quench. Figures 4-1 and 4-2 illustrate the yield strengths and carbon content, based on percent of heats, of the head adapter penetrations in the Millstone Unit 2 vessels relative to a sample of the French head adapters which have experienced cracking. Note that the French plants do not contain the large diameter ICIs, but only tubes the size of CEDMs. The general trends for the head adapter penetrations in Millstone Unit 2 are a higher carbon content, higher mill annealing temperature and lower yield strength relative to those on the French vessels. These factors should all have a beneficial effect on the material resistance to PWSCC in the head penetrations.

4.2 CRACK GROWTH PREDICTION

The cracks in the penetration region have been determined to result from primary water stress corrosion cracking in the Alloy 600 base metal, and in some cases the Alloy 182 weld metal. There are a number of available measurements of static load crack growth rates in primary water environment, and in this section the available results will be compared and a representative growth rate established.

Direct measurements of SCC growth rates in Alloy 600 are relatively rare, and care should be used in interpreting the results because the materials may be excessively cold worked, or the loadings applied may be near or exceeding the limit load of the tube, meaning there will be an interaction between tearing and crack growth. In these cases the crack growth rates may not be representative of service conditions.

The effort to develop a reliable crack growth rate model for Alloy 600 began in the spring of 1992, when the Westinghouse Owners Group was developing a safety case to support continued operation of plants. At the time there was no available crack growth rate data for head penetration materials, and only a few publications existed on growth rates of Alloy 600 in any product form.

The best available publication was found to be that of Peter Scott of Framatome, who had developed a growth rate model for PWR steam generator materials [1]. His model was based on a study of results obtained by McIlree and Smialowska [2] who had tested short steam generator tubes which had been flattened into thin compact specimens.

An equation was fitted to the data of reference [2] for the results obtained in water chemistries that fell within the standard specification for PWR primary water. Results for chemistries outside the specification were not used. The following equation was fitted to the data at 330°C (626°F):

$$\frac{da}{dt} = 2.8 \times 10^{-11} (K - 9)^{1.16} \text{ m/sec} \qquad (4\text{-}1)$$

where:

K is in MPa$\sqrt{m}$

The next step was to correct these results for the effects of cold work. Based on work by Cassagne and Gelpi [3], Scott concluded that dividing the above equation by a factor of 10 would be appropriate to account for the effects of cold work. The crack growth law for 330°C (626°F) then becomes:

$$\frac{da}{dt} = 2.8 \times 10^{-12} (K - 9)^{1.16} \text{ m/sec} \qquad (4\text{-}2)$$

Scott further corrected this law for the effects of temperature. This forms the basis for the PWR Materials Reliability Program (MRP) recommended crack growth rate (CGR) curve for the evaluation of SCC where a power-law dependence on stress intensity factor was assumed [4H]. The MRP recommended CGR curve was used in this report for determining the primary water stress corrosion crack growth rate and a brief discussion on this recommended curve is as follows:

[

]^{a,c,e}

[

]^{a,c,e}

There is a general agreement that crack growth in Alloy 600 materials in the primary water environment can be modeled using a stress intensity factor relationship with differences in temperature accounted for by an activation energy (Arrhenius) model for thermally controlled processes. Figure 4-3 shows the recommended CGR curve along with the laboratory data from Huntington materials used to develop the curve.

[

]^{a,c,e}

[

.]^{a,c,e}

The applicability of the MRP recommended model to head penetrations was recently confirmed by two independent approaches. The first was a collection of all available data from Standard Steel and Huntington Alloys materials tested over the past ten years [4H]. The results are shown in Figure 4-3, along with the Scott model for the test temperature.

The MRP crack growth curve was structured to bound 75 percent of the 26 heats for which test results were available. Fits were done on the results for each heat, and the constant term was determined for each heat. This was done to eliminate the concern that the curve might be biased from a large number of results from a single heat. The 75th percentile was then determined from these results. The MRP expert panel on crack growth endorsed the resulting curve unanimously in a meeting on March 6th and 7th 2002. This approach is consistent with the Section XI flaw evaluation philosophy, which is to make a best estimate prediction of future growth of a flaw. Margins are incorporated in the allowable flaw sizes. The entire data set is shown in Figure 4-3, where the data have been adjusted to a single temperature of 325°C.

A second independent set of data were used to validate the model, and these data were obtained from the two inspections carried out on penetration no. 75 of D.C. Cook Unit 2, which was first found to be cracked in 1994 [4G]. The plant operated for one fuel cycle before the penetration was repaired in 1996 and the flaw was measured again before being repaired. These results were used to estimate the PWSCC growth rate for both the length of the flaw and its depth. These two points are also shown in Figure 4-4, and are consistent with the laboratory data for Huntington materials. In fact, Figure 4-4 demonstrates that the MRP model is nearly an upper bound for these materials. The D.C. Cook Unit 2 penetrations were made from Huntington materials.

Since Millstone Unit 2 operates at a temperature of 312°C (594°F) in the head region [11], and the crack growth rate is strongly affected by temperature, a temperature adjustment is necessary. This temperature correction was obtained from study of both laboratory and field data for stress corrosion crack growth rates for Alloy 600 in primary water environments. The available data showing the effect of temperature are summarized in Figure 4-5. Most of the results shown here are from steam generator tube materials, with several sets of data from operating plants, and results from two heats of materials tested in a laboratory [4A].

Study of the data shown in Figure 4-5 results in an activation energy of 31-33 Kcal/mole, which can then be used to adjust for the lower operating temperature. This value is slightly lower than the generally accepted activation energy of 44-50 Kcal/mole used to characterize the effect of temperature on crack initiation, but the trend of the actual data for many different sources is unmistakable.

[

].[a,c,e] Therefore the following crack growth rate model was used for the Millstone Unit 2 head penetration for crack growth in all the cases analyzed.

$$\frac{da}{dt} = 1.51 \times 10^{-12}(K - 9)^{1.16} \text{ m/sec}$$

where:

K = applied stress intensity factor, in $MPa\sqrt{m}$

This equation implies a threshold for cracking susceptibility, $K_{Iscc} = 9$ $MPa\sqrt{m}$. The crack growth rate is applicable to propagation in both axial and circumferential directions.

(a,c,e

[ ]

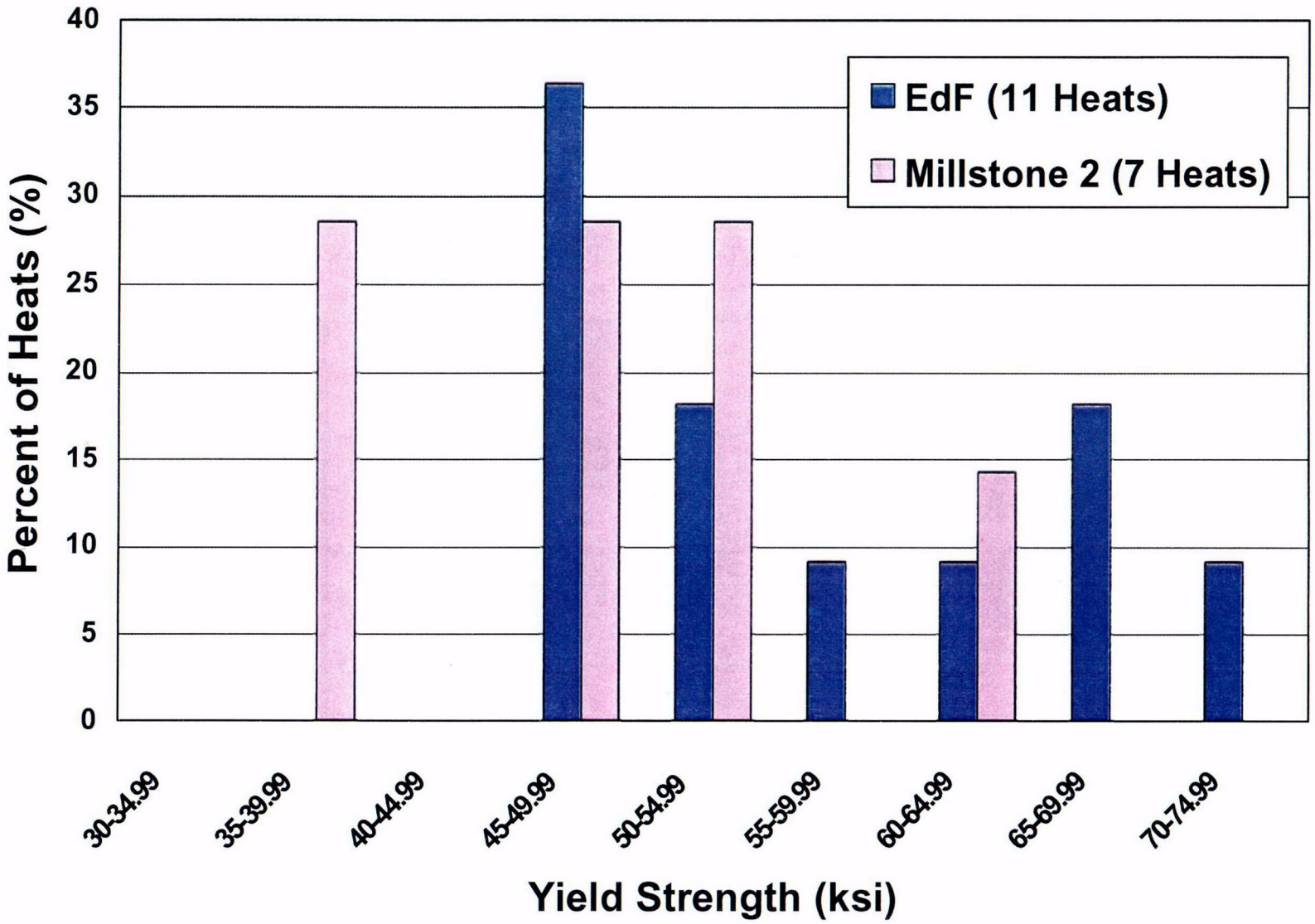

Figure 4-1 Yield Strength of the Various Heats of Alloy 600 Used in Fabricating the Millstone Unit 2 and French Head Penetrations

C02

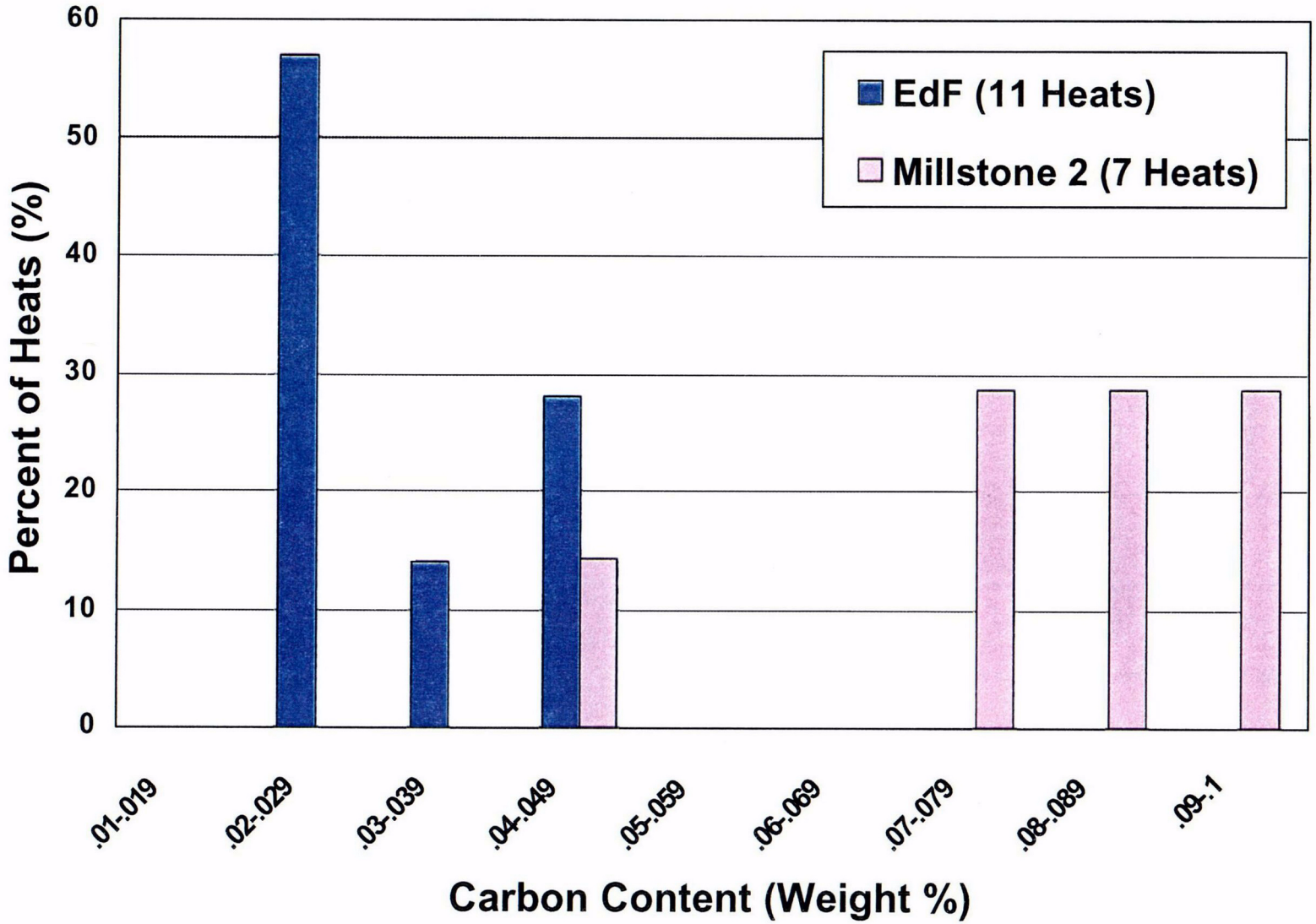

Figure 4-2 Carbon Content of the Various Heats of Alloy 600 Used in Fabricating the Millstone Unit 2 and French Head Penetrations

C03

(a,c,e)

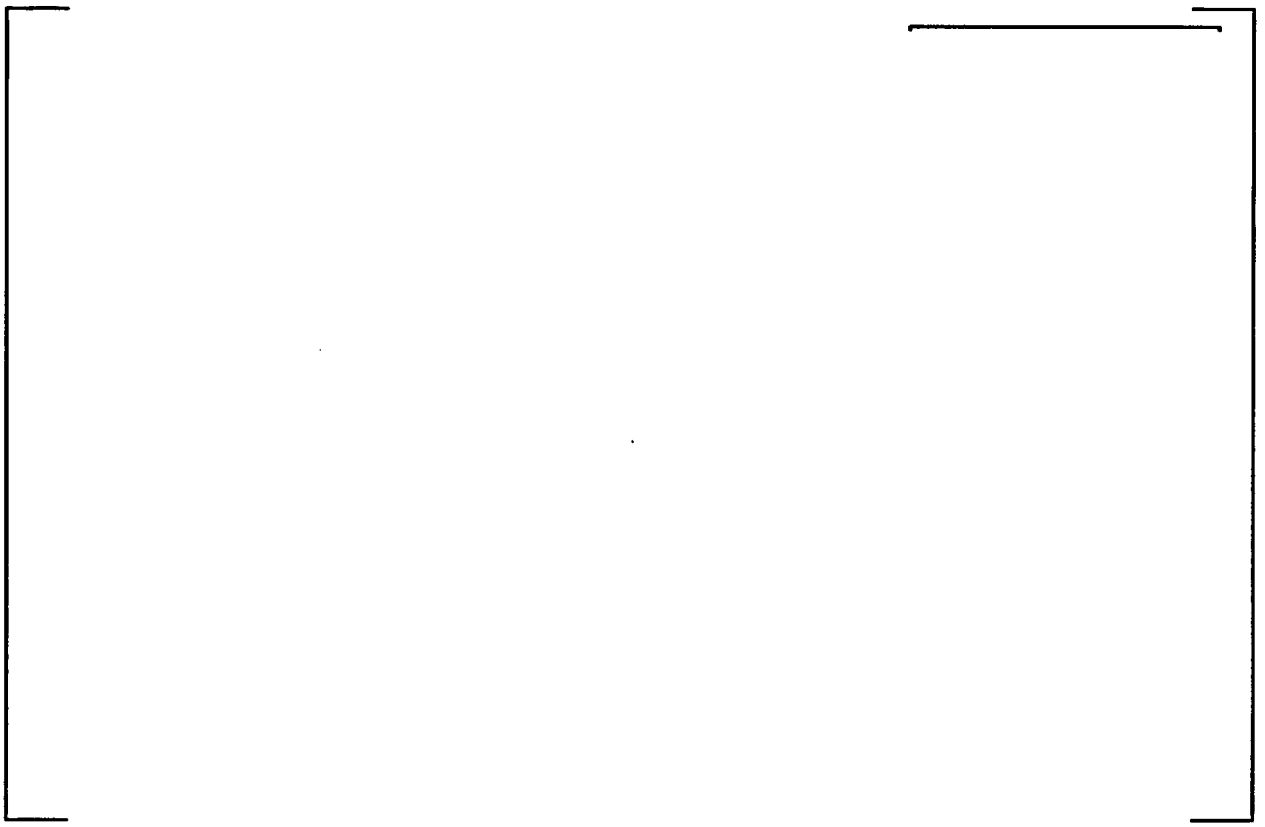

Figure 4-3 Screene d Laboratory Data for Alloy 600 with the MRP Recommended Curve. (Note that the Modified Scott Model is also Shown)

(a,c,e)

Figure 4-4 Model for PWSCC Growth Rates in Alloy 600 in Primary Water Environments (325°C), With Supporting Data from Standard Steel, Huntington, and Sandvik Materials

Note: That the data have been normalized to a temperature of 325°C. The actual test temperatures are listed in parenthesis after the caption. For example, the Huntington data were obtained at temperature ranging from 315°C to 331°C.

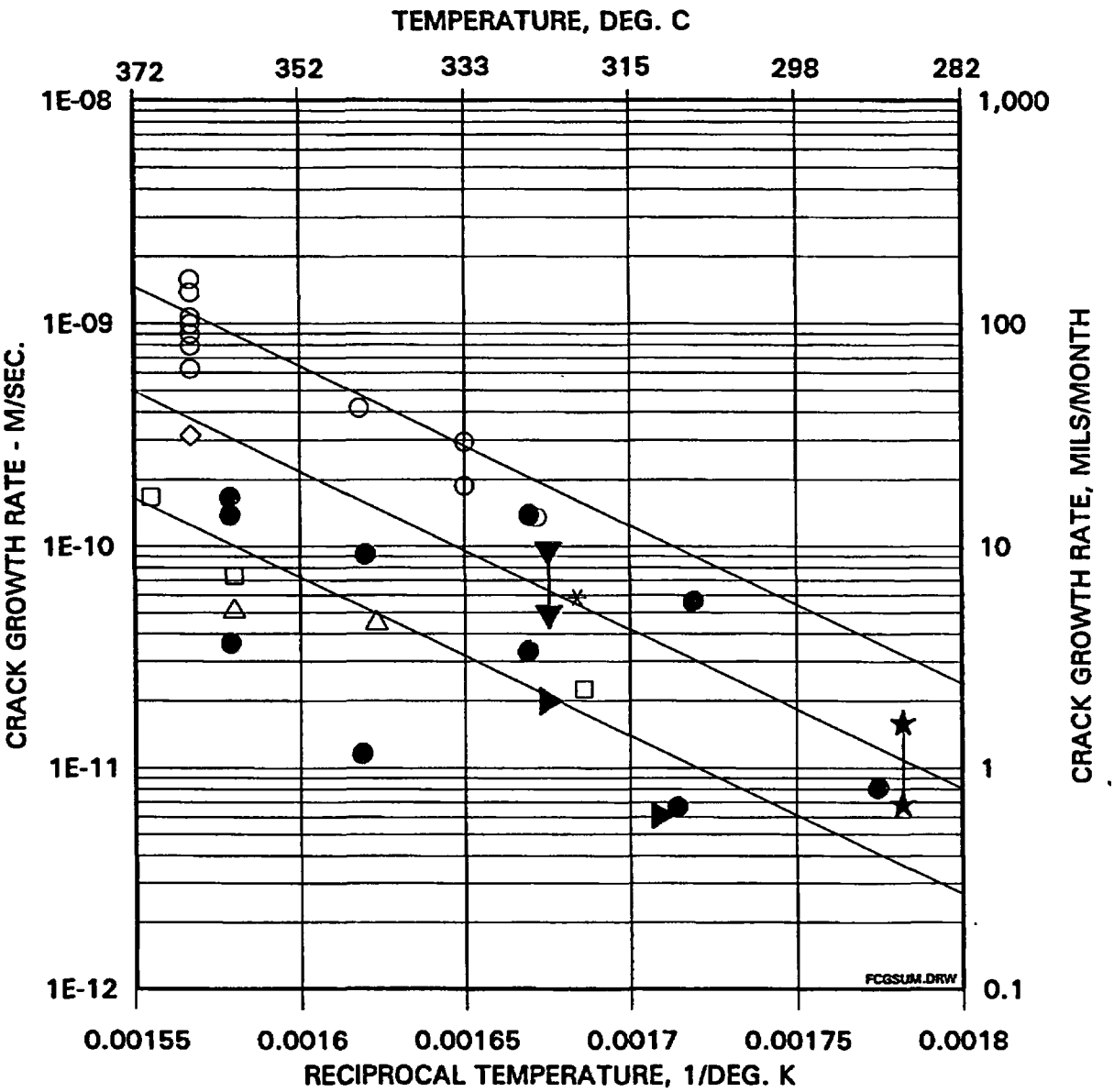

Figure 4-5 **Summary of Temperature Effects on PWSCC Growth Rates for Alloy 600 in Primary Water**

Note:All symbols are for steam generator materials, except the solid circles, which are head penetration laboratory data.

5 STRESS ANALYSIS

5.1 OBJECTIVES OF THE ANALYSIS

The objective of this analysis was to obtain accurate stresses in each CEDM or ICI housing and its immediate vicinity. To do so requires a three dimensional analysis which considers all the pertinent loadings on the penetration [6A, 6B, 6C]. An investigation of deformations at the lower end of the housing was also performed using the same model. Four CEDM locations were considered: the outermost CEDM row (42.5 degrees), rows at 37.1 degrees, 29.1 degrees, and the center location. In addition, the ICI penetration nozzles (54.8 degrees) were analyzed.

The analyses were used to provide information for the flaw tolerance evaluation in Section 6. Also, the results of the stress analysis were compared to the findings from service experience, to help assess the causes of the observed cracking.

5.2 MODEL

A three-dimensional finite element model comprised of isoparametric brick and wedge elements with mid-side nodes on each face was used to obtain the stresses and deflections. Views of CEDM and ICI models are shown in Figures 5-1 and 5-2 respectively. Taking advantage of the symmetry of the vessel head, only half of the CEDM penetrations were modeled. Similarly, only half of the center penetration was modeled.

In the models, the lower portion of the Control Element Drive Mechanism (CEDM) penetration nozzle, In-Core Instrumentation (ICI) nozzle, the head vent, the adjacent section of the vessel closure head, and the joining weld were modeled. The vessel to penetration nozzle weld was simulated with two weld passes. The penetration nozzle, and weld metal were modeled as Alloy 600 and the vessel head shell as carbon steel.

The only loads used in the analysis are the steady state operating loads. External loads, such as seismic loads, have been studied and have no impact since the penetration nozzles are captured by the full thickness of the reactor vessel head (about 7 and 1/2 inches of steel [10B]) into which the penetrations are shrunk fit during construction. The area of interest is in the penetration near the attachment weld, which is unaffected by these external loads.

5.3 STRESS ANALYSIS RESULTS – OUTERMOST CEDM PENETRATION NOZZLE (42.5 DEGREES)

Figure 5-3 presents the hoop and axial stresses for the steady state condition for the outermost CEDM penetration.

[

]^{a,c,e}

[

]a,c,e

5.4 STRESS ANALYSIS RESULTS 37.1 DEGREE AND 29.1 DEGREE CEDM PENETRATION NOZZLES

[

]a,c,e

5.5 STRESS ANALYSIS RESULTS-CENTER CEDM PENETRATION NOZZLE

[

]a,c,e

5.6 STRESS ANALYSIS RESULTS: ICI NOZZLES

The ICI nozzles are located further from the reactor vessel centerline than any of the other head penetration nozzles. They are larger in diameter and thinner than the CEDMs. The stress contour plots for the ICI nozzles at steady state conditions are shown in Figure 5-8.

5.7 STRESS ANALYSIS RESULTS: HEAD VENT NOZZLE

The head vent is a smaller penetration than the CEDM or ICI head penetration nozzles, but is also constructed of Alloy 600 material, with a partial penetration weld at the inside of the reactor vessel head. The head vent is located 8.2 inches from the centerline of the head dome.

[

]a,c,e

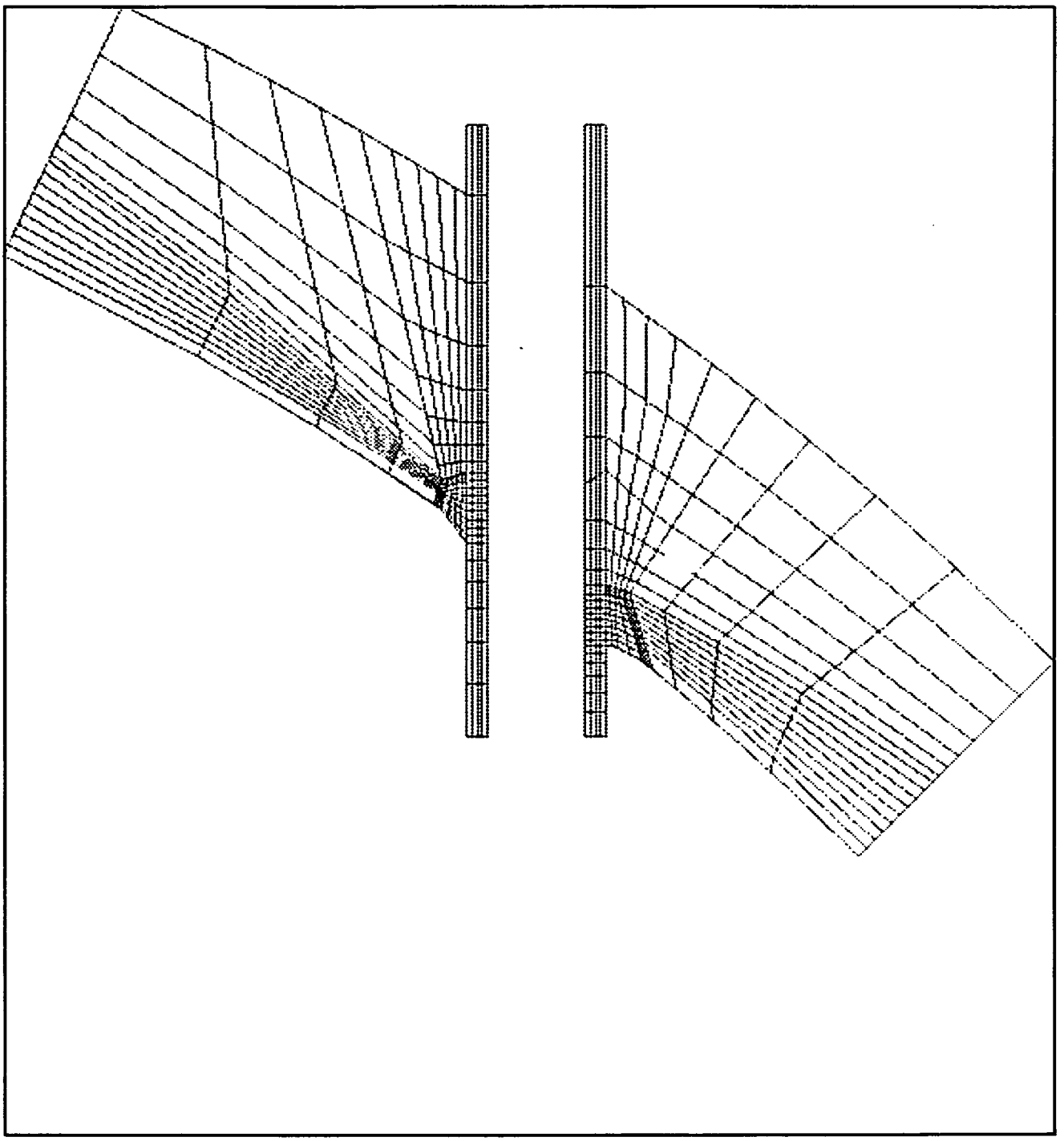

Figure 5-1 Finite Element Model of CEDM Penetration (42.5 Degrees)

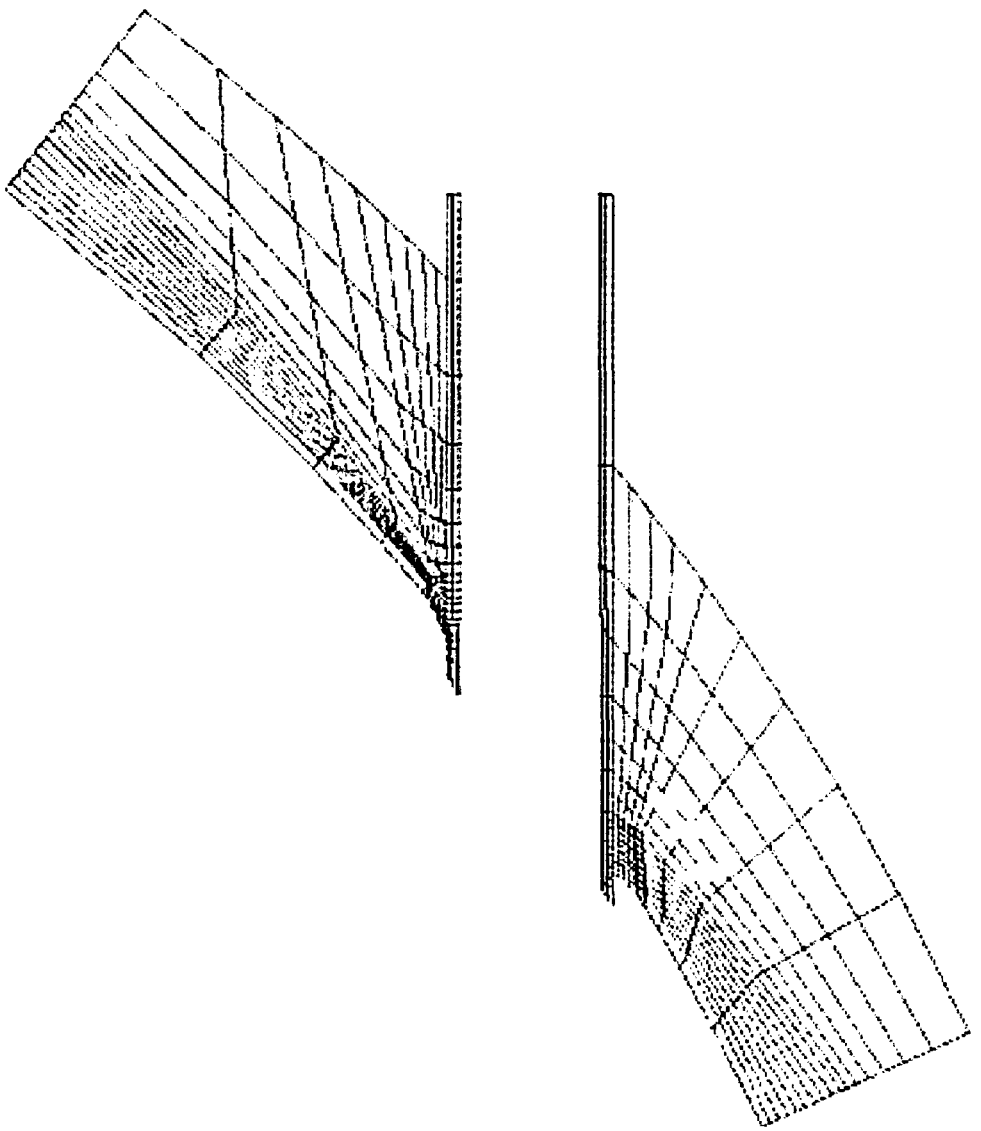

Figure 5-2 Three Dimensional Model of the ICI Penetration Nozzle (54.8 Degrees)

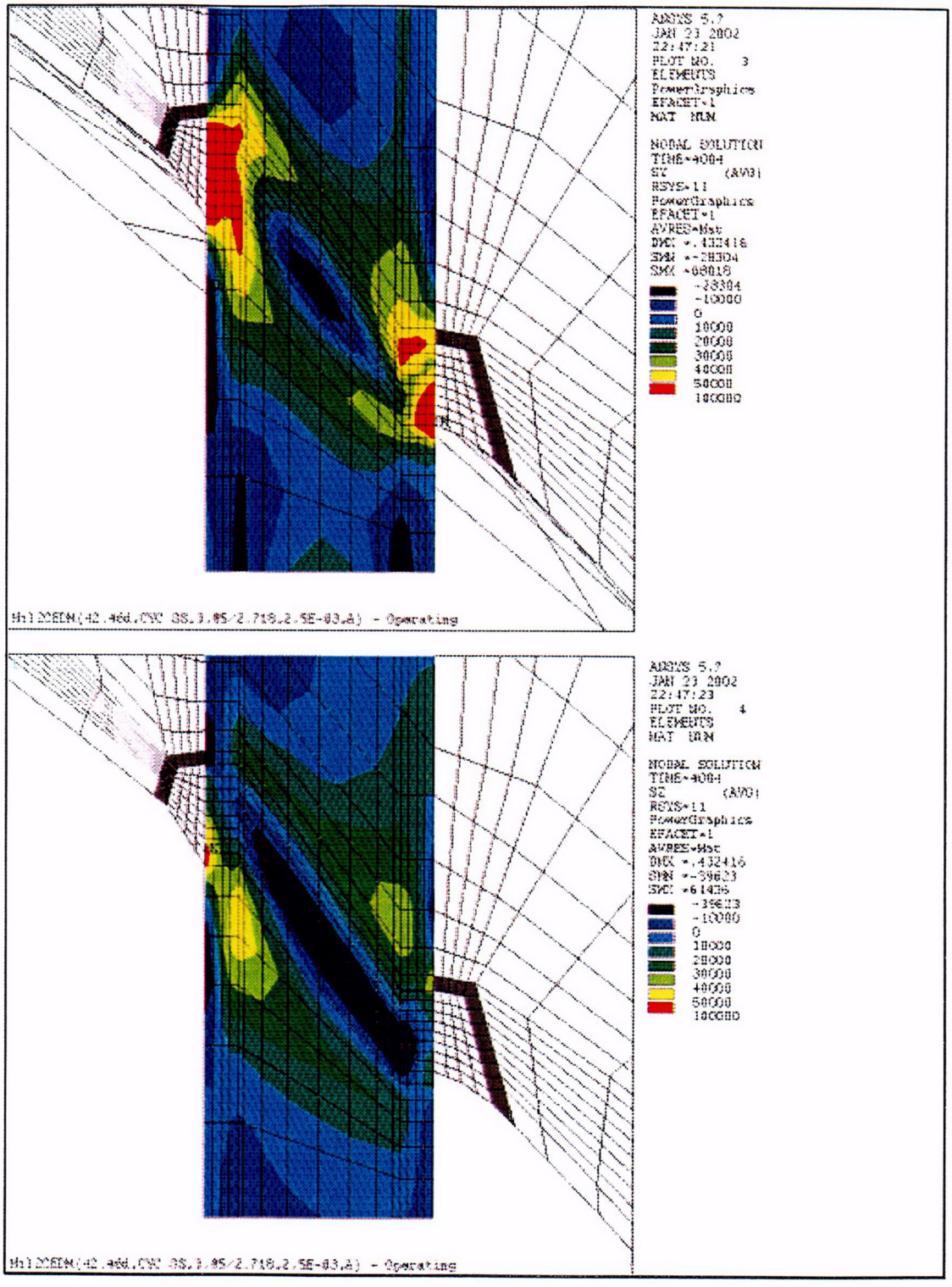

Figure 5-3 Stress Distributions at Steady State Conditions: Outermost CEDM Penetration Nozzle (42.5 Degrees) (Hoop Stress is the Top Figure; Axial Stress is the Bottom Figure)

C04

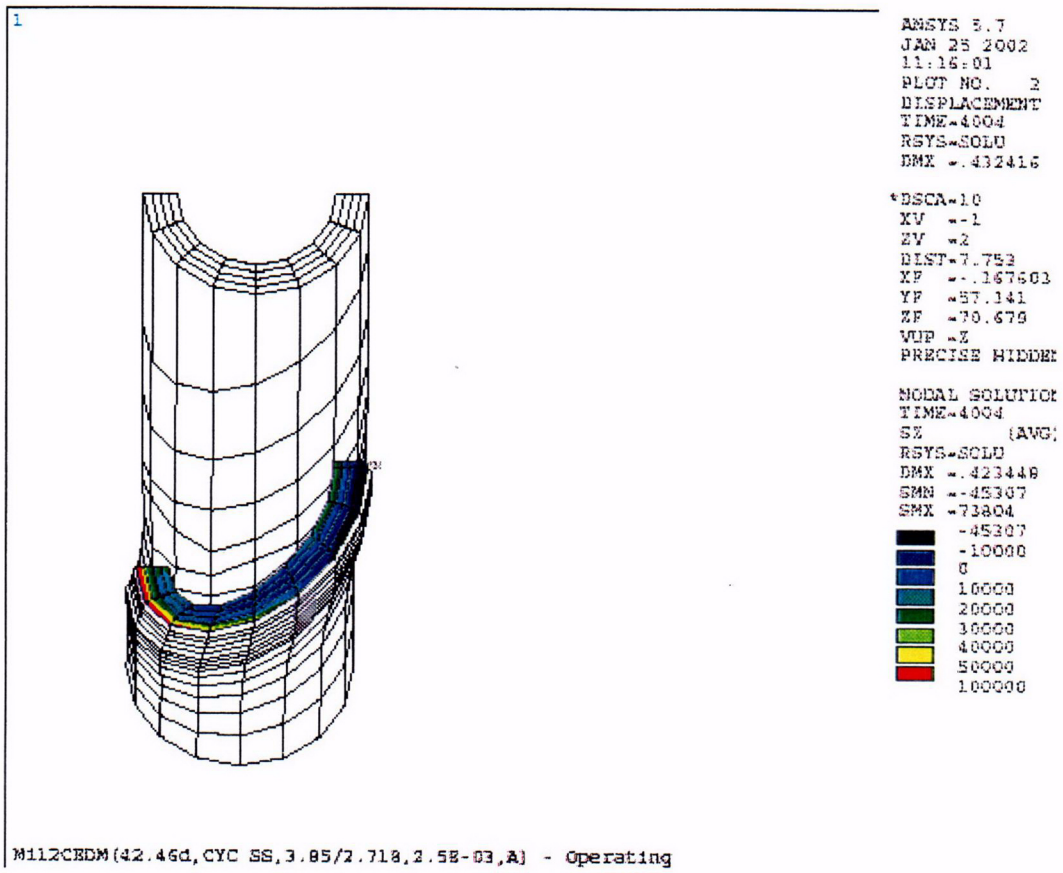

Figure 5-4 Axial Stress Distribution at Steady State Conditions for the Outermost CEDM (42.5 Degrees) Penetration, Along a Plane Oriented Parallel to, and Just Above, the Attachment Weld

C05

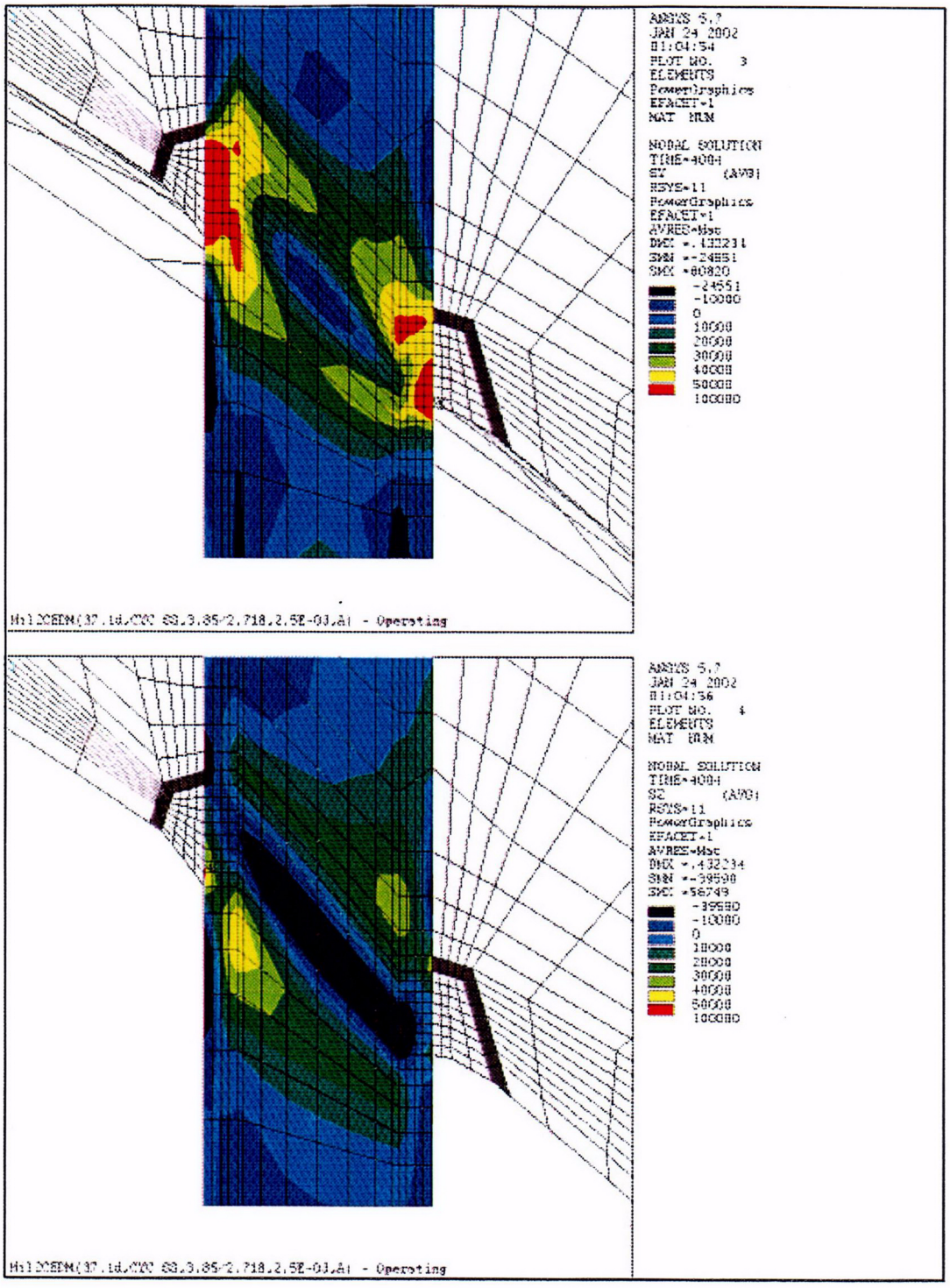

Figure 5-5 Stress Distribution at Steady State Condition for the 37.1 Degrees CEDM Penetration Nozzle (Hoop Stress is the Top Figure; Axial Stress is the Bottom Figure)

C06

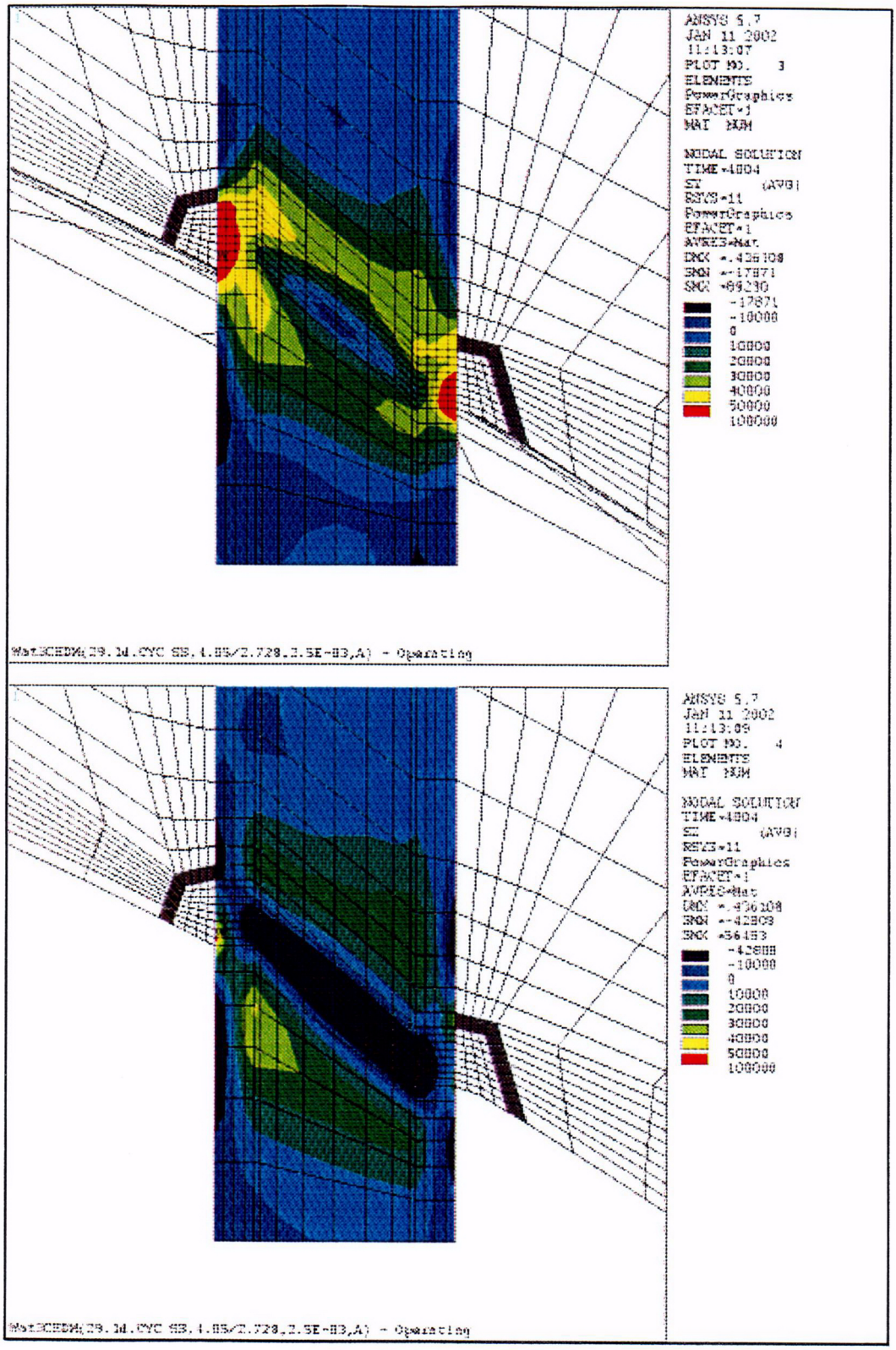

Figure 5-6 Stress Distribution at Steady State Condition for the 29.1 Degrees CEDM Penetration Nozzle (Hoop Stress is the Top Figure; Axial Stress is the Bottom Figure)

C07

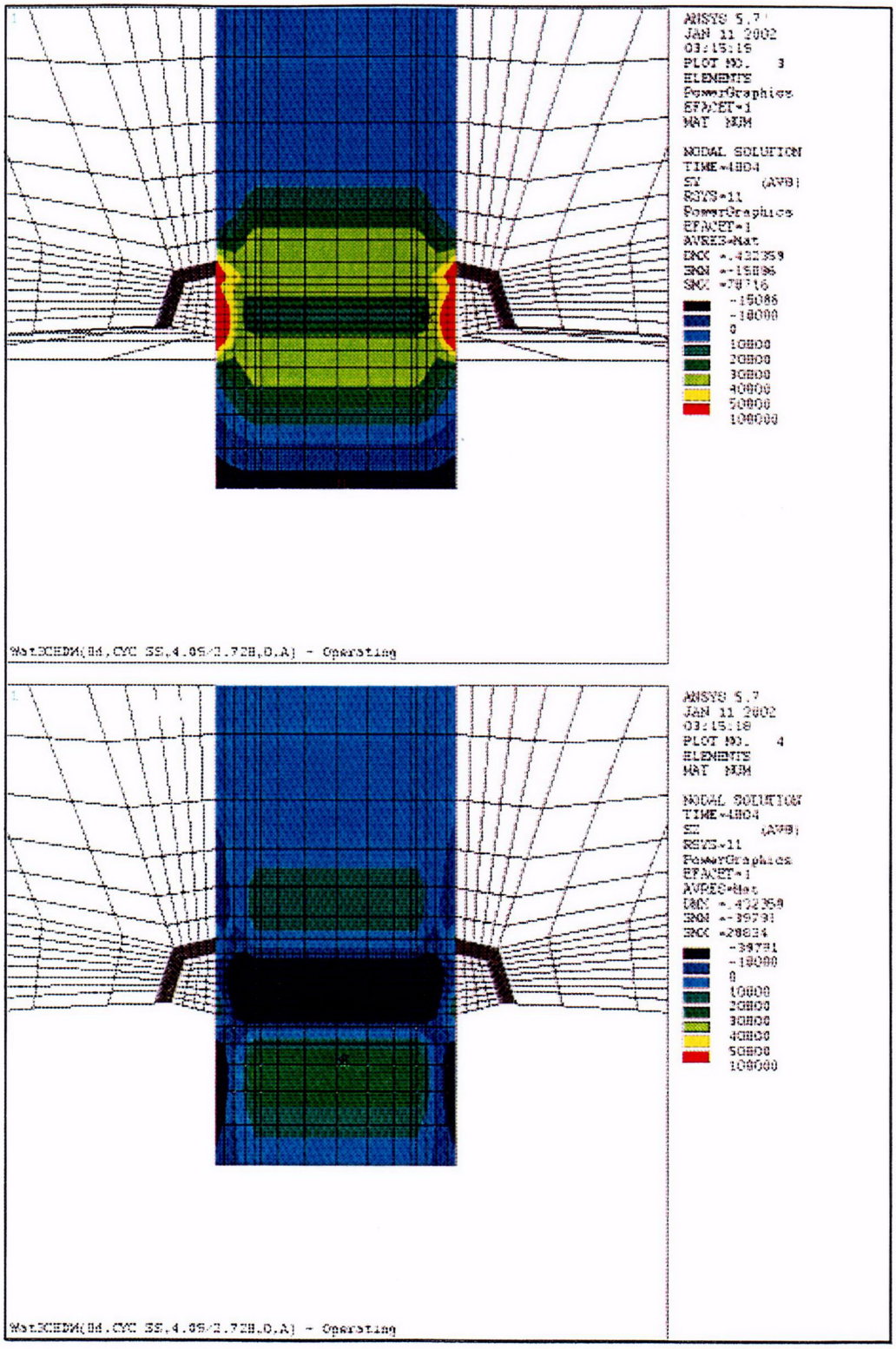

Figure 5-7 Stress Distribution at Steady State Condition for the Center CEDM Penetration Nozzle (Hoop Stress is the Top Figure; Axial Stress is the Bottom Figure)

C08

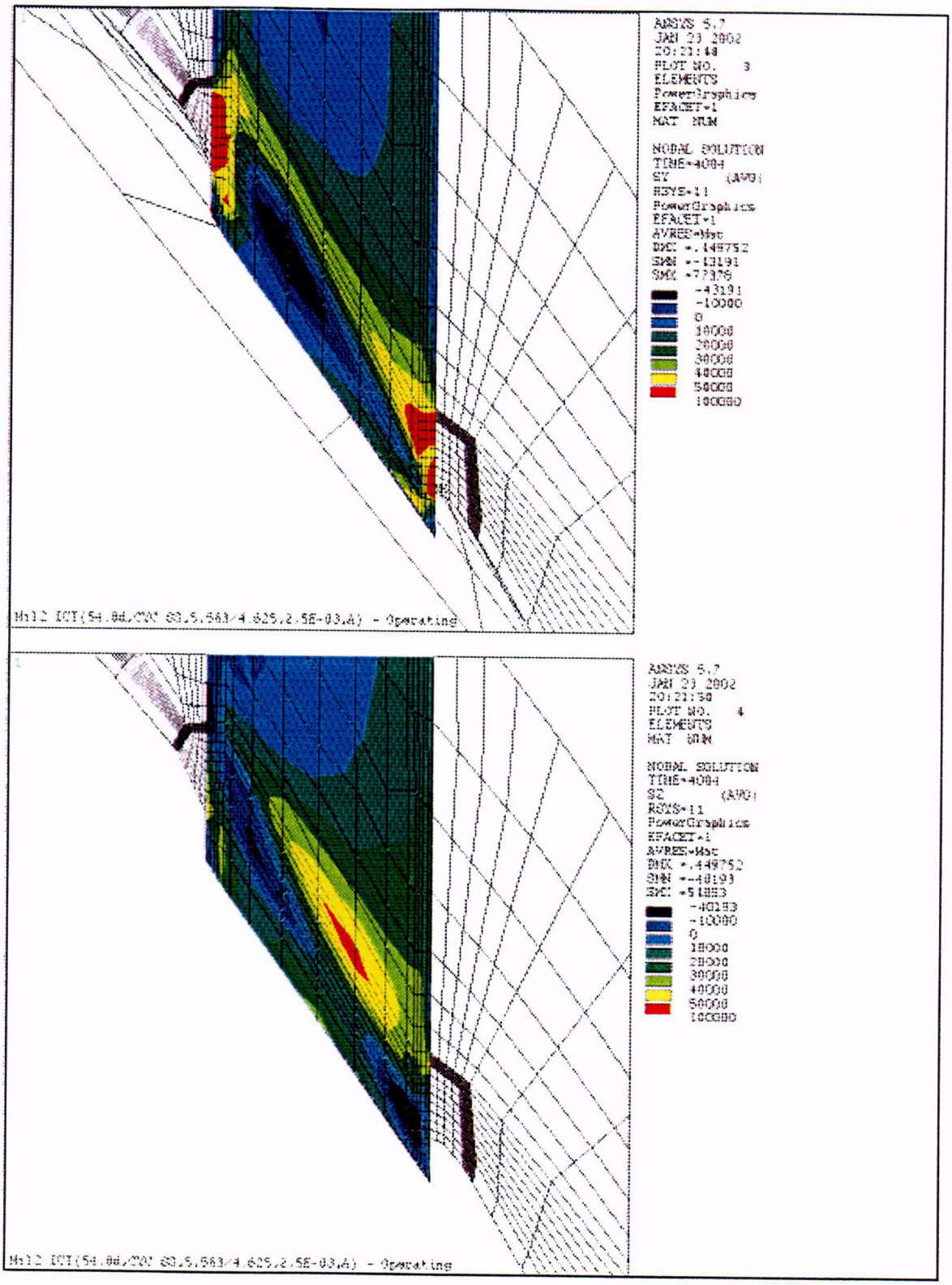

Figure 5-8 Stress Distribution at Steady State Conditions for the ICI Penetration (Hoop Stress is the Top Figure; Axial Stress is the Bottom Figure)

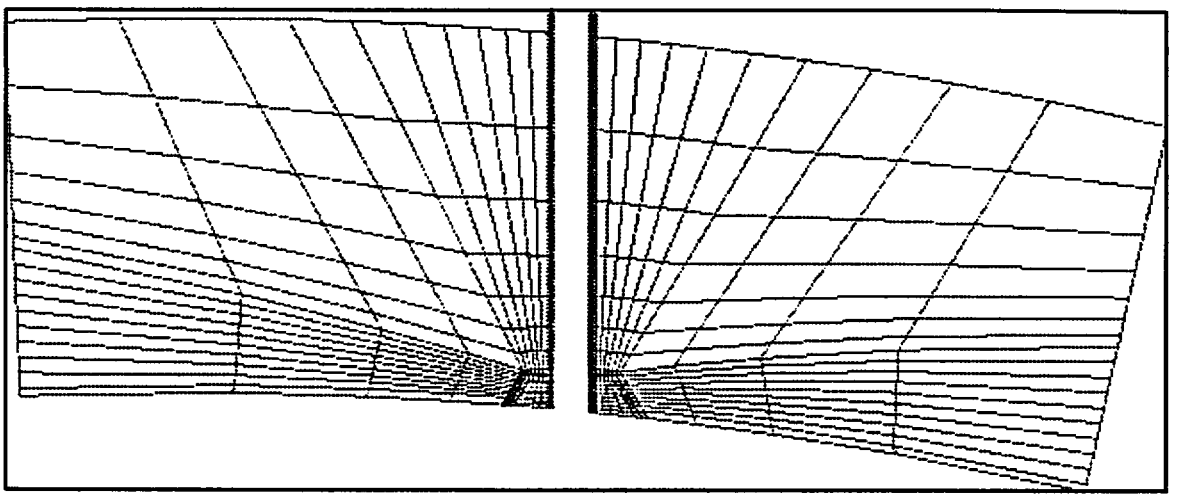

Figure 5-9 Head Vent Nozzle Finite Element Model

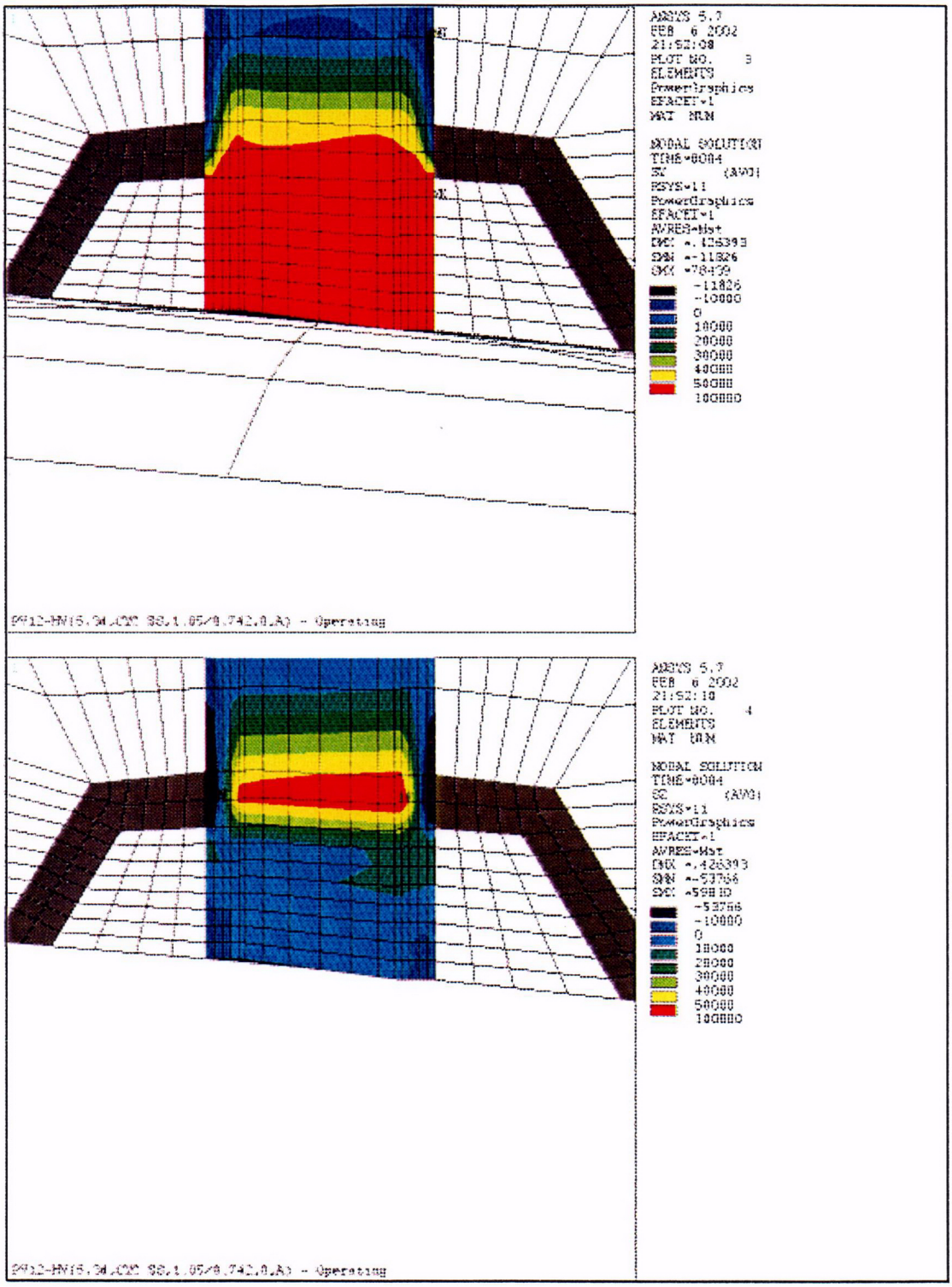

Figure 5-10 Stress Contours in the Head Vent Nozzle as a Result of Residual Stresses and Operating Pressure (Hoop stress is the Top Figure; Axial Stress is the Bottom Figure)

C10

6 FLAW EVALUATION CHARTS

6.1 INTRODUCTION

The flaw evaluation charts were developed from the stress analysis of each of the penetration locations, as discussed in Section 5. The crack growth law developed for Millstone Unit 2 in Section 4.2 was used for each case, and several flaw tolerance charts were developed for each penetration location. The first series of charts characterizes the growth of a part through flaw, and the second series of charts characterizes the growth of a through-wall flaw in the length direction. The allowable safe operating life of the penetration nozzle may then be directly determined, using the combined results of the two charts. All times resulting from these calculations are effective full power years, since crack growth will only occur at operating temperatures.

6.2 OVERALL APPROACH

The results of the three-dimensional stress analysis of the penetration locations were used directly in the flaw tolerance evaluation.

The crack growth evaluation for the part-through flaws was based on the worst stress distribution through the penetration wall at the location of interest of the penetration. The highest stressed location was found to be in the immediate vicinity of the weld for both the center and outermost penetrations.

The stress profile was represented by a cubic polynomial:

$$\sigma(x) = A_0 + A_1 x + A_2 x^2 + A_3 x^3 \qquad (6\text{-}1)$$

where:

x	=	the coordinate distance into the nozzle wall
σ	=	stress perpendicular to the plane of the crack
A_i	=	coefficients of the cubic polynomial fit

For the surface flaw with length six times its depth, the stress intensity factor expression of Raju and Newman [5A] was used. The stress intensity factor $K_I(\Phi)$ can be calculated anywhere along the crack front. The point of maximum crack depth is represented by $\Phi = 0$, and this location was also found to be the point of maximum K_I for the cases considered here. The following expression is used for calculating $K_I(\Phi)$, where Φ is the angular location around the crack. The units of $K_I(\Phi)$ are $ksi\sqrt{in}$.

$$K_I(\Phi) = \left[\frac{\pi a}{Q}\right]^{0.5} \sum_{j=0}^{3} G_j(a/c,\ a/t,\ t/R,\ \Phi)\, A_j\, a^j \qquad (6\text{-}2)$$

The boundary correction factors $G_0(\Phi)$, $G_1(\Phi)$, $G_2(\Phi)$ and $G_3(\Phi)$ are obtained by the procedure outlined in reference [5A]. The dimension "a" is the crack depth, and "c" is the semi crack

length, while "t" is the wall thickness. "R" is the inside radius of the tube, and "Q" is the shape factor.

[

]^{a,c,e}

6.3 RESULTS: AXIAL FLAWS

CEDM and ICI Surface Flaws

The results of the calculated growth through the wall thickness of the CEDM penetration nozzles for surface flaws are shown in Figures 6-2 through 6-7 for inside surface flaws. For outside surface flaws the results are shown in Figures 6-8 and 6-9. Based on the discussion in MRP-55 report [4H], the use of stress intensity factors less than $15\,\text{MPa}\sqrt{\text{m}}$ involves assumption not currently substantiated by actual CGR data for neither CEDM nor ICI nozzle materials. Therefore, these crack growth curves begin at a flaw depth that results in a stress intensity factor of $15\,\text{MPa}\sqrt{\text{m}}$, which exceeds the threshold value of $9\,\text{MPa}\sqrt{\text{m}}$. This may result in curves with

different initial flaw sizes, as seen for example in Figure 6-3. Note that results are only provided for the uphill and downhill sides of each penetration nozzle; the stresses for the regions 90 degrees from these locations are compressive. If flaws are found in such a location, the results for either the uphill or downhill location, whichever is closer, can be used.

Each of these figures allows the future allowable service time to be estimated graphically, as discussed in Section 3. Results are shown for each of the penetration nozzles analyzed in each of these figures. The stresses are much higher near the attachment weld than at 0.5 inch below or above it, so separate figures have been provided for these three regions. For more than 0.5 inch below the weld, the crack growth will eventually come to rest since the stresses are compressive as shown for CEDM nozzles in Appendix E. Also, the stresses are different on the downhill side of the penetration as opposed to the uphill side, so these two cross sections have also been treated separately.

CEDM and ICI Through-Wall Flaws

The projected crack growth of a through-wall flaw in the CEDM and ICI penetration nozzles are the primary concern in evaluating the structural integrity of head penetrations. In some cases, the through-wall flaw may be located sufficiently below the attachment weld that additional time may be required for the flaw to grow to the attachment weld. To provide a means to evaluate the duration of this additional time, a series of flaw tolerance charts for through-wall flaws were prepared.

Charts were prepared for each of the penetrations evaluated, for both the uphill and downhill locations, as shown in Figures 6-12 through 6-20. In each figure, the upper extremity of the thru-weld crack is measured from the bottom of the nozzle. Note that in all the cases, the crack slows down significantly as it grows above the weld, due to the decreasing magnitude of the stress field. This provides further assurance that axial flaws will not extend to a critical length which exceeds 15 inches, regardless of the duration of crack growth.

Head Vent

The only flaw tolerance chart that is necessary for the head vent region is for flaws at and above the weld, since there is no portion of the head vent which projects below the weld. Figure 6-11 provides the projected growth of a part through flaw in the head vent just above the attachment weld. The growth through the wall is relatively rapid, because the thickness of the head vent is small.

6.4 CIRCUMFERENTIAL CRACK PROPAGATION

Since circumferentially oriented flaws have been found at five plants (Bugey 3, Oconee 2, Crystal River 3, Davis Besse, and Oconee 3), it is important to consider the possibility of crack extension in the circumferential direction. The first case was discovered as part of the destructive examination of the tube with the most extensive circumferential cracking at Bugey 3. The crack was found to have extended to a depth of 2.25 mm in a wall thickness of 16 mm. The flaw was found at the outside surface of the penetration (number 54) at the downhill side location, just above the weld.

The circumferential flaws in Oconee Unit 3 were discovered during the process of repairing a number of axial flaws, whereas the circumferential flaw in Oconee Unit 2 and Crystal River Unit 3 were discovered by UT. Experience gained from these findings has enabled the development of UT procedures capable of detecting circumferential flaws reliably.

To investigate this issue completely, a series of crack growth calculations were carried out for a postulated surface circumferential flaw located just above the head penetration weld, in a plane parallel to the weld itself. This is the only flaw plane that could result in a complete separation of the penetration nozzle, since all others would result in propagation below the weld, and therefore there is no chance of complete separation because the remaining weld would hold the penetration nozzle in place.

[

]^{a,c,e}

[

]^{a,c,e}

[

]^{a,c,e} The results of this calculation are shown in Figure 6-21. From Figure 6-21, it can be seen that the time required for propagation of a circumferential flaw to a point where the integrity of the CEDM penetration nozzle would be affected (330-350 degrees [11]) would be about 25 years. From the same figure, the required time for propagation of a circumferential flaw to a point where the integrity of the ICI penetration nozzles would be affected is about 38 years. Due to the conservatism in the calculations (the time period for a surface flaw to become a through-wall flaw was conservatively ignored) the service life is likely to be even longer. In addition, due to uncertainties in the exact composition of the chemical environment in contact with the nozzle OD, a multiplicative factor of 2.0 is used in the CGR for all circumferential surface flaws on the OD of the head penetration nozzles located above the elevation of the J-groove weld.

6.5 FLAW ACCEPTANCE CRITERIA

Now that the projected crack growth curves have been developed, the question remains as to what flaw size would be acceptable for further service.

Acceptance criteria have been developed for indications found during inspection of reactor vessel upper head penetration as part of an industry program coordinated by NEI (formerly NUMARC). Such criteria are normally found in Section XI of the ASME Code, but Section XI does not require in-service inspection of these regions and therefore acceptance criteria are not available. In developing the enclosed acceptance criteria, the approach used was very similar to that used by Section XI, in that an industry consensus was reached using input from both operating utility technical staff and each of the three PWR vendors. The criteria developed are applicable to all PWR plant designs.

Since the discovery of the leaks at Oconee and ANO-1, the acceptance criteria have been revised slightly, to cover flaws on the outside diameter of the penetration below the attachment weld, and flaws in the attachment weld. These revised criteria are now formally endorsed by the NRC [12].

The criteria presented herein are limits on flaw sizes, which are acceptable. The criteria are to be applied to inspection results. It should be noted that determination of the future service during which the criteria are satisfied is plant-specific and dependent on flaw geometry and loading conditions.

It has been previously demonstrated by each of the owners groups that the penetration nozzles are very tolerant of flaws and there is only a small likelihood of flaw extensions to larger sizes. Therefore, it was concluded that complete fracture of the penetration nozzle is highly unlikely. The approach used here is more conservative than that used in Section XI applications where the

acceptable flaw size is calculated by placing a margin on the critical flaw size. For the current application, the critical flaw size would be far too large to allow a practical application of the approach used in Section XI applications, so protection against leakage is the priority.

The acceptance criteria presented herein apply to all the flaw types regardless of orientation and shape. Similar to the approach used in Section XI, flaws are first characterized according to established rules and then compared with acceptance criteria.

Flaw Characterization

Flaws detected must be characterized by the flaw length and preferably flaw depth. The proximity rules of Section XI for considering flaws as separate, may be used directly (Section XI, Figure IWA 3400-1). This figure is reproduced here as Figure 6-22.

When a flaw is detected, its projections in both the axial and circumferential directions must be determined. Note that the axial direction is always the same for each penetration, but the circumferential direction will be different depending on the angle of intersection of the penetration nozzle with the vessel head. The "circumferential" direction of interest here is along the top of the attachment weld, as illustrated in Figure 6-23. It is this angle which will change for each penetration nozzle and the top of the attachment weld is also the plane which could cause separation of the penetration nozzle from the vessel head. The location of the flaw relative to both the top and bottom of the partial penetration attachment weld must also be determined since a potential leak path exists when a flaw propagates through the penetration nozzle wall and up the penetration nozzle past the attachment weld. Schematic of a typical weld geometry is shown in Figure 6-24.

Flaw Acceptance Criteria

The maximum allowable depth (a_f) for axial flaws on the inside surface of the penetration nozzle, at or above the weld is 75 percent of the penetration wall thickness. The term a_f is defined as the maximum size to which the detected flaw is calculated to grow in a specified time period. This 75 percent limitation was selected to be consistent with the maximum acceptable flaw depth in Section XI and to provide an additional margin against through wall penetration. There is no concern about separation of the penetration nozzle from the vessel head, unless the flaw is above the attachment weld and oriented circumferentially. Calculations have been completed to show that the geometry of all penetrations can support a continuous circumferential flaw with a depth of 75 percent of the wall thickness.

Axial inside surface flaws found below the weld are acceptable regardless of depth as long as their upper extremity does not reach the bottom of the weld during the period of service until the next inspection. Axial flaws that extend above the weld are limited to 75 percent of the wall thickness.

Axial flaws on the outside surface of the penetration nozzle below the attachment weld are acceptable regardless of depth, as long as they do not extend into the attachment weld during the

period of service until next inspection. Outside surface flaws above the attachment weld must be evaluated on a case by case basis, and must be discussed with the regulatory authority.

Circumferential flaws located below the weld are acceptable regardless of their depth, provided the length is less than 75 percent of the penetration nozzle circumference for the period of service until the next inspection. Circumferential flaws detected in this area have no structural significance except that loose parts must be avoided. To this end, intersecting axial and circumferential flaws shall be removed or repaired. Circumferential flaws at and above the weld must be discussed with the regulatory authority on a case by case basis.

Surface flaws located in the attachment welds themselves are not acceptable regardless of their depth. This is because the crack growth rate is several times faster than that of the Alloy 600 material, and also because depth sizing capability does not yet exist for indications in the attachment weld.

The flaw acceptance criteria are summarized in Table 6-1. Flaws that exceed these criteria must be repaired unless analytically justified for further service. These criteria have been reviewed and endorsed by the NRC, as documented in references [7, 8, & 12]. These criteria are identical with the draft acceptance criteria now being considered for Section XI, for head penetrations.

It is expected that the use of these criteria and crack growth curves will provide conservative predictions of the allowable service time.

Table 6-1 Summary of R.V. Head Penetration Acceptance Criteria (Limits for Future Growth)				
Location	Axial		Circumferential	
	a_f	l	a_f	l
Below Weld (ID)	t	no limit	t	.75 circ.
At and Above Weld (ID)	0.75 t	no limit	*	*
Below Weld (OD)	t	no limit	t	.75 circ.
Above Weld (OD)	*	*	*	*

Note: Surface flaws of any size in the attachment weld are not acceptable.

* Requires case-by-case evaluation and discussion with regulatory authority.

a_f = Flaw Depth
l = Flaw Length
t = Wall Thickness

Table 6-2 Millstone Unit 2 Penetration Geometries [10A, 10C]		
Penetration Type	Wall Thickness (in.)	Penetration OD (in.)
CEDM	0.566	3.850
ICI	0.469	5.563
Head Vent	0.154	1.050

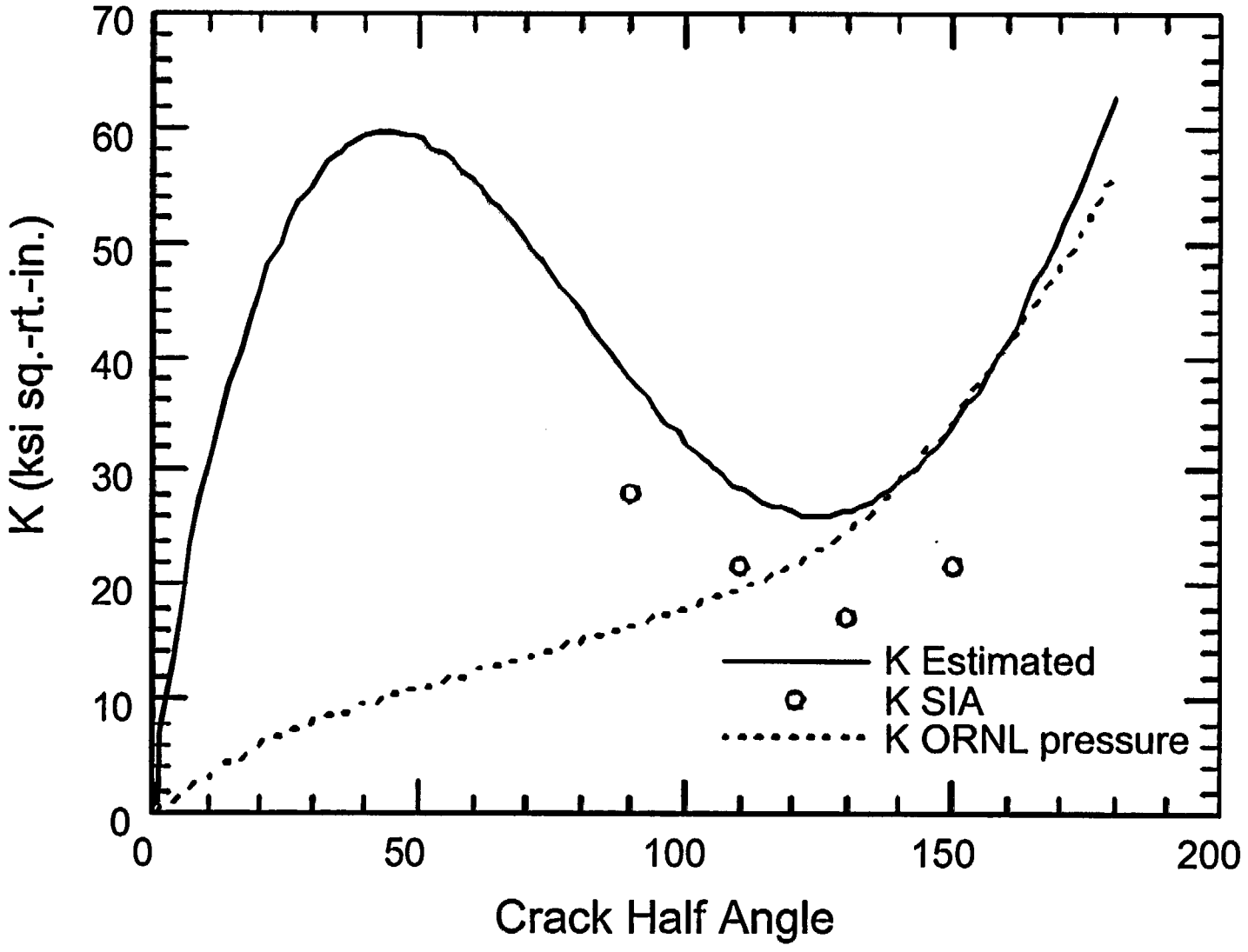

Figure 6-1 Stress Intensity Factor for a Through-Wall Circumferential Flaw in a Head Penetration Nozzle

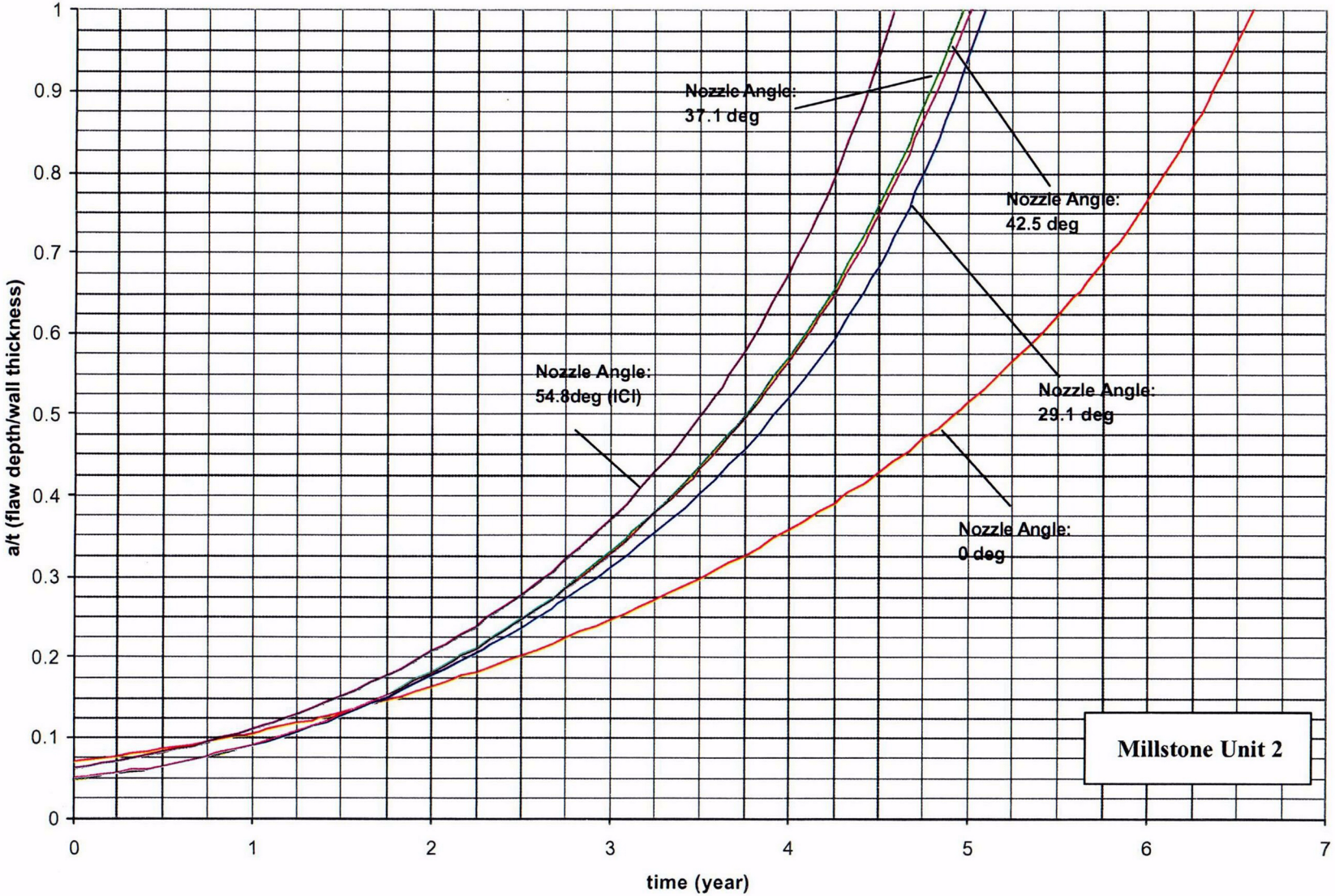

Figure 6-2 Inside, Axial Surface Flaws, .5" Below the Attachment Weld, Nozzle Uphill Side - Crack Growth Predictions

C11

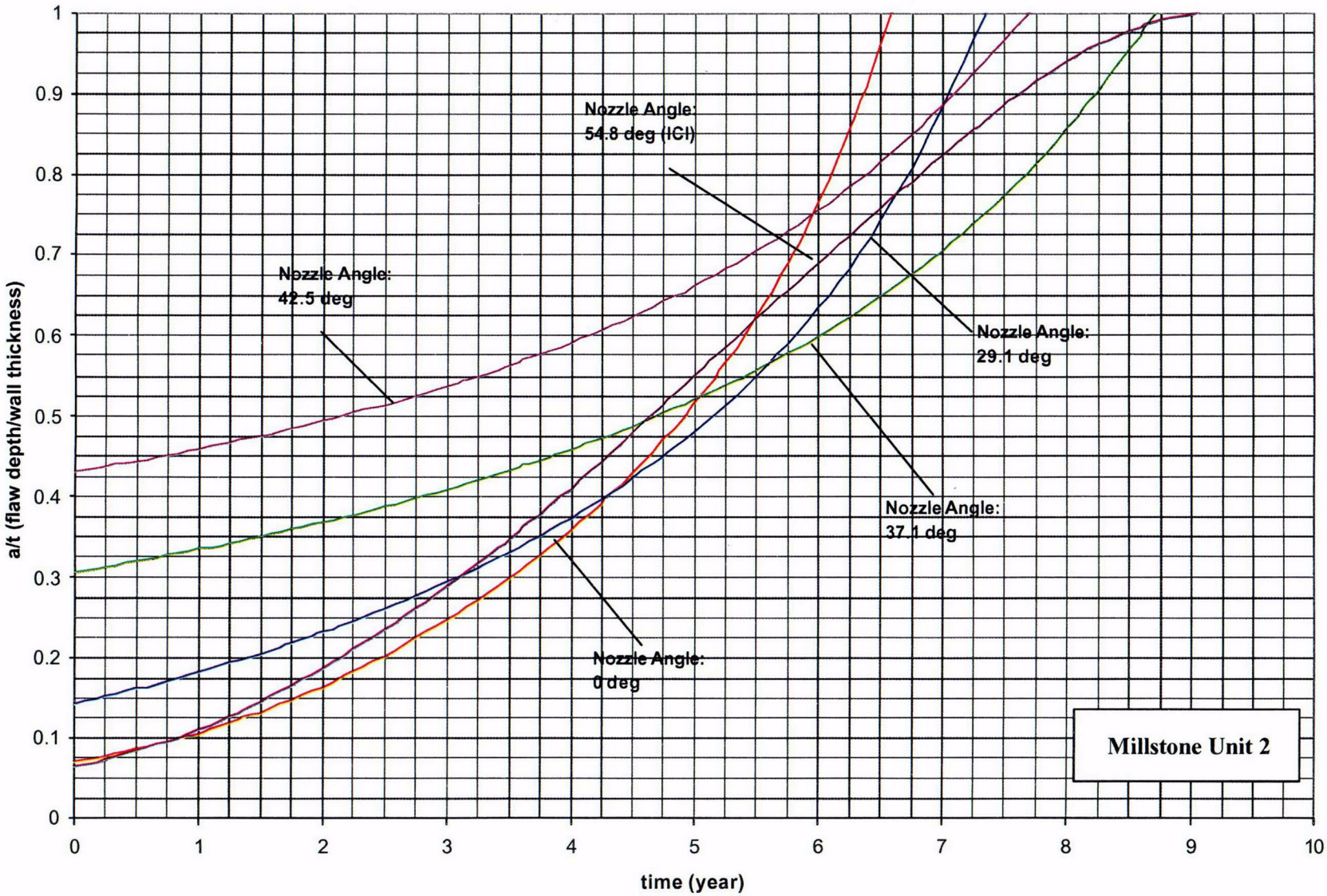

Figure 6-3 Inside, Axial Surface Flaws, .5" Below the Attachment Weld, Nozzle Downhill Side - Crack Growth Predictions

C12

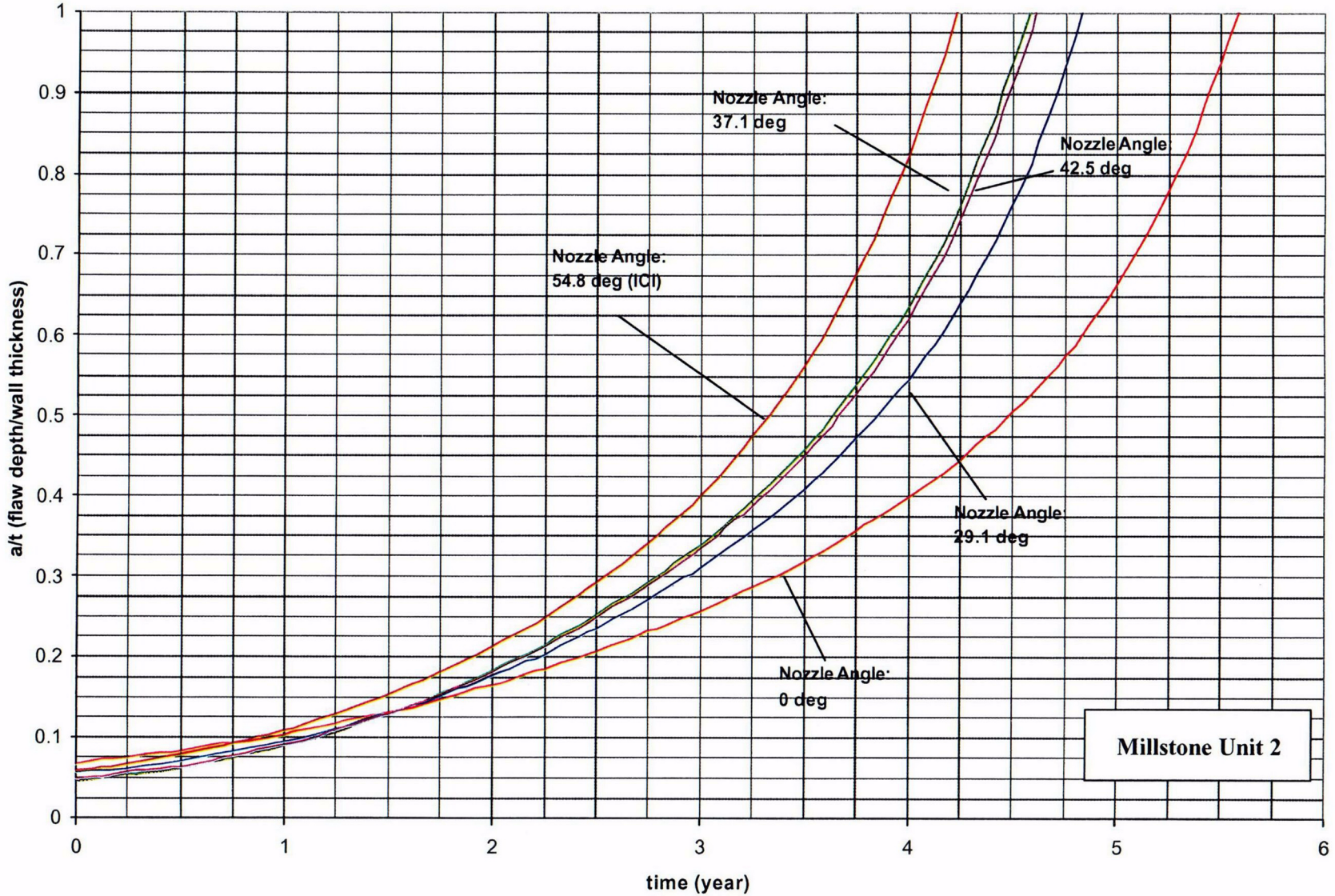

Figure 6-4 Inside, Axial Surface Flaws, at the Attachment Weld, Nozzle Uphill Side - Crack Growth Predictions

C13

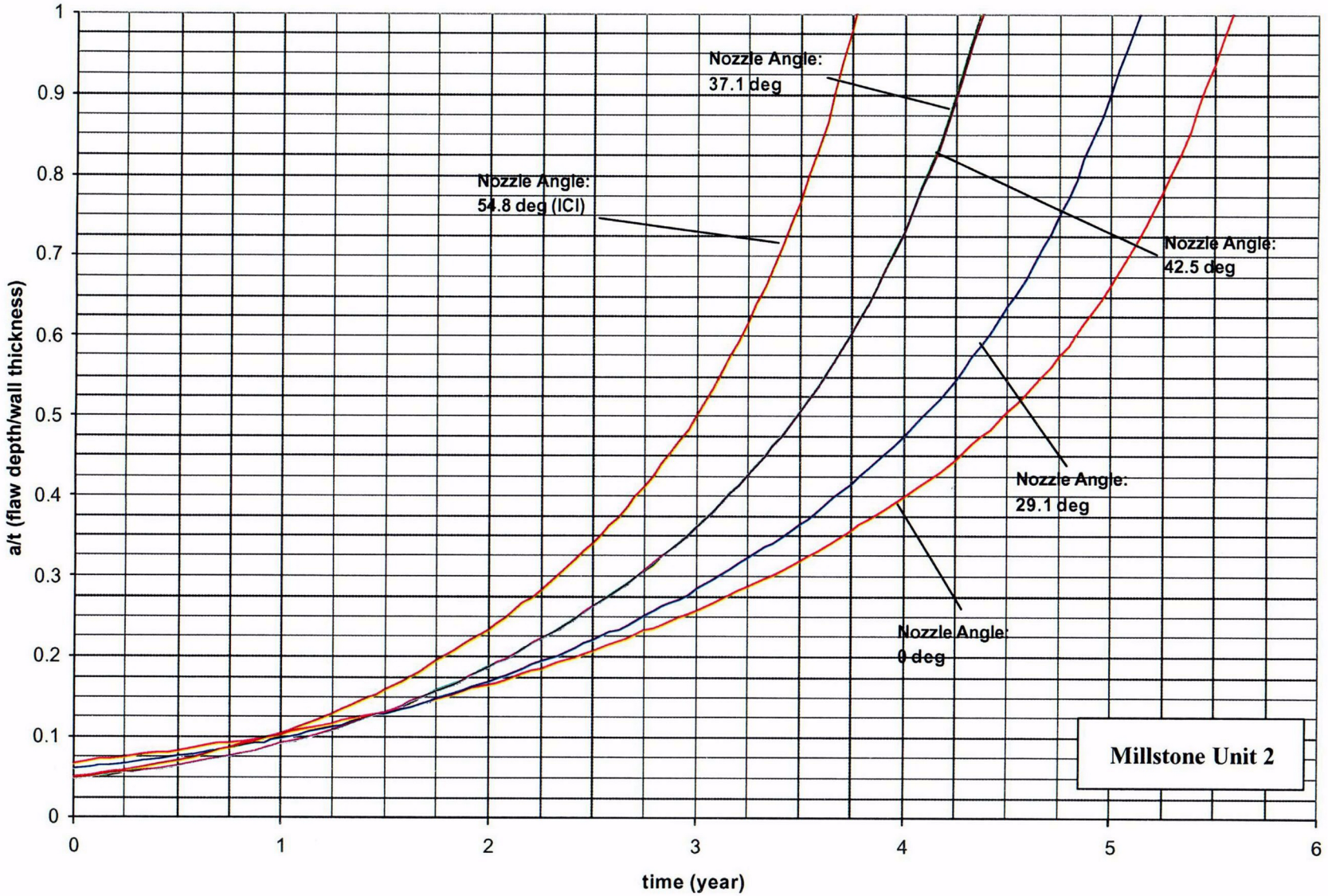

Figure 6-5 Inside, Axial Surface Flaws, at the Attachment Weld, Nozzle Downhill Side - Crack Growth Predictions

C14

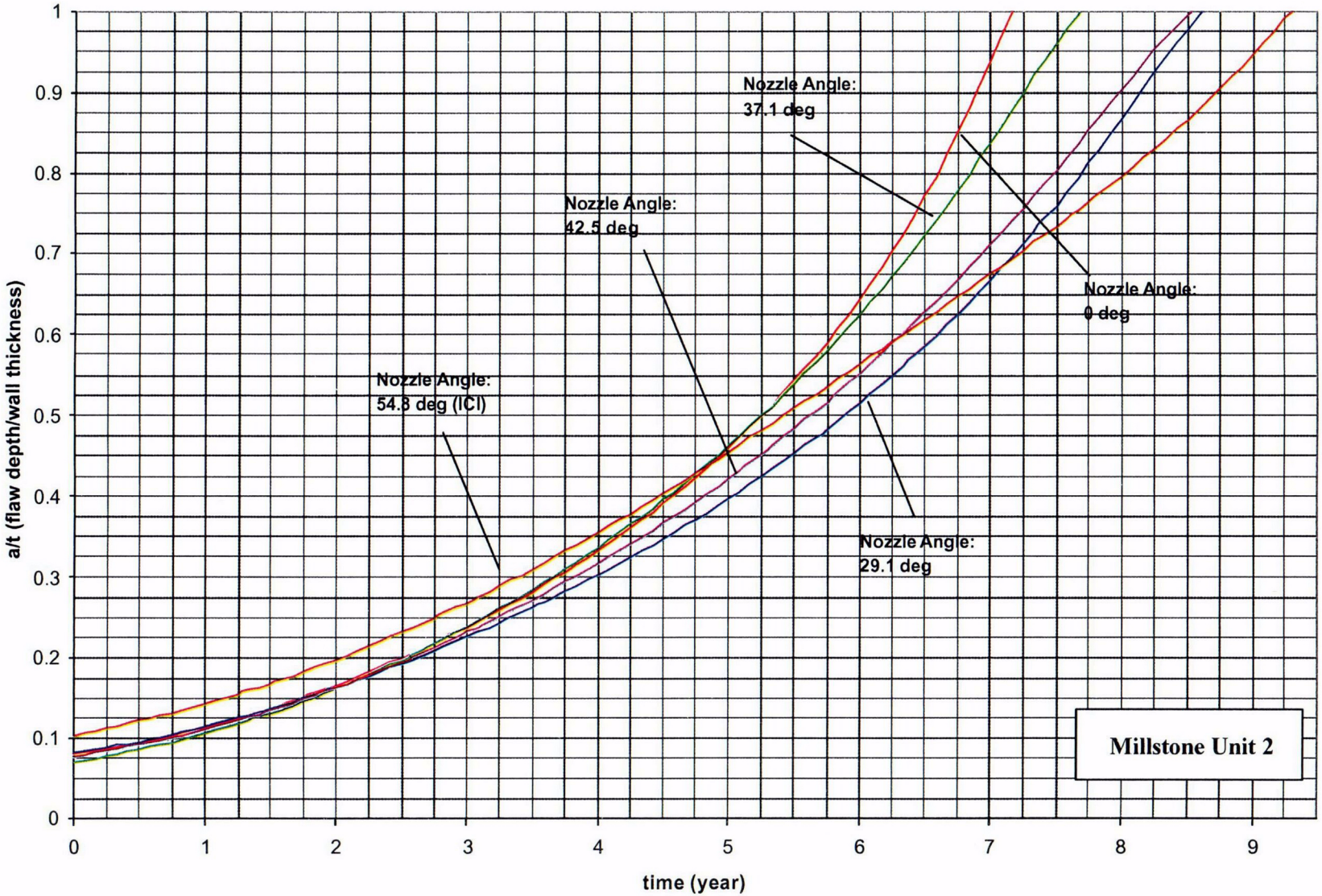

Figure 6-6 Inside, Axial Surface Flaws, .5" Above the Attachment Weld, Nozzle Uphill Side - Crack Growth Predictions

C15

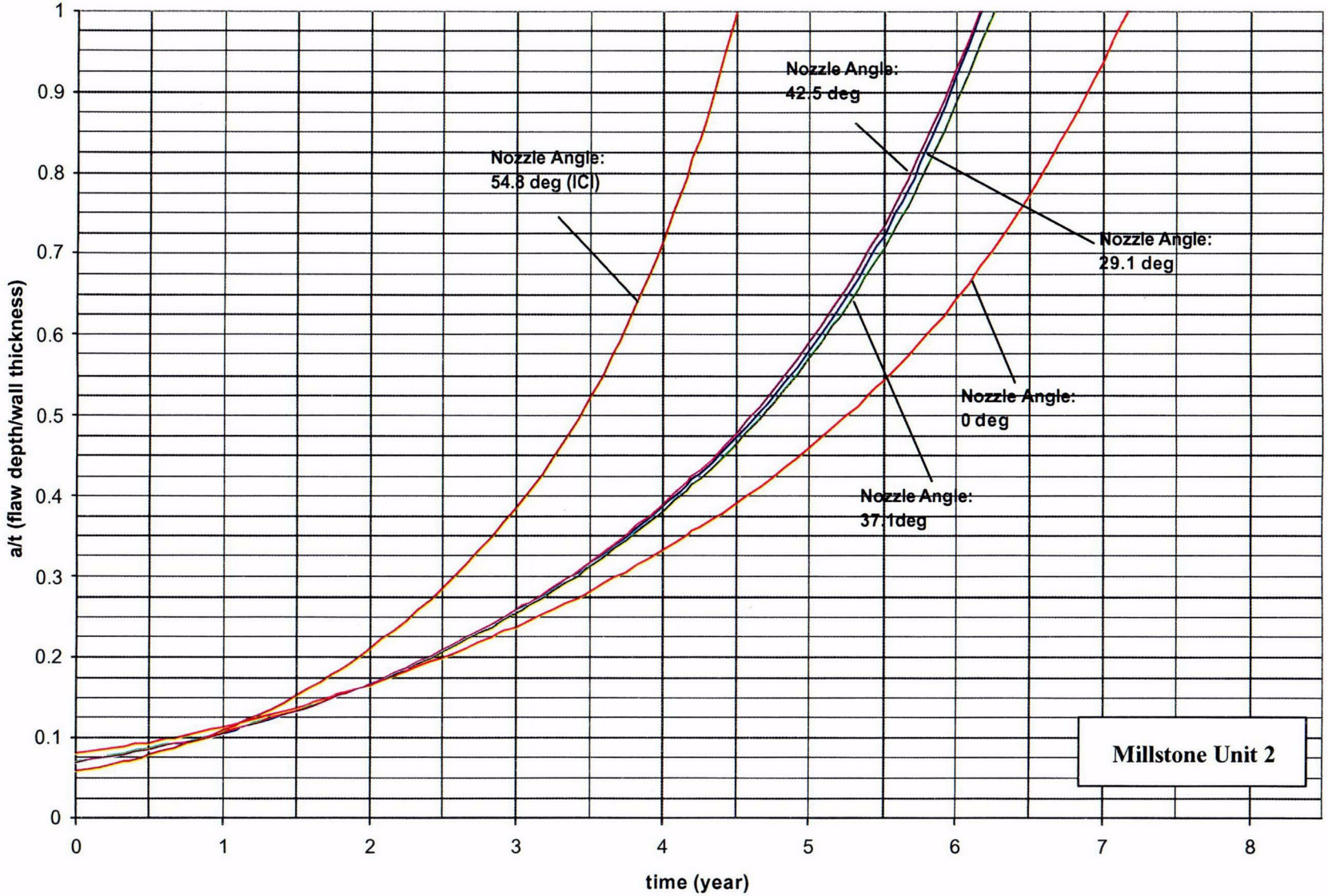

Figure 6-7 Inside, Axial Surface Flaws, .5" Above the Attachment Weld, Nozzle Downhill Side - Crack Growth Predictions

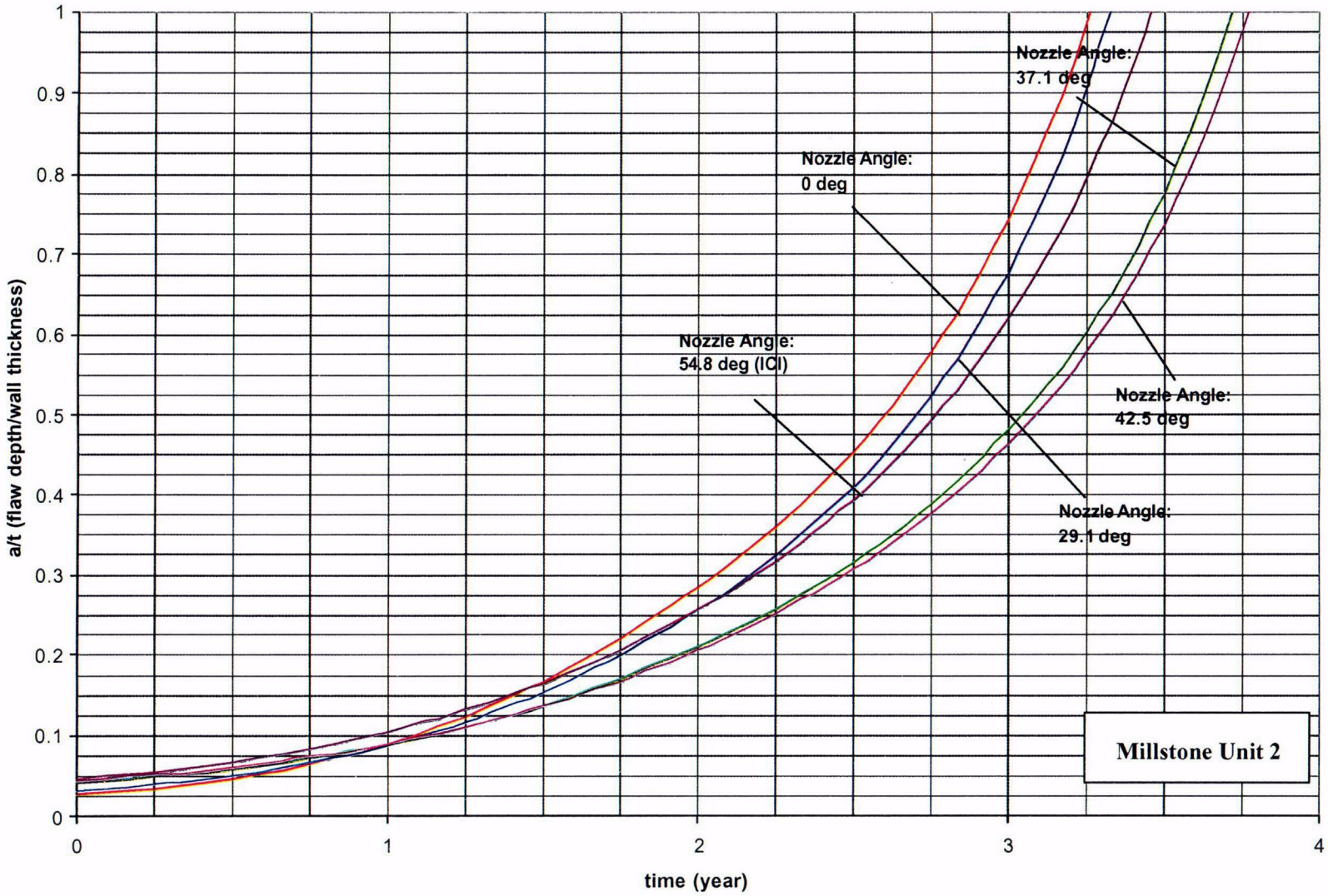

Figure 6-8 Outside, Axial Surface Flaws, Below the Attachment Weld, Nozzle Uphill Side – Crack Growth Predictions

C17

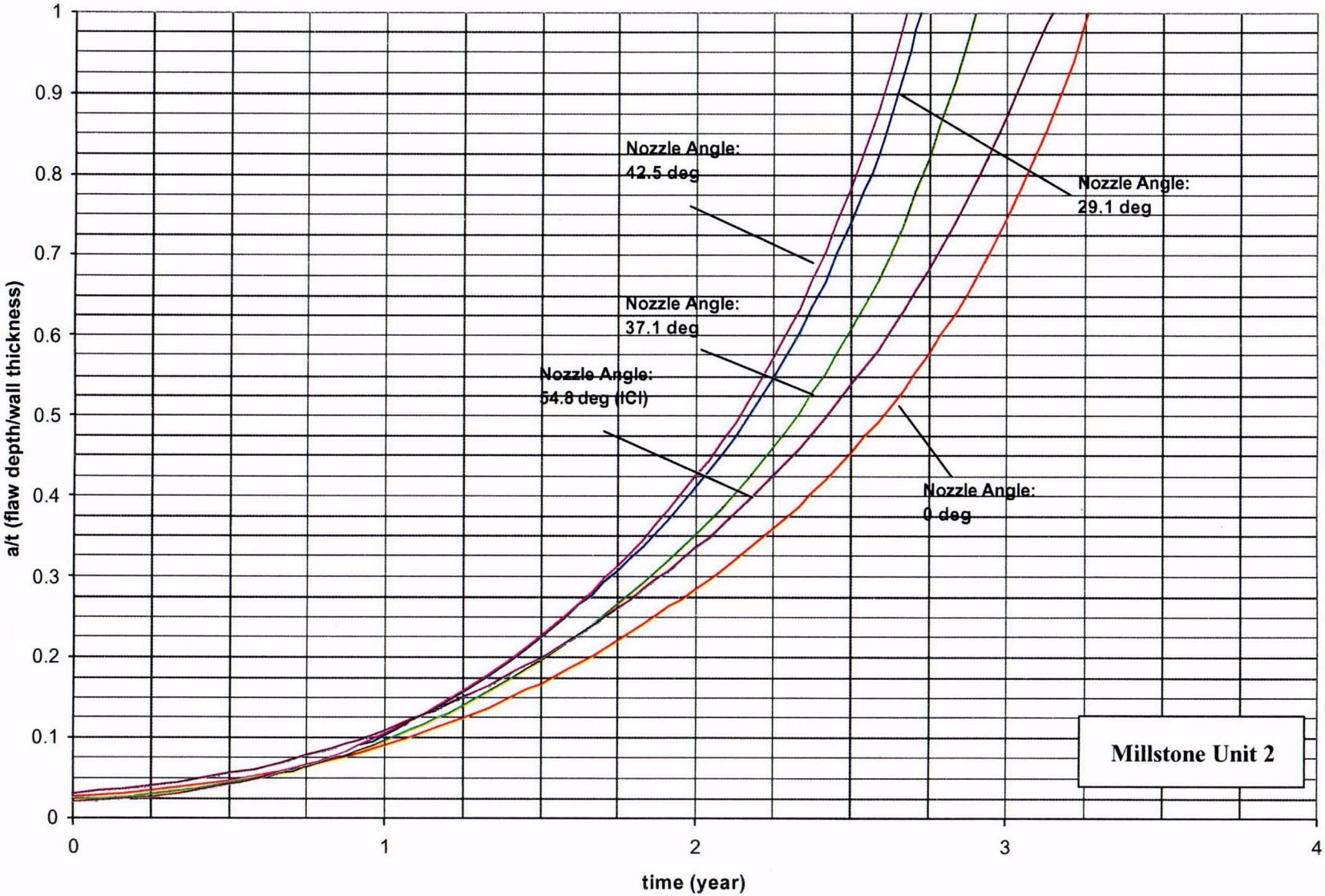

Figure 6-9 Outside, Axial Surface Flaws, Below the Attachment Weld, Nozzle Downhill Side– Crack Growth Predictions

C18

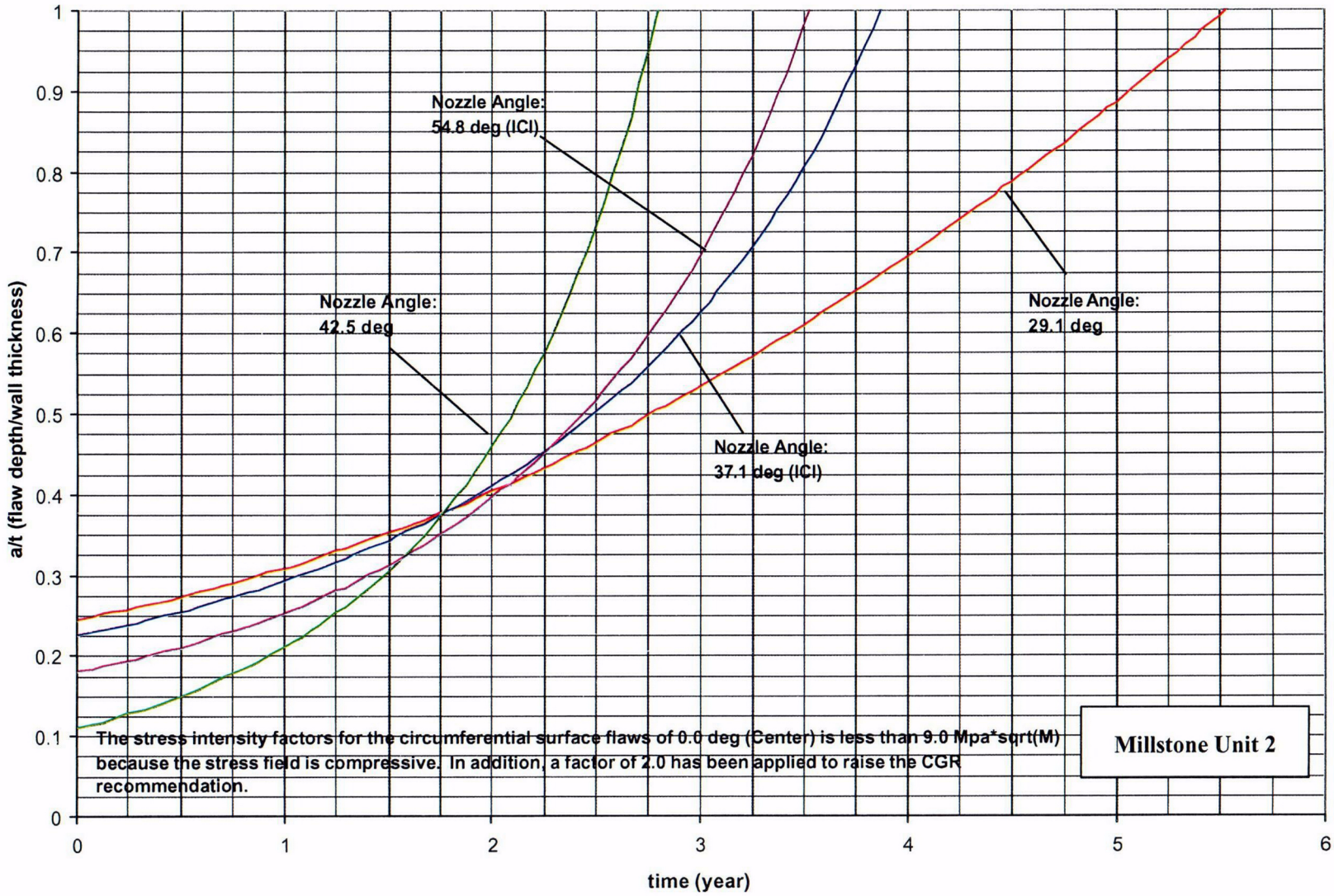

Figure 6-10 Outside, Circumferential Surface Flaws, Along the Top of the Attachment Weld - Crack Growth Predictions (MRP Factor of 2.0 Included)

C19

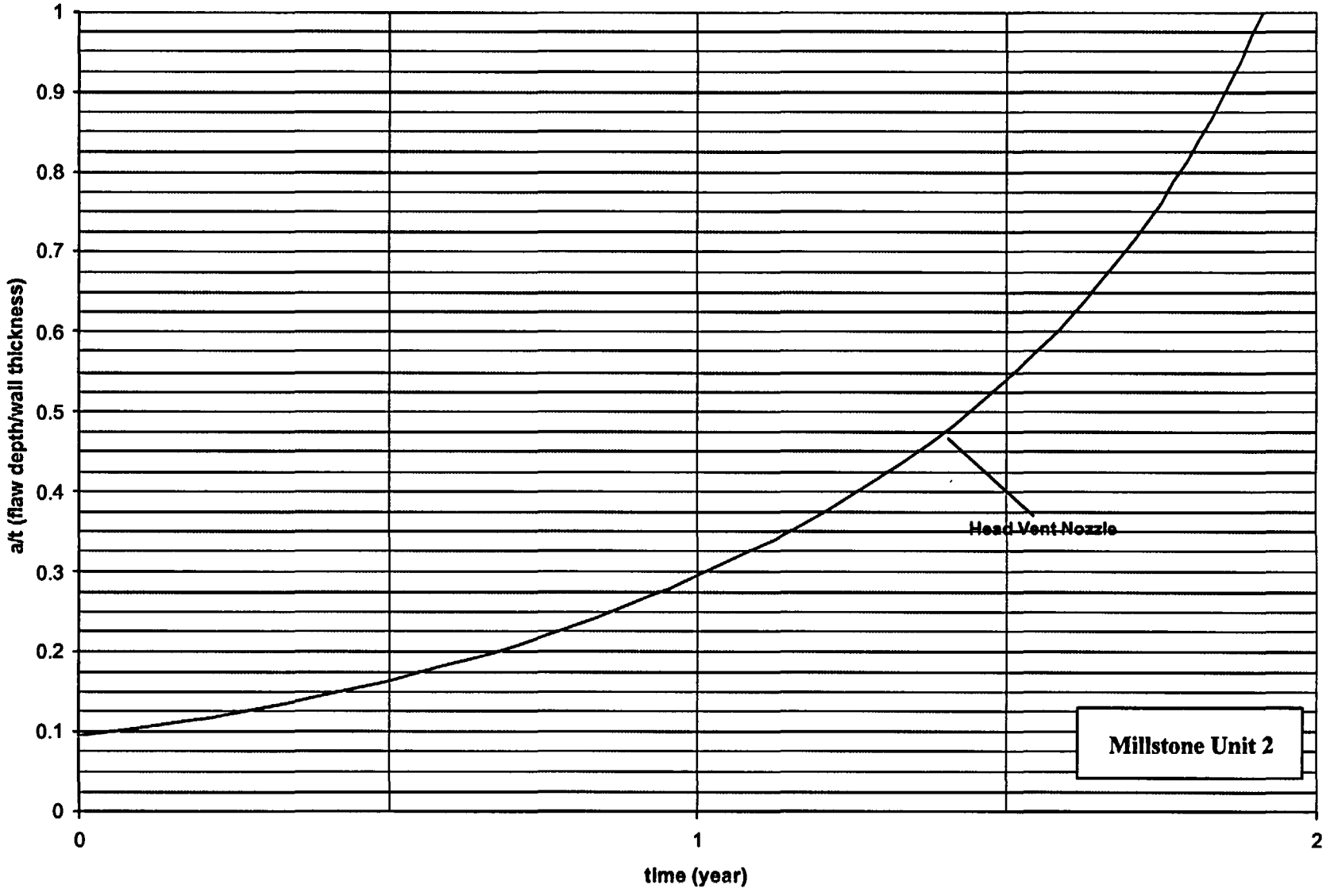

Figure 6-11 Inside, Axial Surface Flaws, At the Attachment Weld, Head Vent, Nozzle Downhill Side - Crack Growth Predictions

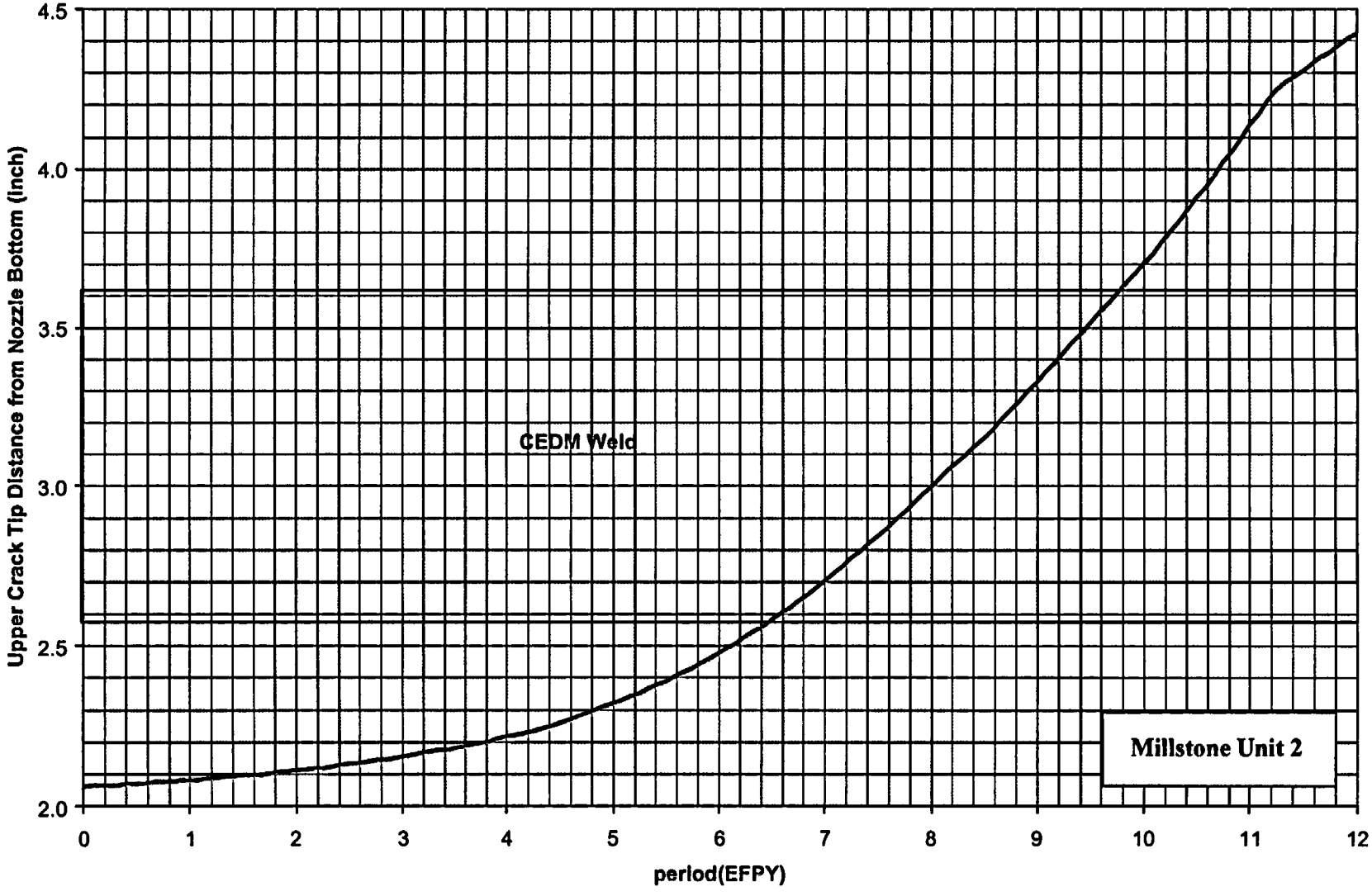

Figure 6-12 Through-Wall Axial Flaws Located in the Center CEDM (0.0 Degrees) Penetration, Uphill and Downhill Side - Crack Growth Predictions

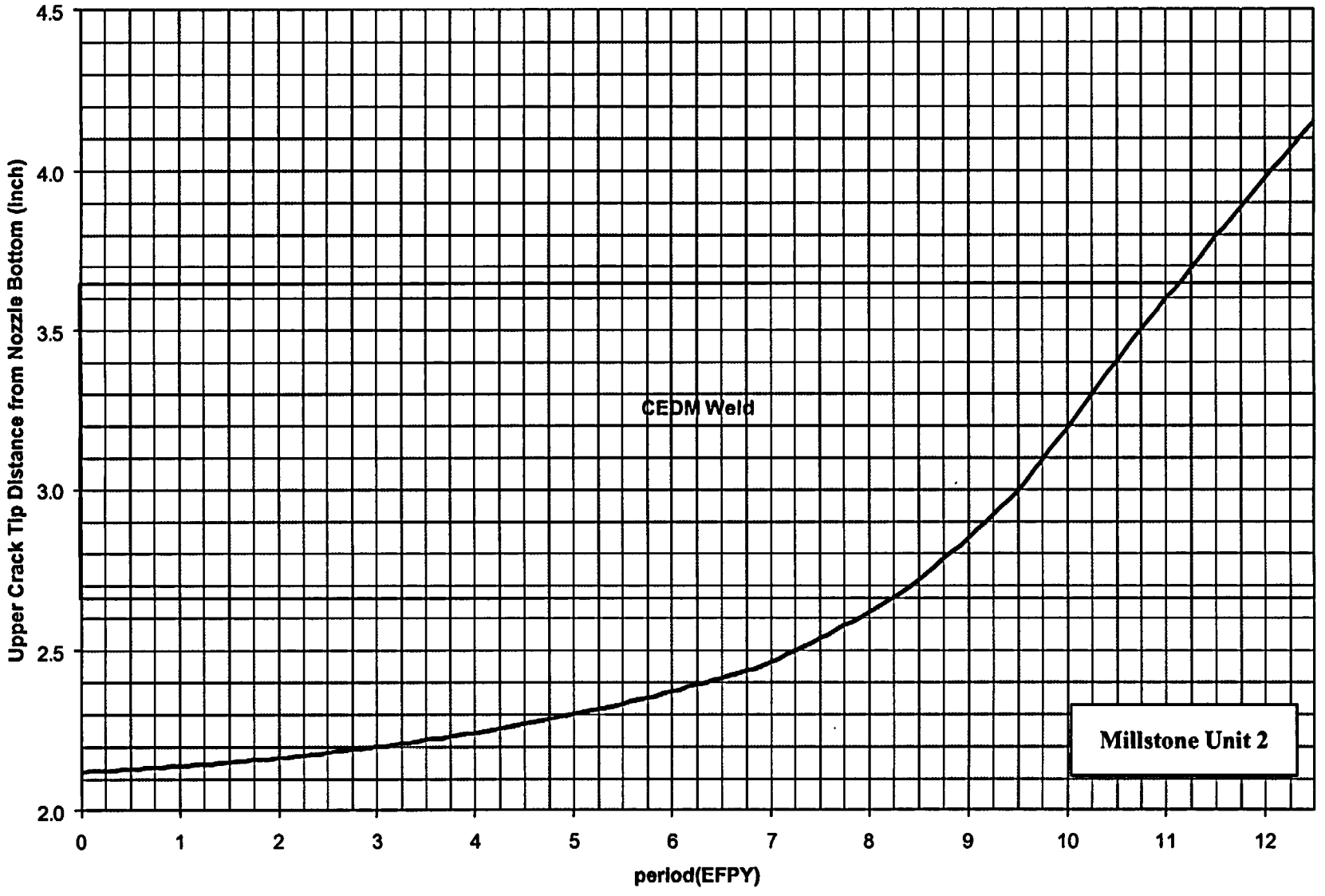

Figure 6-13 Through-Wall Axial Flaws Located in the 29.1 Degree Row of Penetrations, Downhill Side– Crack Growth Predictions

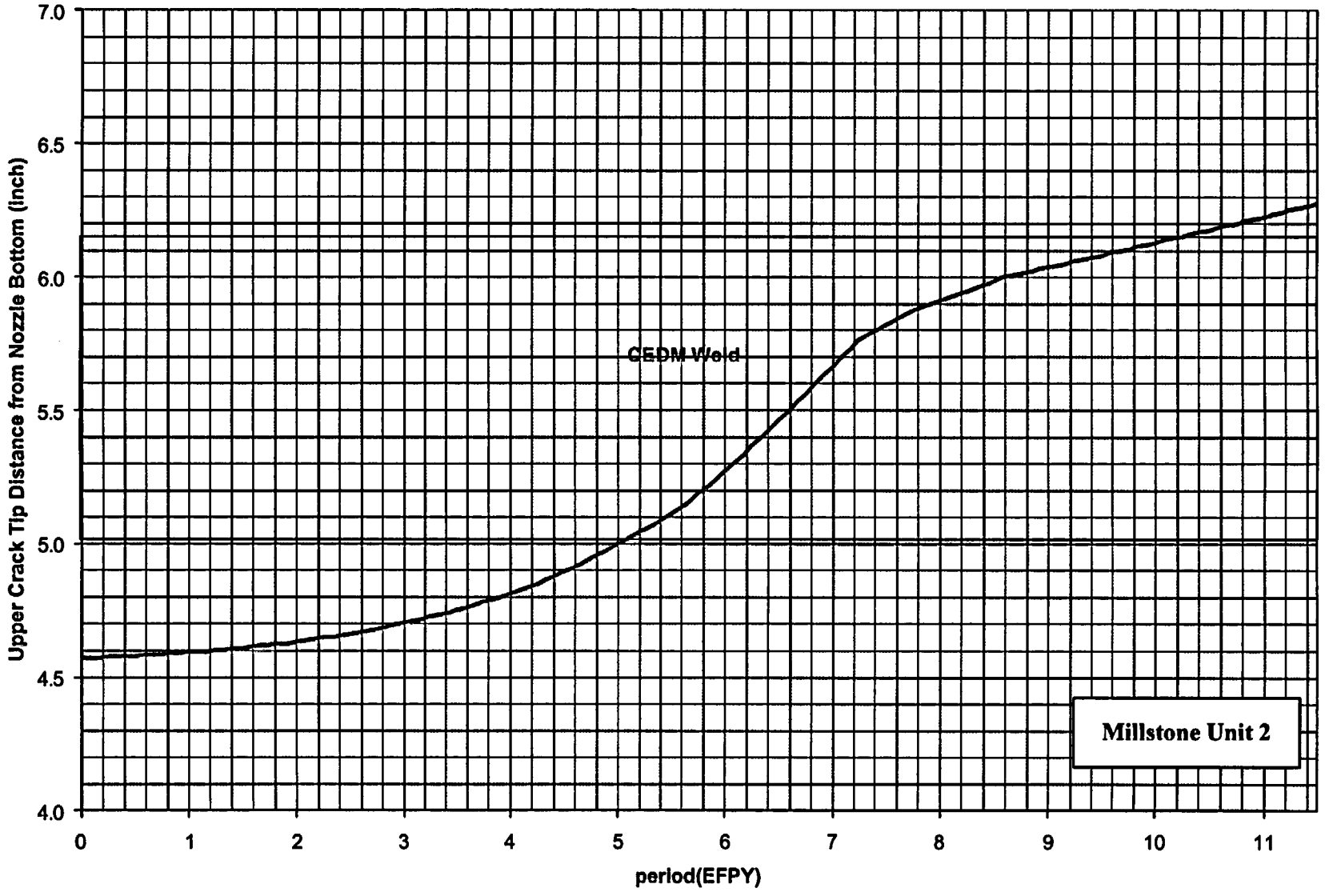

Figure 6-14 Through-Wall Axial Flaws Located in the 29.1 Degree Row of Penetrations, Uphill Side– Crack Growth Predictions

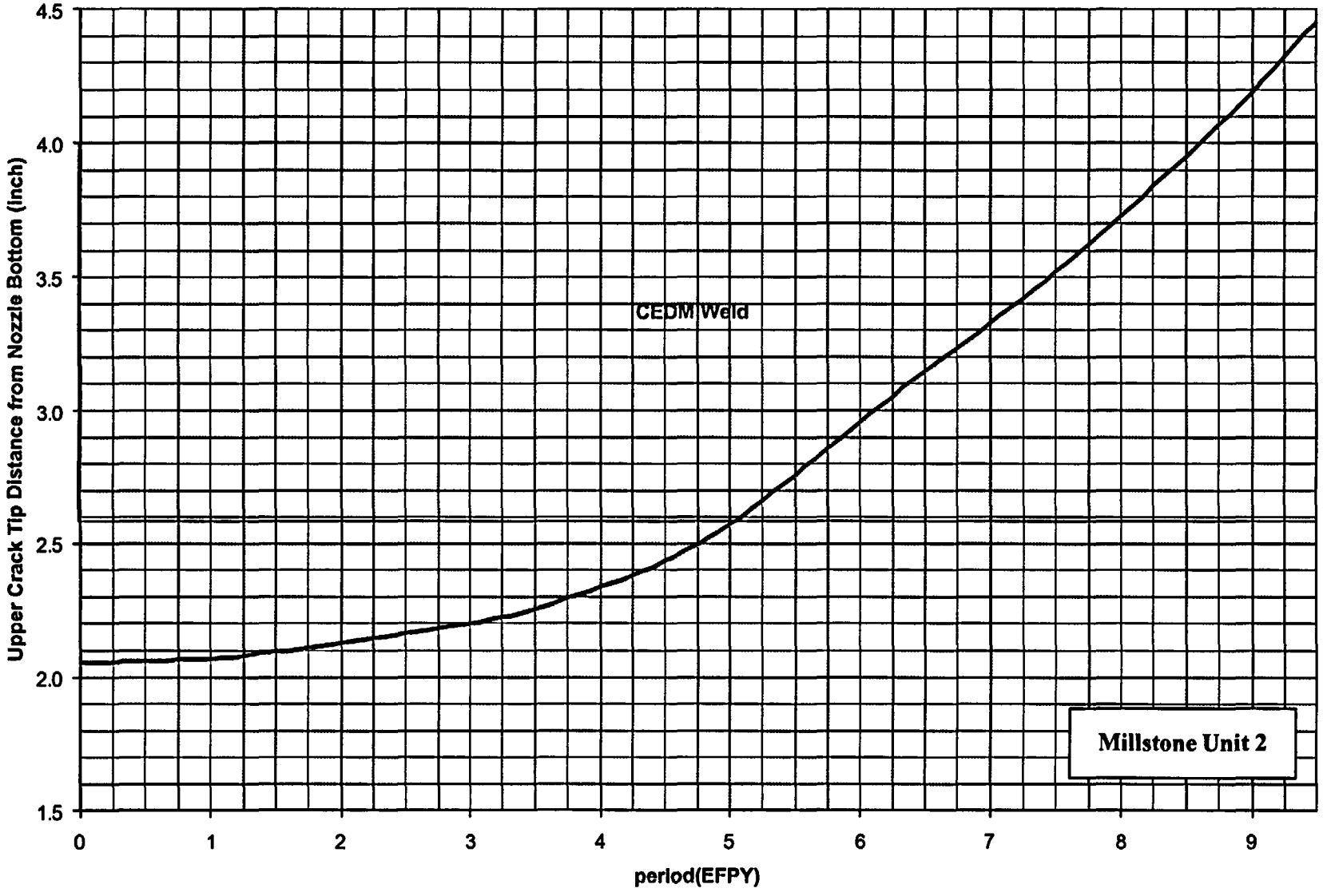

Figure 6-15 Through-Wall Axial Flaws Located in the 37.1 Degree Row of Penetrations, Downhill Side– Crack Growth Predictions

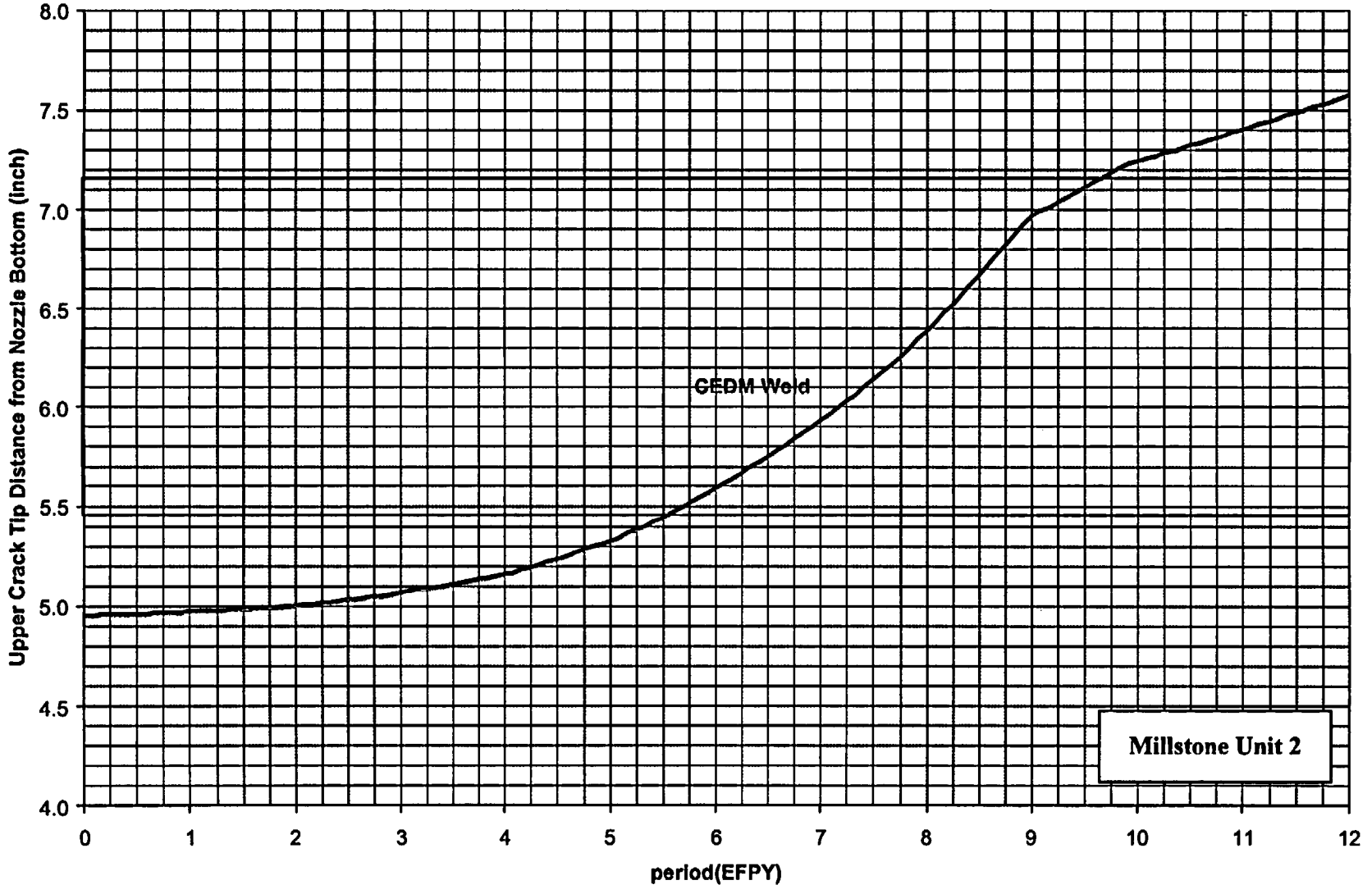

Figure 6-16 Through-Wall Axial Flaws Located in the 37.1 Degree Row of Penetrations, Uphill Side– Crack Growth Predictions

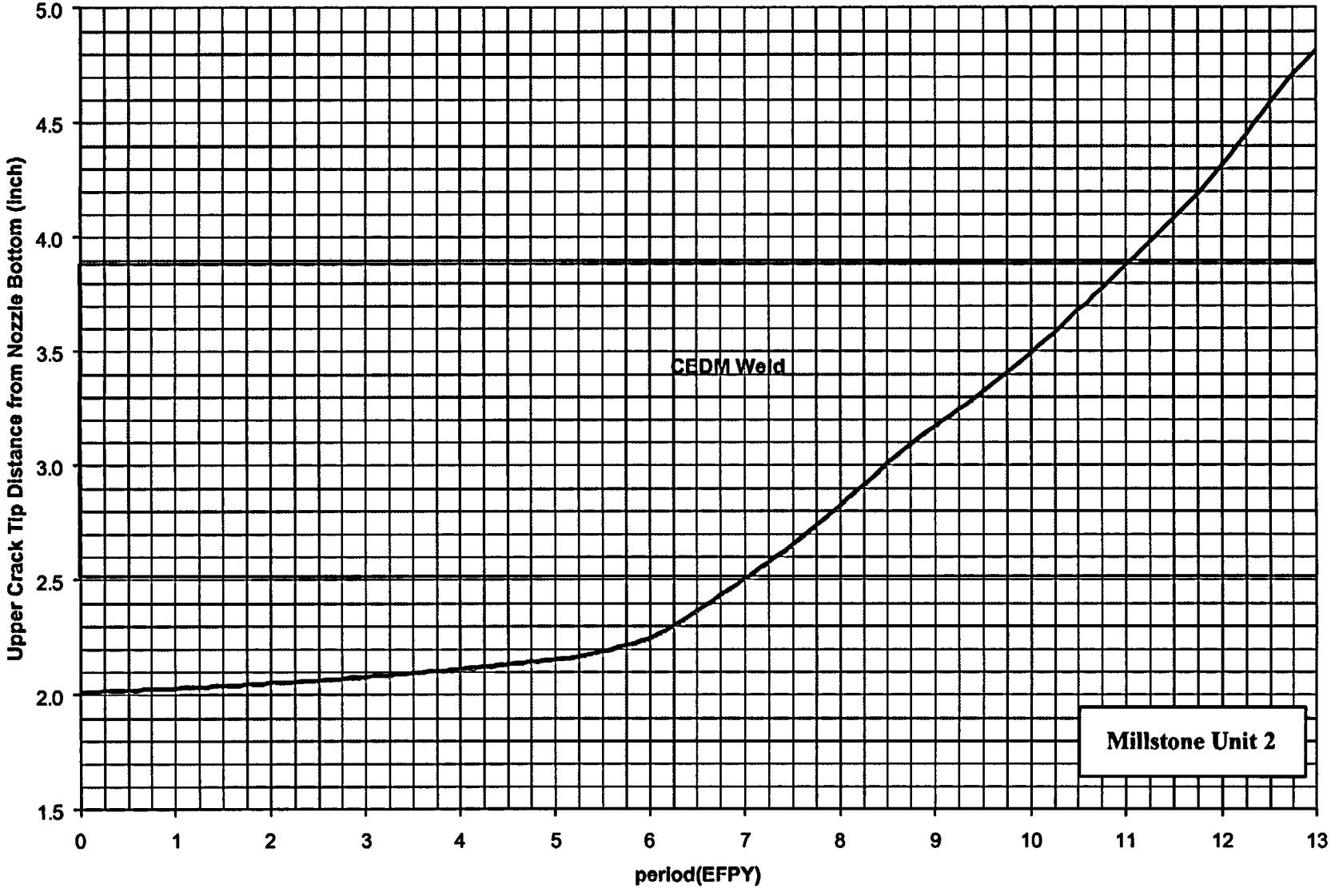

Figure 6-17 Through-Wall Axial Flaws Located in the 42.5 Degree Row of Penetrations, Downhill Side– Crack Growth Predictions

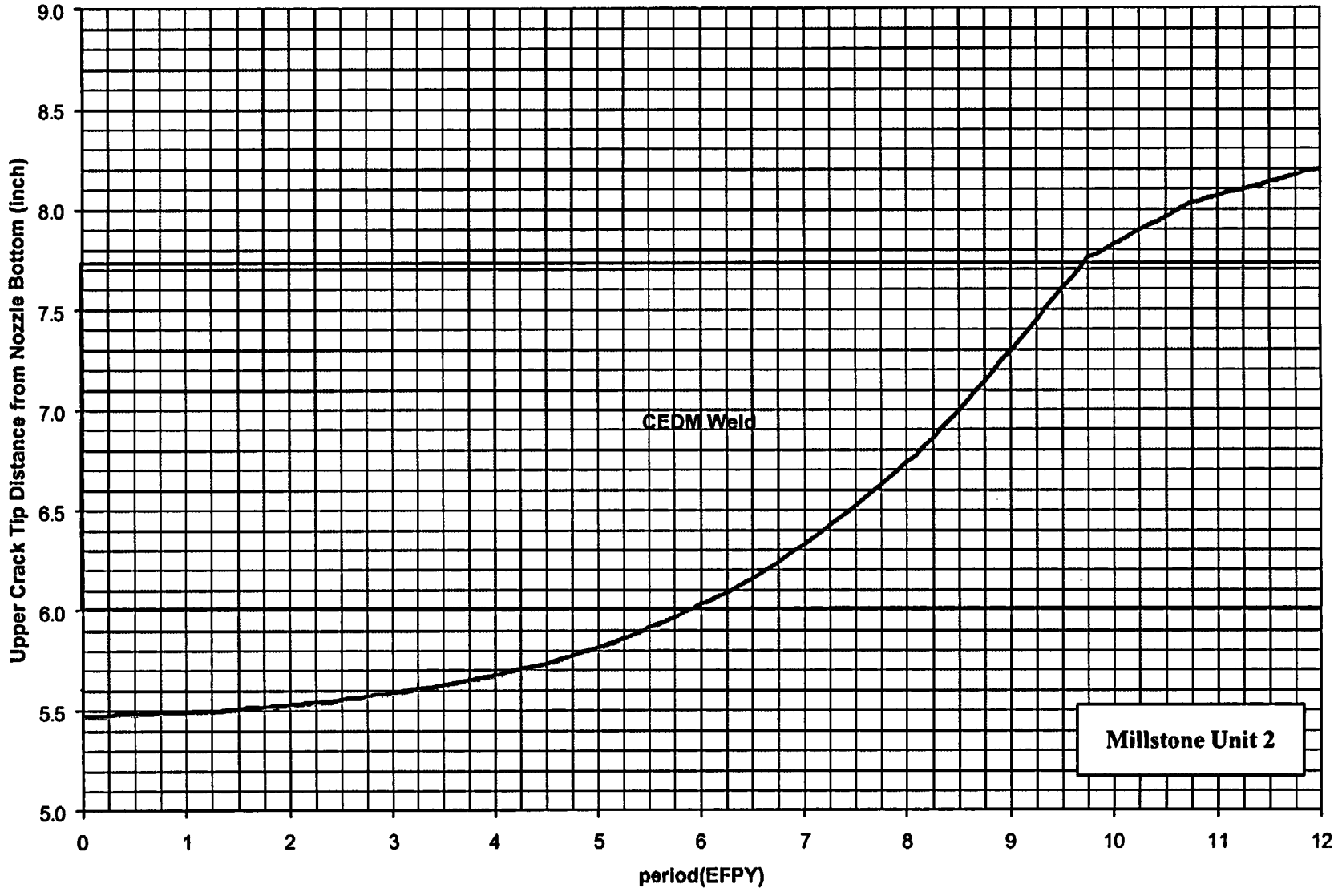

Figure 6-18 Through-Wall Axial Flaws Locatedin the 42.5 Degree Row of Penetrations, Uphill Side– Crack Growth Predictions

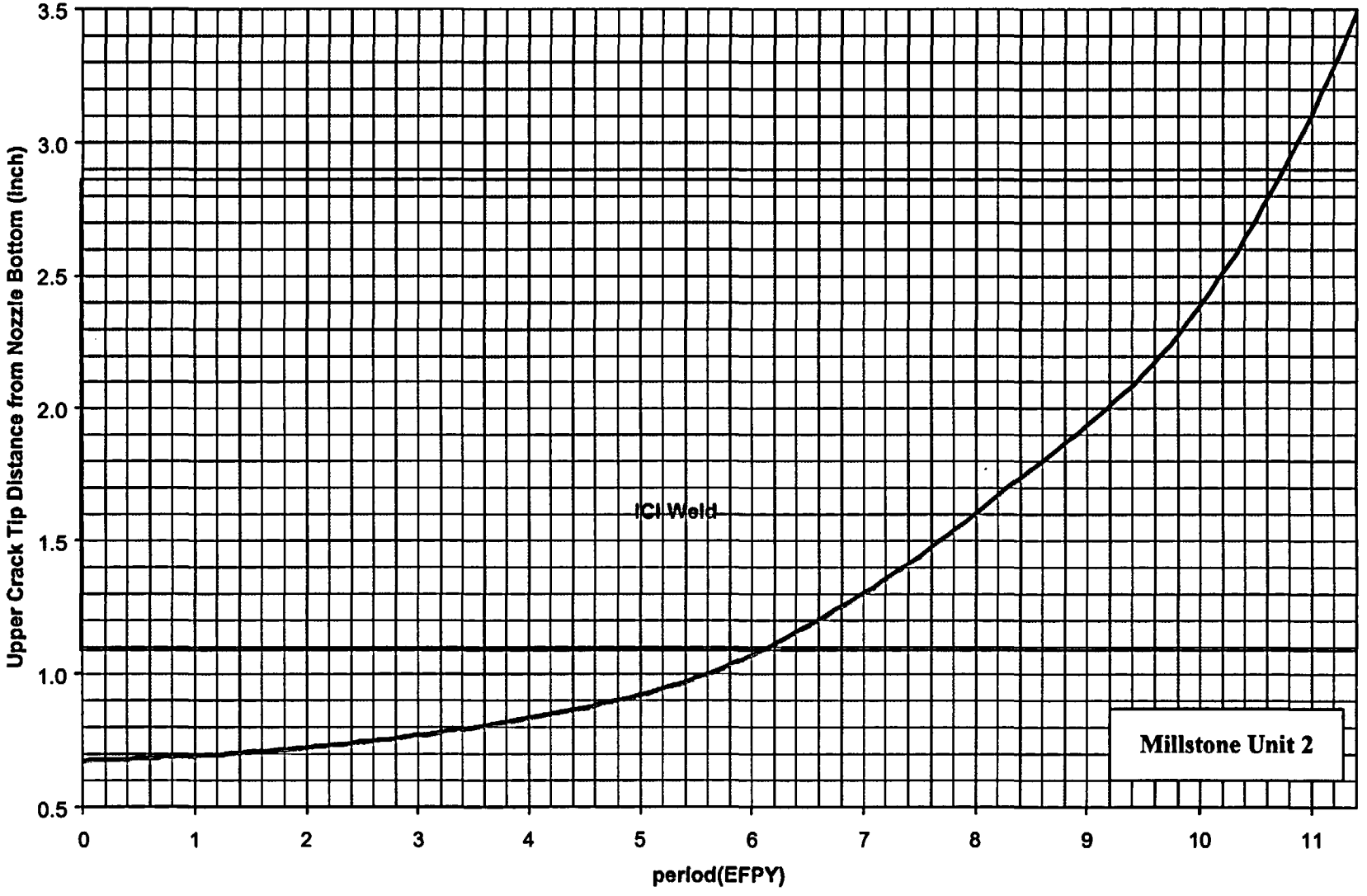

Figure 6-19 Through-Wall Axial Flaws Located in the 54.8 Degree Row of Penetrations, Downhill Side– Crack Growth Predictions

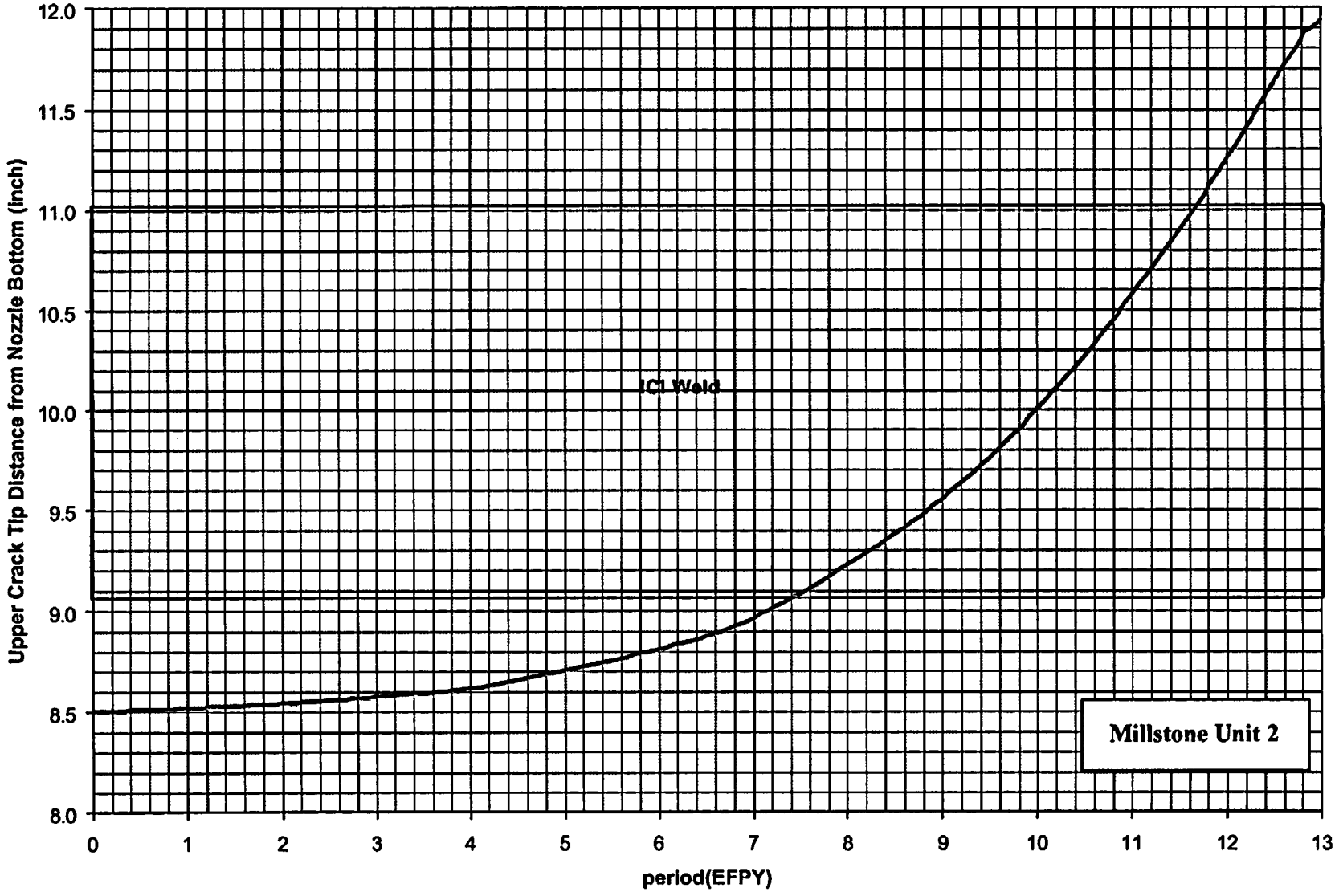

Figure 6-20 Through-Wall Axial Flaws Located in the 54.8 Degree Row of Penetrations, Uphill Side– Crack Growth Predictions

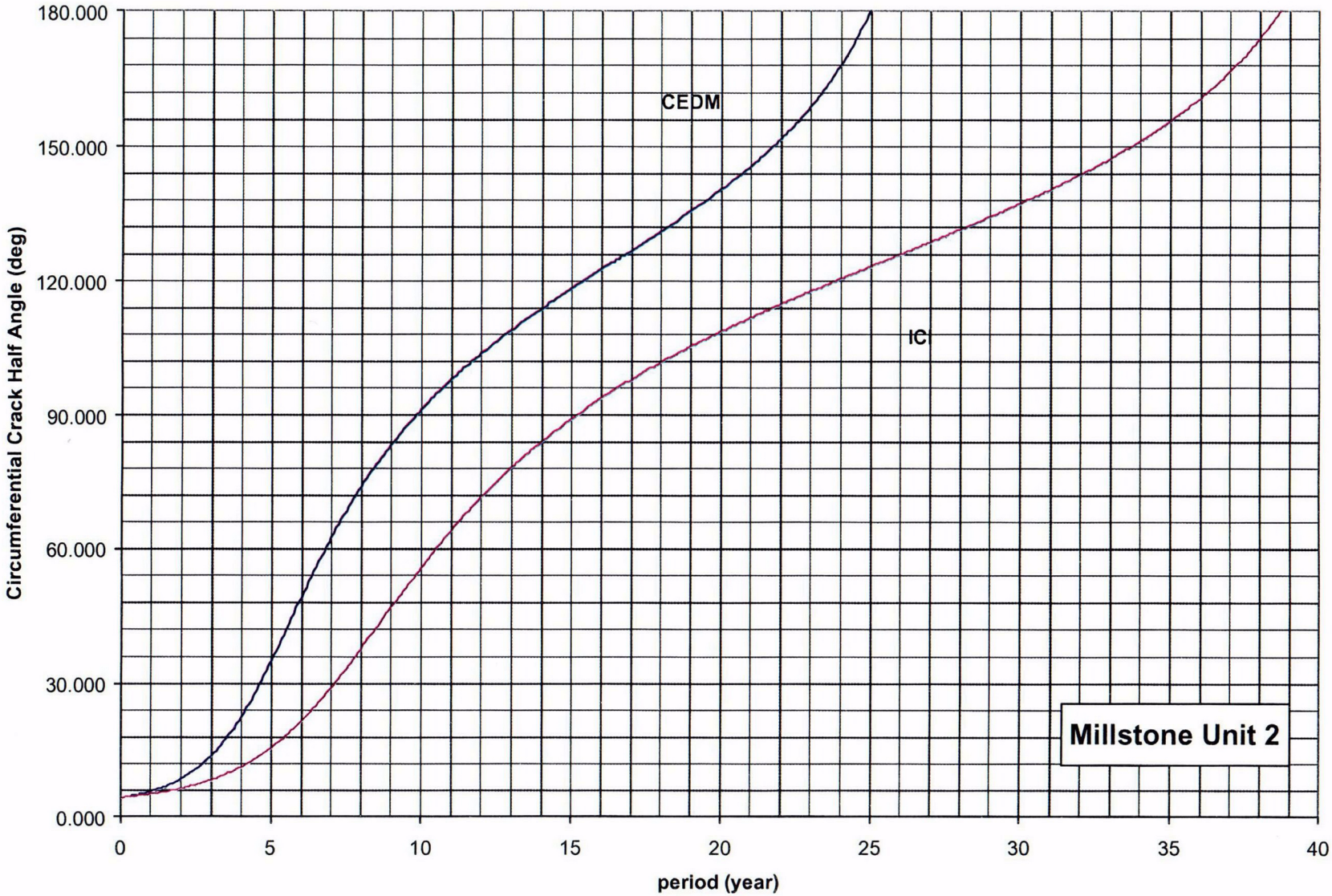

Figure 6-21 Through-Wall Circumferential Flaws Near the Top of the Attachment Weld for CEDM and ICI Nozzles – Crack Growth Predictions (MRP Factor of 2.0 Included)

C20

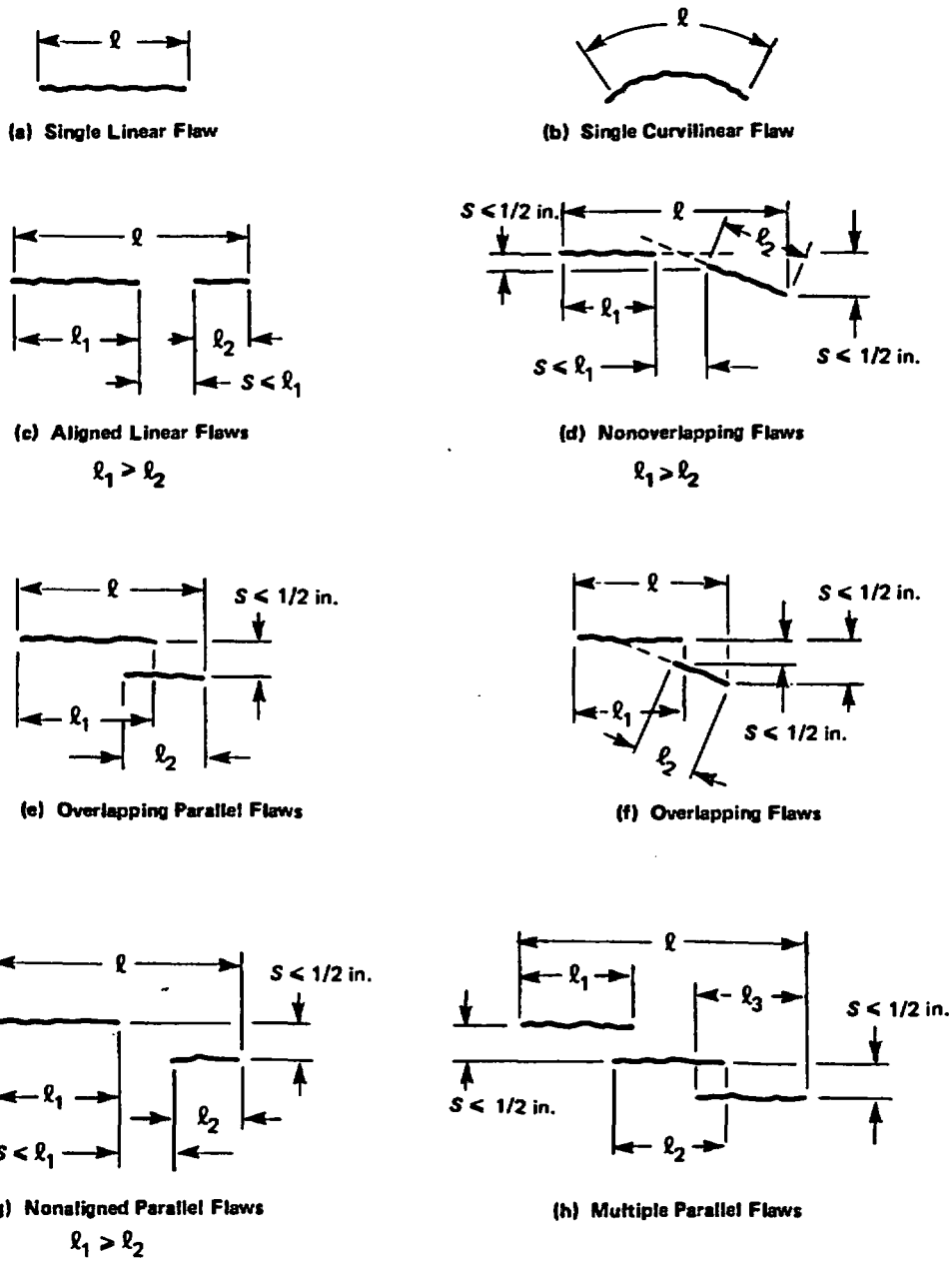

Figure 6-22 Section XI Flaw Proximity Rules for Surface Flaws (Figure IWA-3400-1)

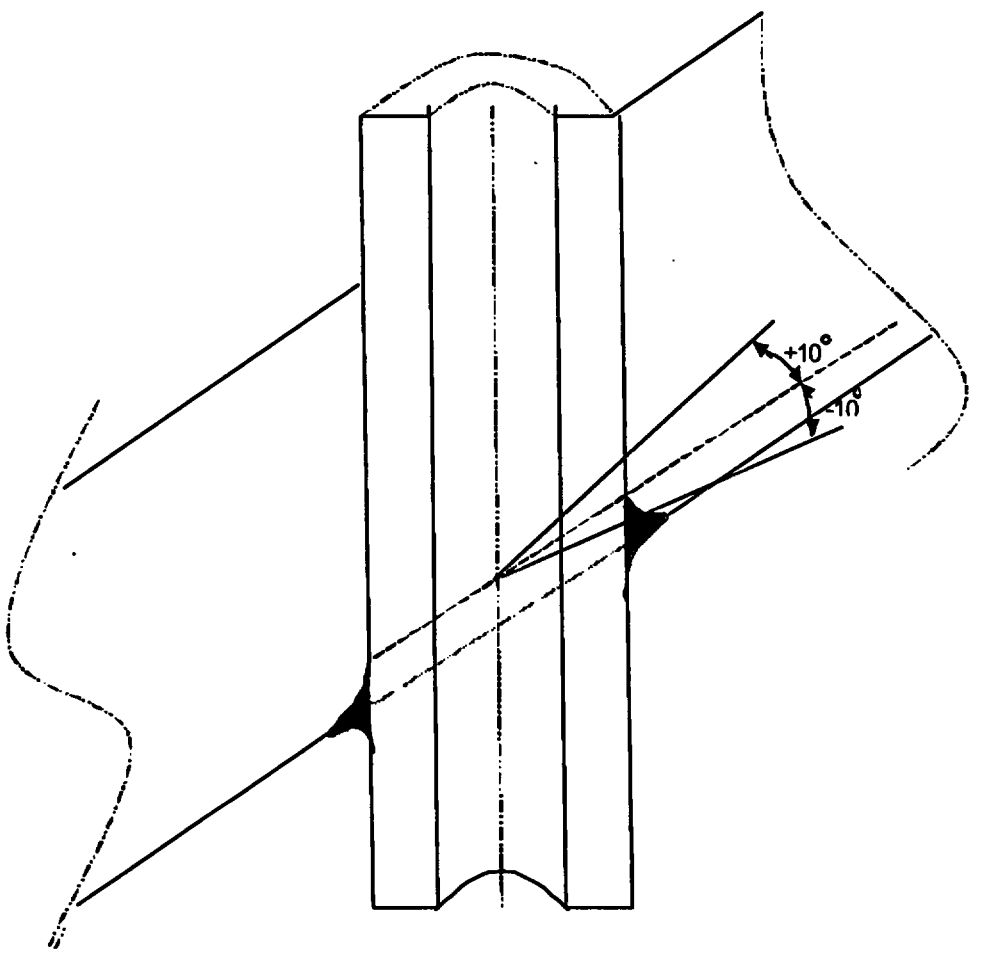

Figure 6-23 Definition of "Circumferential"

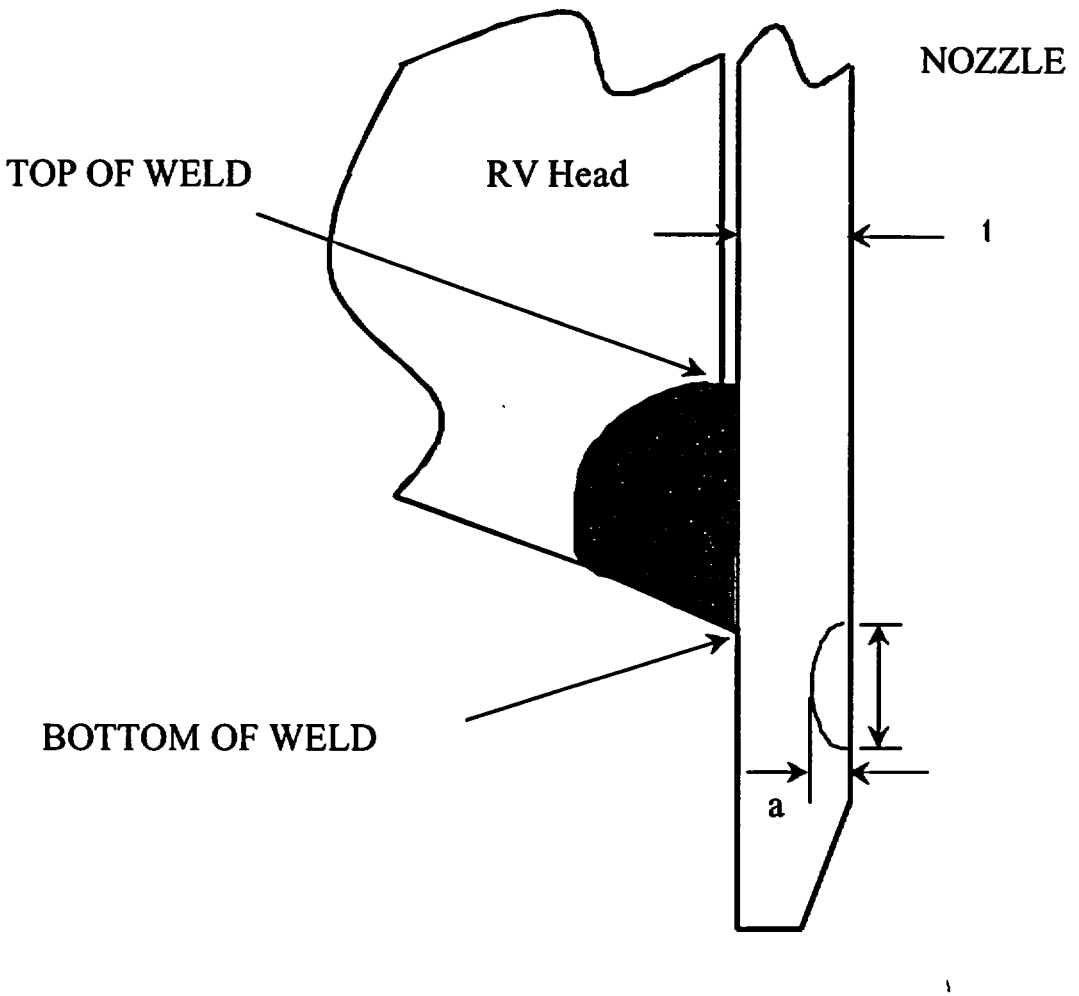

Figure 6-24 Schematic of Head Penetration Geometry

7 SUMMARY AND EXAMPLE PROBLEMS

An extensive evaluation has been carried out to characterize the loadings and stresses which exist in the head penetrations at Millstone Unit 2. Three-dimensional finite element models were constructed, and all pertinent loadings on the penetrations were analyzed [6A, 6B, 6C]. These loadings included internal pressure and thermal expansion effects typical of steady state operation. In addition, residual stresses due to the welding of the penetrations to the vessel head were considered.

Results of the analyses reported here are consistent with the axial orientation and location of flaws which have been found in service in a number of plants, in that the largest stress component is the hoop stress, and the maximum stresses were found to exist in the locations nearest and farthest away from the center of the vessel. The most important loading conditions were found to be those which exist on the penetration for the majority of the time, which are the steady state loading and the residual stresses.

These stresses are important because the cracking which has been observed to date in operating plants has been determined to result from primary water stress corrosion cracking (PWSCC). These stresses were used in fracture calculations to predict the future growth of flaws postulated to exist in the head penetrations. A crack growth law was developed specifically for the operating temperature of the head at Millstone Unit 2, based on the EPRI recommendation, which is consistent with laboratory data as well as crack growth results for operating plants.

The crack growth predictions contained in Section 6 show that the future growth of cracks which might be found in the penetrations will be very slow, and that a number of effective full power years will be required for any significant extensions. An exception is the vent line, where the time is less because of the smaller thickness.

7.1 SAFETY ASSESSMENT

It is appropriate to examine the safety consequences of an indication which might be found. The indication, even if it were to propagate through the penetration wall, would have only minor consequences, since the pressure boundary would not be broken, unless it were to propagate above the weld.

Further propagation of the indication would not change its orientation, since the hoop stresses in the penetration are much larger than the axial stresses. Therefore, it is extremely unlikely that the head penetration would be severed.

If the indication were to propagate to a position above the weld, a leak could result, but the magnitude of such a leak would be very small, because the crack could not open significantly due to the tight fit between the penetration and the vessel head. Such a leak would have no immediate impact on the structural integrity of the system, but could lead to minor wastage in the ferritic steel of the vessel head, as the borated primary water concentrates due to evaporation. Davis Besse has demonstrated the consequence of ignoring such leaks.

Any indication is unlikely to propagate very far up the penetration nozzle above the weld since the hoop stresses decrease in this direction, causing the indication to slow down and stop before it reaches the outside surface of the head.

The high likelihood that the indication will not propagate up the penetration nozzle beyond the vessel head ensures that no catastrophic failure of the head penetration will occur. The indication will be enveloped in the vessel head itself, which precludes the opening of the crack and limits leakage.

7.2 EXAMPLE PROBLEMS

The crack growth prediction curves in Figures 6-2 through 6-21 can be used with the acceptance criteria of Section 6.5 to determine the available service time. In this section, a few examples will be presented to illustrate the use of these figures. The example cases are listed in Table 7-1.

Example 1. – Determine the service life of an axially oriented inside surface flaw whose upper extremity is located 1.3" below the weld on the uphill side of penetration no. 30, the penetration locality angle must first obtained from Table 1-1. In this case, the locality angle is 29.1 degrees and the initial flaw depth is 0.0425" ($a_{initial}$) and the initial flaw length is 0.085" ($2c_{initial}$). Assuming that the initial aspect ratio of 2:1 is maintained throughout the time that the inside surface flaw becomes a through-wall flaw, the final length of the flaw ($2c_{final}$) will be 1.132". The upper extremity of the flaw is now located 0.7765" below the weld and validates the use of a single crack growth curve. The crack growth curve for the 29.1 degrees nozzle angle of Figure 6-2 is applicable and Figure 6-2 has been reproduced as Figure 7-1. The flaw is initially 7.5 percent of the wall thickness, and a straight line is drawn horizontally at a/t = 0.075 that intersects the crack growth curve. Using the acceptance criteria in Table 6-1, the service life can then be determined as the remaining time for this flaw to grow to the limit of 100 percent of the wall thickness or approximately 4.4 years (labeled as Service Life in Figure 7-1).

Example 2. In this case, the flaw is identical in size to that used in Example 1, but located on the outside surface and on the downhill side of penetration no. 50. This flaw, just as the flaw in Example 1, will not cross into the weld region. The applicable curve to use is Figure 6-9. The ratio a/t and initial reference time are likewise found using the same approach as used in Example 1. Using the acceptance criteria in Table 6-1, the determination of service life is illustrated in Figure 7-2, where we can see that the result is approximately 2.1 years.

Example 3. An axial inside surface flaw is located at the weld and on the uphill side of penetration no. 70. The initial length of the flaw is 0.250" and the initial depth is 0.05". From Table 1-1, the angle of this penetration nozzle is 54.8 degrees. The applicable curve is Figure 6-4 and is reproduced here as Figure 7-3. In this case, the initial flaw depth is 10.7 percent of the wall thickness. The initial reference time can be found by drawing a horizontal line at a/t = 0.107. Using the acceptance criteria in Table 6-1, the allowable service life can then be determined as the time for the flaw to reach a depth of 75 percent of the wall thickness. The final reference time is found through a horizontal line drawn at a/t = 0.75. The service life can be determined through the intersection points of these lines and the crack growth curve. The resulting service life is approximately 2.85 years, as shown in Figure 7-3.

Example 4. In this case, we have postulated an axial inside surface flaw that will require the use of two flaw charts for its evaluation because the upper extremity of this flaw will reach within 0.5 inch below the attachment weld as it propagates into the nozzle wall. The flaw has an initial depth of 0.079 inch (2mm) and is located on the downhill side of penetration no. 1, which is the center nozzle at 0.0°. The length of the initial flaw is 0.395 inches and its upper extremity is located 1.0 inch below the attachment weld. Assuming that the initial aspect ratio of 5:1 is maintained as the flaw propagates into the nozzle wall, the final length of a through-wall flaw would be 2.83 inches long. The location of the upper extremity of this flaw would have reached within 0.5 inch below the weld as it propagates into the nozzle wall.

For this postulated flaw, the first step is to estimate the time required for the initial flaw to grow to within 0.5 inch of the weld. This can be accomplished with the use of Figure 6-2 or 6-3 (Figure 6-3 is used) because CGR is the same for both uphill and downhill side of the center penetration and is reproduced here as Figure 7-4A. The crack tip is 1 inch below the weld and is assumed to grow until the tip is 0.5 inches below. The final half-length of the flaw when it reaches 0.5 inches below the weld is the sum of the initial half-length and the 0.5 inches it has grown (0.5 +0.395/2). Then by dividing the aspect ratio and multiplying by two, the flaw depth when the crack tip is 0.5 inches below the weld is 0.279 in. The required time to reach such a flaw size (a/t=0.49) is estimated as 3.35 years in Figure 7-4A. Using the flaw depth calculated previously (49 percent) as the initial flaw depth, the curves in Figure 6-4 or 6-5 can be used, because CGR is the same for both uphill and downhill side of the center penetration, for inside surface flaws near the weld can be used to determine the service life before the flaw reaches the allowable flaw size. Using the acceptance criteria in Table 6-1 and Figure 6-5 as the source figure, Figure 7-4B shows an additional 0.75 years of service life for a total of 4.1 years. (See Guideline 5 below, for a quick and conservative approach to evaluate flaws that are more than 0.5" below the weld and will extend to within 0.5" of the weld).

Example 5. This case is an axial through-wall flaw whose upper-most end is 0.40 inches below the weld region on the uphill side of penetration 65, which is in the 42.5 degree row of penetrations, as seen in Table 1-1. From Figure 6-18 we obtain the appropriate curve for the crack growth prediction, and this is reproduced as Figure 7-5. This figure gives a service life estimate of approximately 2.8 years to grow to the bottom of the weld as illustrated in Figure 7-5.

It is clear from these examples that the most important figures for use in evaluating flaws in head penetrations are the surface flaw Figures 6-2 through 6-9 for axial flaws and 6-10 for circumferential flaws. The figures which project the growth of through-wall flaws are valuable, but may be of limited practical use with the acceptance criteria. There is an important safety aspect to the through-wall flaw charts, however, in that they demonstrate that flaw propagation above the weld will be very limited.

Several guidelines are important to understand when using these charts.

1. If a flaw is found in a penetration nozzle for which no specific analysis was performed and there is a uniform trend as a function of penetration nozzle angle, interpolation between penetration nozzles is the best approach.

2. If a flaw is found in a penetration nozzle for which no specific analysis was performed and there is no apparent trend as a function of penetration nozzle angle, the result for the penetration nozzle with the closest angle should be used.

3. If a flaw is found which has a depth smaller than any depth shown for the penetration nozzle angle of interest, the initial flaw depth should be assumed to be the same as the smallest depth analyzed for that particular penetration nozzle.

4. The flaw evaluation charts are applicable for aspect ratio of 6 or less. Consult with Westinghouse if the as-found flaw has an aspect ratio larger than 6.0.

5. As shown in Example 4, flaws whose upper extremities grow within 0.5" below the weld require the use of both the 0.5" below the weld and "at the weld" flaw tolerance charts. To avoid the use of these two charts, the "at the weld" charts may solely be used in determining the service life. This shall provide a conservative estimate of the crack growth due to a larger stress field.

6. Results are only provided for the uphill and downhill sides of the selected penetration nozzles. If flaws are found in locations between the uphill and downhill side, use the results for either the uphill or downhill location, whichever is closer

Table 7-1 Example Problem Inputs: Initial Flaw Sizes and Locations

No.	Orientation	Vertical Location	Circum. Location	Penetration Angle	Length (2c)	Depth (a)	a/t	Wall Thick. (t)	Pen. No.	Source Figure
1	Axial - Inside Surface	1.3" Below Weld	Uphill	29.1°	0.085"	0.0425"	0.075	0.566"	30	6-2
2	Axial – Outside Surface	1.3" Below Weld	Downhill	37.1°	0.085"	0.0425"	0.075	0.566"	50	6-9
3	Axial - Inside Surface	At Weld	Uphill	ICI (54.8°)	0.250"	0.05"	0.107	0.469"	70	6-4
4	Axial - Inside Surface	1.0" Below Weld	--	0.0°	0.395"	0.079"	0.14	0.566"	1	6-3, 6-5
5	Axial Through-Wall	0.4" Below Weld	Uphill	42.5	--	--	--	0.566"	65	6-18

No.	Orientation	Crack Tip Location	Circum. Location	Pen No.	Length (2c)	Depth (a)	Penetration Angle	Source Figure	a/t	Wall Thick. (t)
1	Axial – Inside Surface	1.3" Below Weld	Uphill	30	0.085"	0.0425"	29.1°	6-2	0.075	0.566"

Acceptance Criteria (Table 6-1)

Location	Axial	
	a_f	L
Below Weld (ID)	t	No Limit

Locality Angles (Table 1-1)

Nozzle No.	Type	Angle
30	CEDM	29.1

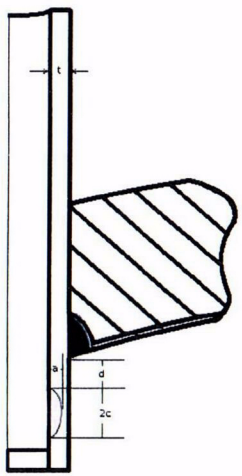

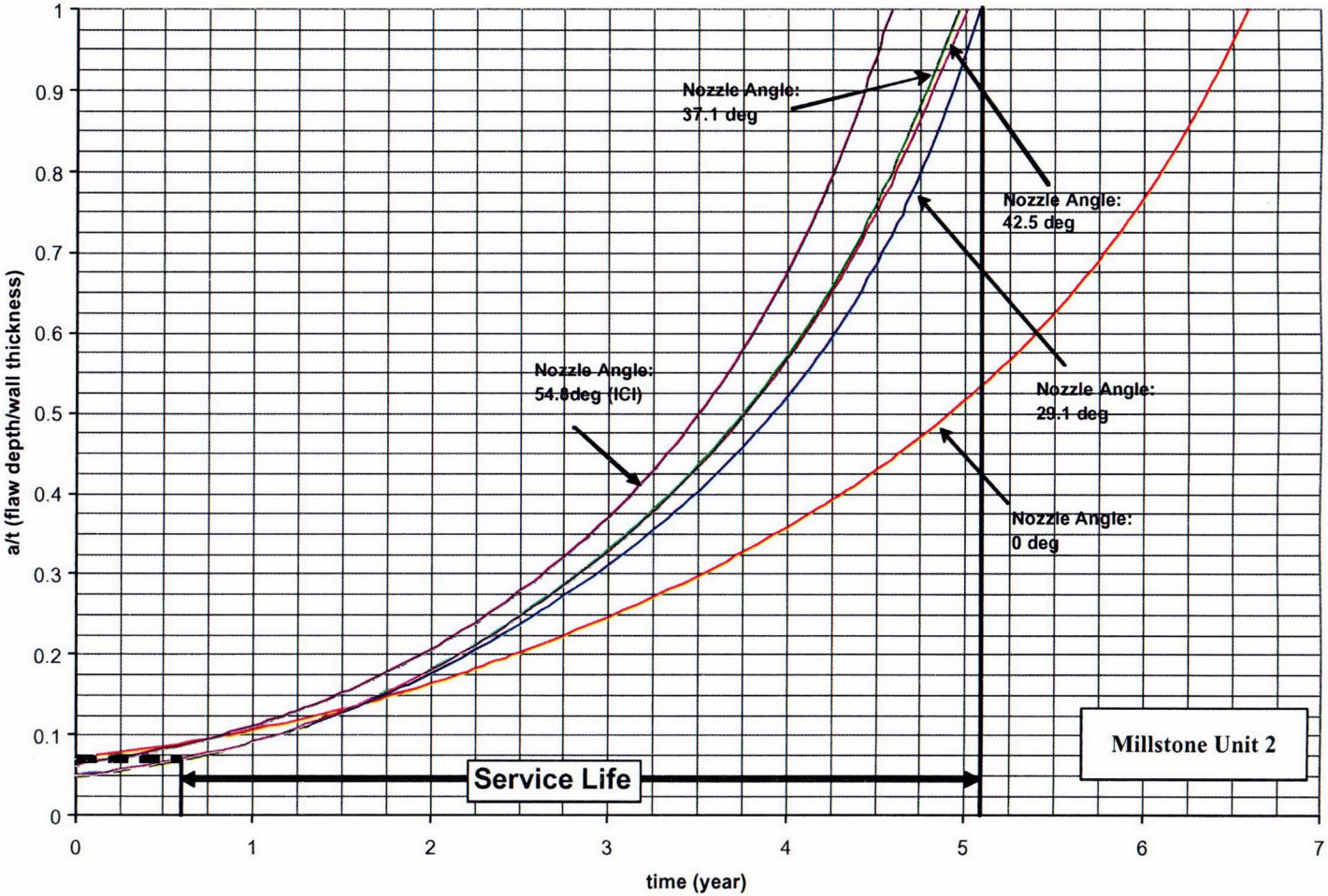

Figure 7-1 Example Problem 1

C21

No.	Orientation	Crack Tip Location	Circum. Location	Pen No.	Length (2c)	Depth (a)	Penetration Angle	Source Figure	a/t	Wall Thick. (t)
2	Axial – Outside Surface	1.3" Below Weld	Downhill	50	0.085"	0.0425"	37.1°	6-9	0.075	0.566"

Acceptance Criteria (Table 6-1)

Location	Axial	
	a_f	L
Below Weld (OD)	t	No Limit

Locality Angles (Table 1-1)

Nozzle No.	Type	Angle
50	CEDM	37.1

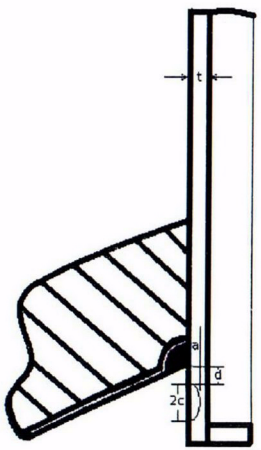

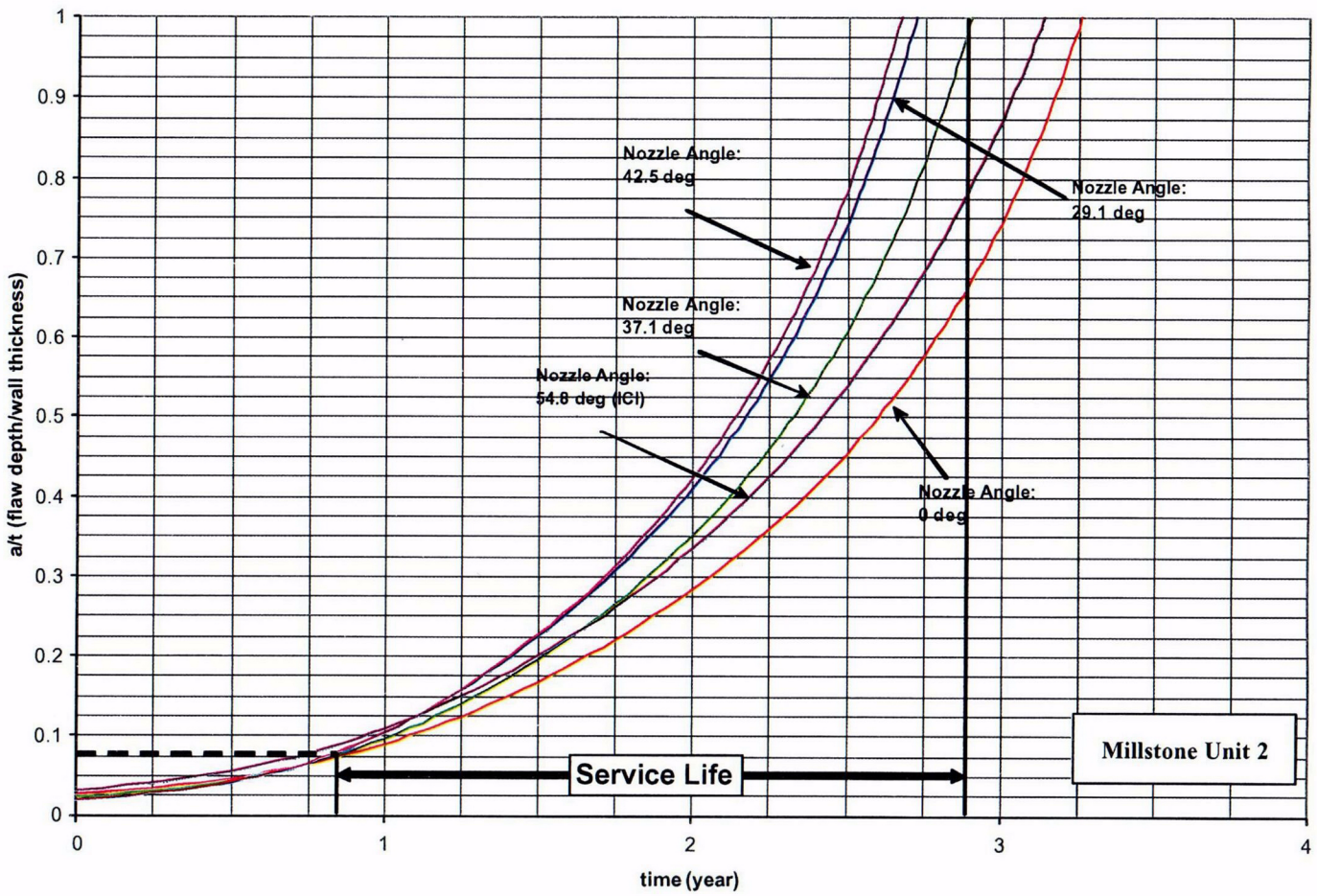

Figure 7-2 Example Problem 2

No.	Orientation	Crack Tip Location	Circum. Location	Pen No.	Length (2c)	Depth (a)	Penetration Angle	Source Figure	a/t	Wall Thick. (t)
3	Axial – Inside Surface	At Weld	Uphill	70	0.250"	0.050"	ICI (54.8°)	6-6	0.107	0.469"

Acceptance Criteria (Table 6-1)

Location	Axial	
	a_f	L
At and Above Weld (ID)	0.75 t	No Limit

Locality Angles (Table 1-1)

Nozzle No.	Type	Angle
70	CEDM	ICI (54.8)

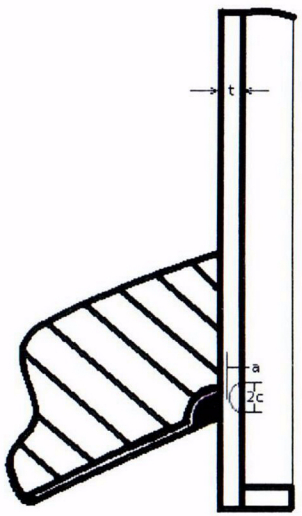

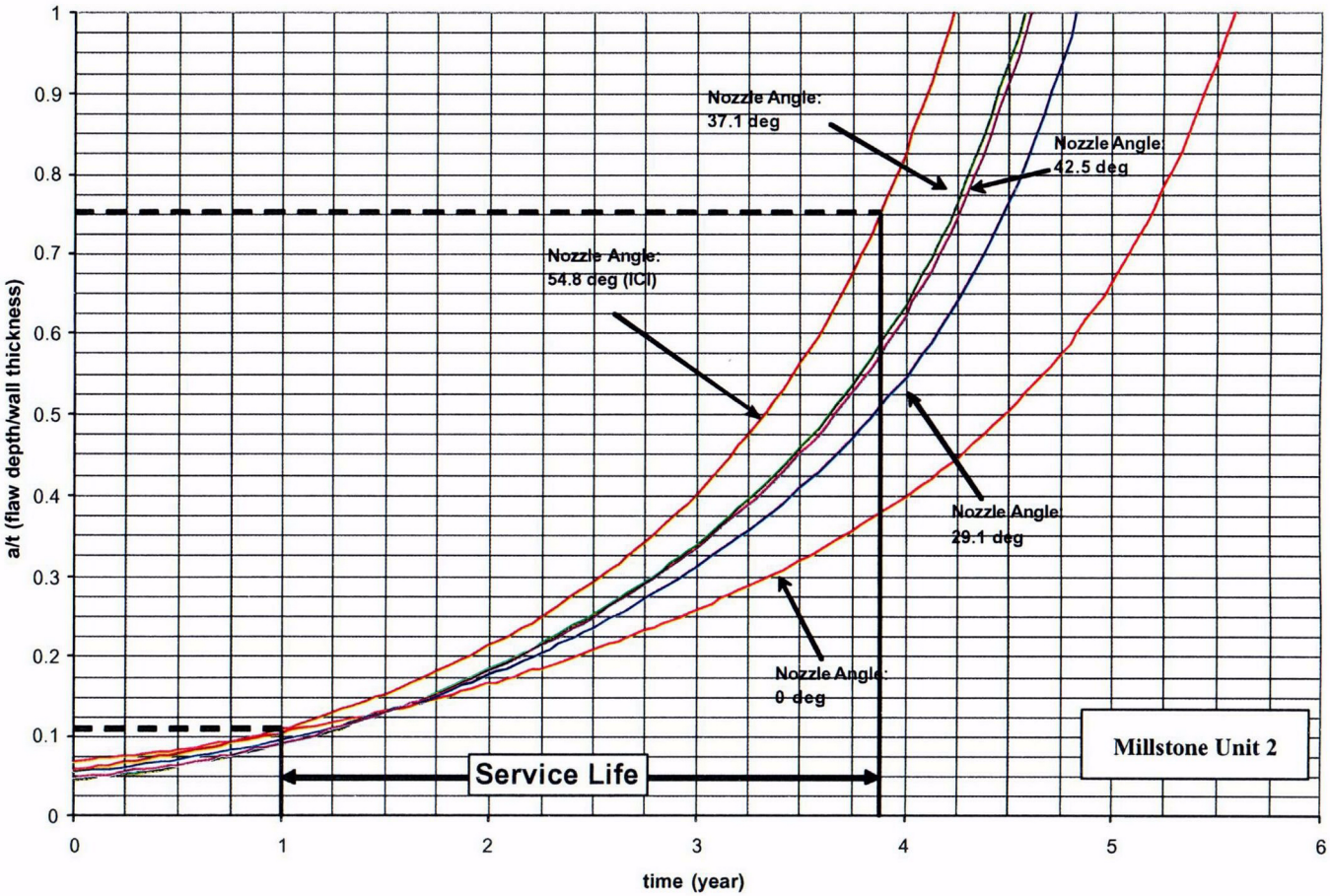

Figure 7-3 Example Problem 3

C23

No.	Orientation	Crack Tip Location	Circum. Location	Pen No.	Length (2c)	Depth (a)	Penetration Angle	Source Figure	a/t	Wall Thick. (t)
4	Axial – Inside Surface	1.0" Below Weld	--	1	0.395"	0.079"	0.0°	6-3, 6-5	0.14	0.566"

Acceptance Criteria (Table 6-1)

Location	Axial	
	a_f	L
Below Weld (ID)	t	No Limit

Locality Angles (Table 1-1)

Nozzle No.	Type	Angle
1	CEDM	0.0

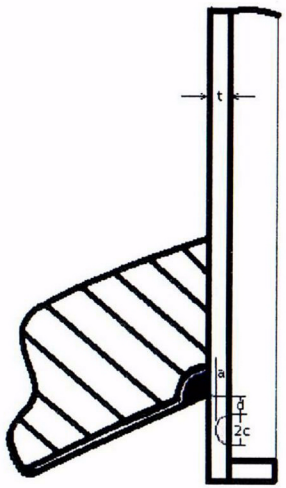

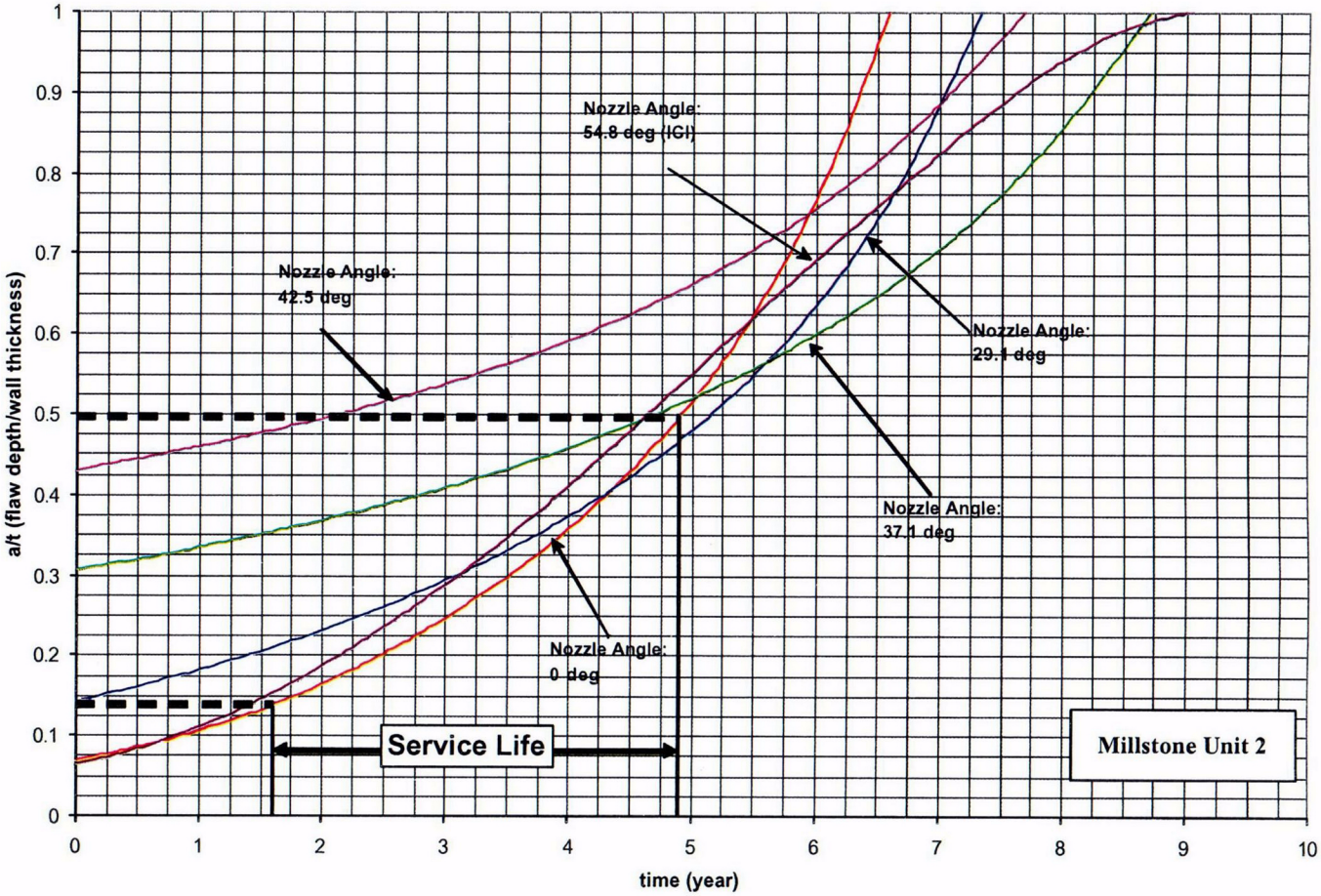

Figure 7-4a Example Problem 4 (also see Figure 7-4b)

C24

No.	Orientation	Crack Tip Location	Circum. Location	Pen No.	Length (2c)	Depth (a)	Penetration Angle	Source Figure	a/t	Wall Thick. (t)
4	Axial – Inside Surface	1.0" Below Weld	--	1	0.395"	0.079"	0.0°	6-3, 6-5	0.14	0.566"

Acceptance Criteria (Table 6-1)

Location	Axial	
	a_f	L
Below Weld (ID)	t	No Limit

Locality Angles (Table 1-1)

Nozzle No.	Type	Angle
1	CEDM	0.0

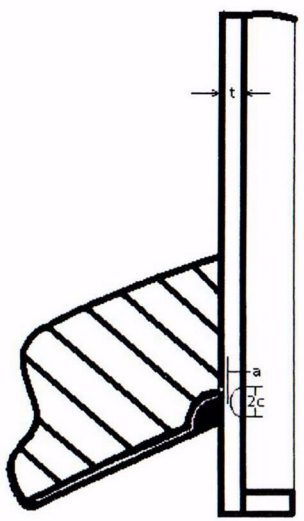

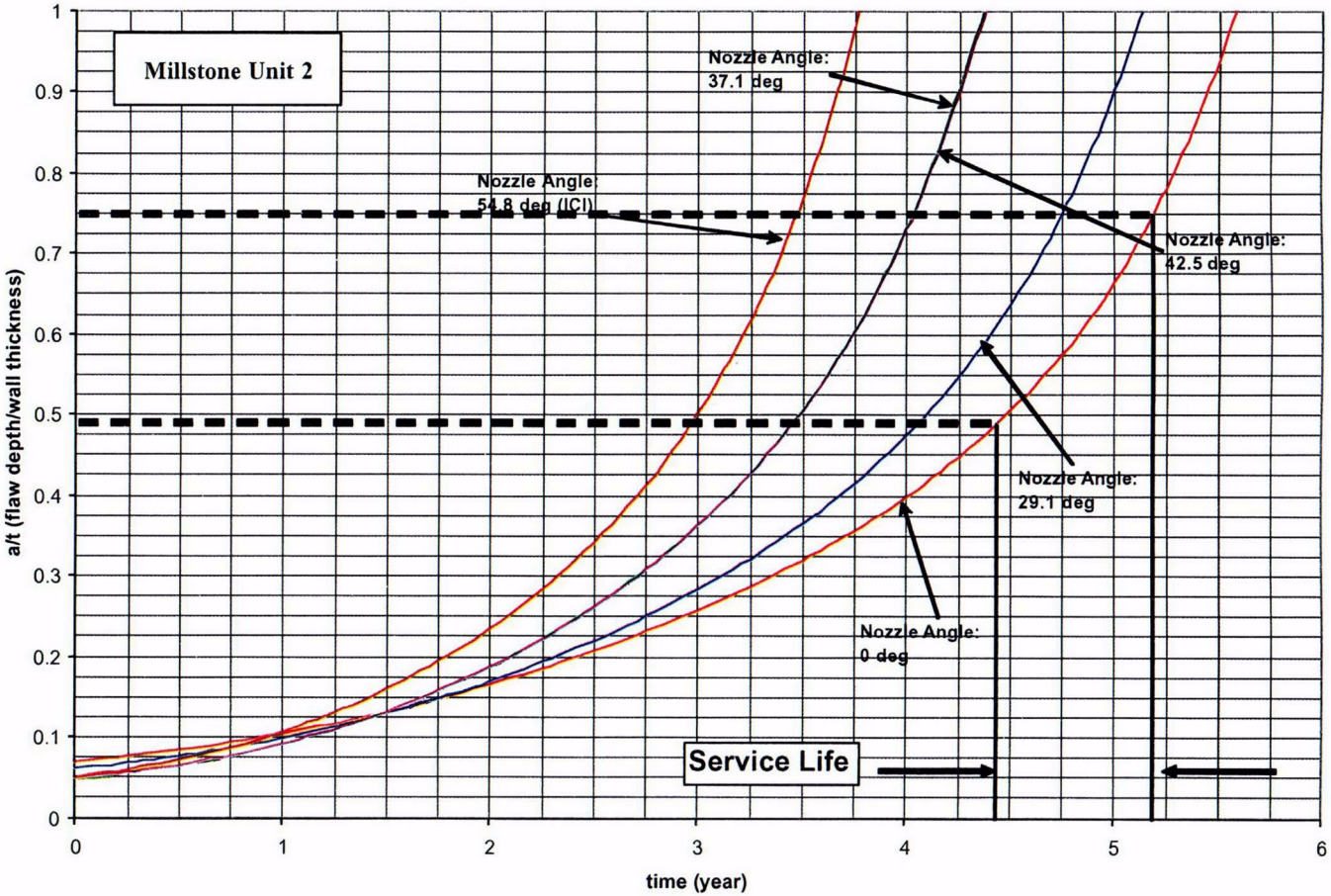

Figure 7-4b Example Problem 4 (also see Figure 7-4a)

C25

No.	Orientation	Crack Tip Location	Circum. Location	Pen No.	Length (2c)	Depth (a)	Penetration Angle	Source Figure	a/t	Wall Thick. (t)
5	Axial – Through Wall	0.4" Below Weld	Uphill	65	--	--	42.5°	6-18	--	0.566"

Acceptance Criteria (Table 6-1)

Location	Axial	
	a_f	L
Below Weld (ID)	t	Bottom Weld

Locality Angles (Table 1-1)

Nozzle No.	Type	Angle
65	ICI	42.5

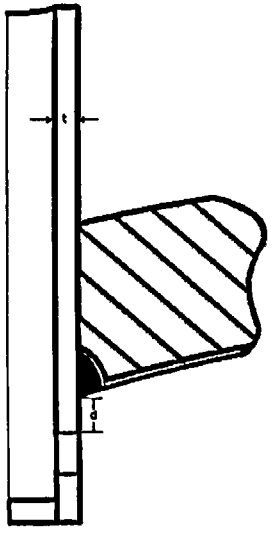

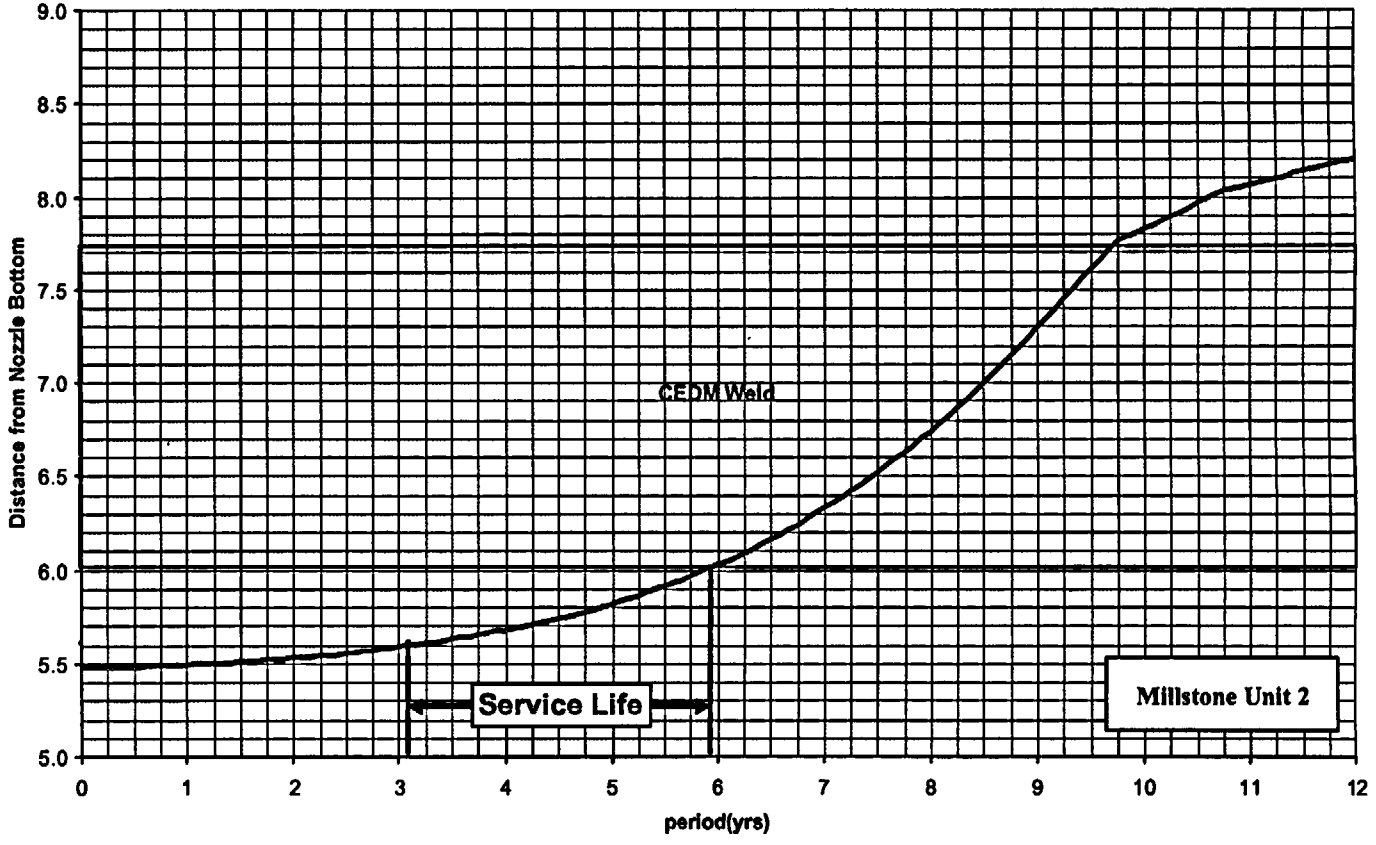

Figure 7-5 Example Problem 5

8 REFERENCES

1. Scott, P. M., "An Analysis of Primary Water Stress Corrosion Cracking in PWR Steam Generators," in Proceedings, Specialists Meeting on Operating Experience With Steam Generators, Brussels Belgium, Sept. 1991, pages 5, 6.

2. McIlree, A. R., Rebak, R. B., Smialowska, S., "Relationship of Stress Intensity to Crack Growth Rate of Alloy 600 in Primary Water," Proceedings International Symposium Fontevraud II, Vol, 1, p. 258-267, September 10-14, 1990.

3. Cassagne, T., Gelpi, A., "Measurements of Crack Propagation Rates on Alloy 600 Tubes in PWR Primary Water, in Proceedings of the 5th International Symposium on Environmental Degradation of Material in Nuclear Power System-Water Reactor," August 25-29, 1991, Monterey, California.

4A. *Crack Growth and Microstructural Characterization of Alloy 600 PWR Vessel Head Penetration Materials,* EPRI, Palo Alto, CA. 1997. TR-109136.

4B. Vaillant, F. and C. Amzallag. "Crack Growth Rates of Alloy 600 in Primary Water," Presentation to the EPRI-MRP Crack Growth Rate (CGR) Review Team, Lake Tahoe, NV, August 10, 2001.

4C. Vaillant, F. and S. Le Hong. *Crack Growth Rate Measurements in Primary Water of Pressure Vessel Penetrations in Alloy 600 and Weld Metal 182,* EDF, April 1997. HT-44/96/024/A.

4D. Framatome laboratory data provided by C. Amzallag (EDF) to MRP Crack Growth Rate Review Team, October 4, 2001 (Proprietary to EDF).

4E. Cassagne, T., D. Caron, J. Daret, and Y. Lefevre. "Stress Corrosion Crack Growth Rate Measurements in Alloys 600 and 182 in Primary Water Loops Under Constant Load," *Ninth International Symposium on Environmental Degradation of Materials in Nuclear Power Systems-Water Reactors* (Newport Beach, CA, August 1-5, 1999), Edited by F. P. Ford, S. M. Bruemmer, and G. S. Was, The Minerals, Metals & Materials Society (TMS), Warrendale, PA, 1999.

4F. Studsvik laboratory data provided by Anders Jenssen (Studsvik) to MRP Crack Growth Rate Review Team, October 3, 2001 (Proprietary to Studsvik).

4G [ ]a,c,e

4H "Materials Reliability Program (MRP) Crack Growth Rates for Evaluating Primary Water Stress Corrosion Cracking (PWSCC) of Thick Wall Alloy 600 Material (MRP-55) Revision 1," EPRI, Palo Alto, CA:, November 2002. 1006695.

4I. "Crack Growth Rate Tests of Alloy 600 in Primary PWR Conditions," Communication from M. L. Castaño (CIEMAT) to J. Hickling (EPRI), March 25, 2002.

4J. Gomez-BriceZo, D., J. LapeZa, and F. Bl<zquez. "Crack Growth Rates in Vessel Head Penetration Materials," *Proceedings of the International Symposium Fontevraud III: Contribution of Materials Investigation to the Resolution of Problems Encountered in Pressurized Water Reactors* (Chinton, France, September 12-16, 1994), French Nuclear Energy Society, Paris, 1994, pp. 209-214.

4K. Gomez-BriceZo, D. and J. LapeZa. "Crack Growth Rates in Vessel Head Penetration Materials," *Proceedings: 1994 EPRI Workshop on PWSCC of Alloy 600 in PWRs* (Tampa, FL, November 15-17, 1994), EPRI, Palo Alto, CA, TR-105406, August 1995, pp. E4-1 through E4-15.

4L. Gomez-BriceZo, D., et al. "Crack Propagation in Inconel 600 Vessel Head Penetrations," Eurocorr 96, Nice, France, September 24-26, 1996.

4M. CastaZo, M. L., D. G.·.mez-BriceZo, M. Alvarez-de-Lara, F. Bl<zquez, M. S. Garcia, F. Hern<ndez, and A. Largares. "Effect of Cationic Resin Intrusions on IGA/SCC of Alloy 600 Under Primary Water Conditions," *Proceedings of the International Symposium Fontevraud IV: Contribution of Materials Investigation to the Resolution of Problems Encountered in Pressurized Water Reactors* (France, September 14-18, 1998), French Nuclear Energy Society, Paris, 1998, Volume 2, pp. 925-937.

5A. Newman, J. C. and Raju, I. S., "Stress Intensity Factor Influence Coefficients for Internal and External Surface Cracks in Cylindrical Vessels," in Aspects of Fracture Mechanics in Pressure Vessels and Piping, PVP Vol. 58, ASME, 1982, pp. 37-48.

5B. Hiser, Allen, "Determinists and Probabilistic Assessments," presentation at NRC/Industry/ACRS meeting, November 8, 2001.

6A. [ ]^{a,c,e}

6B. [ ]^{a,c,e}

6C. Fleming, M.A., "Palo Verde 1 and 2 CEDM and Head Vent Stress Analysis", Dominion Engineering Calculation No. C-7736-00-6, February 2002.

7. USNRC Letter, W. T. Russell to W. Raisin, NUMARC, "Safety Evaluation for Potential Reactor Vessel Head Adapter Tube Cracking," November 19, 1993.

8. USNRC Letter, A. G. Hansen to R. E. Link, "Acceptance Criteria for Control Rod Drive Mechanism Penetrations at Point Beach Nuclear Plant, Unit 1," March 9, 1994.

9. Millstone Unit 2, NRC Bulletin 2001-01 Response (Docket Numbers 50-336 and 50-423, B18466) August 31, 2001.

10A. CE Drawing No. E-233-537, " Closure Head Penetrations", Revision 5, October 1969.

10B. CE Drawing No. E-233-534, " Closure Head Forming & Welding", Revision 8, October 1969.

10C. CE Drawing No. E-233-536, " Closure Head Nozzle Details", Revision 8, December 1969.

11. CEOG Report # CEN-614, "Safety Evaluation of the Potential for and Consequences of Reactor Vessel Head Penetration Alloy 600 OD Initiated Nozzle Cracking," December 1993.

12. USNRC Letter, R. Barrett to A. Marion, "Flaw Evaluation Guidelines," April 11, 2003.

APPENDIX A
ALLOWABLE AREAS OF LACK OF FUSION: WELD FUSION ZONES

There are two fusion zones of interest for the head penetration nozzle attachment welds, the penetration itself (Alloy 600) and the reactor vessel head material (A533B ferritic steel). The operating temperature of the upper head region of the Millstone Unit 2 is 312°C (594°F), so the materials will be very ductile. The toughness of both materials is quite high, so any flaw propagation along either of the fusion zones will be totally ductile.

Two generic calculations were completed for the fusion zones, one for the critical flaw size, and the second for the allowable flaw size, which includes the margins required in the ASME code. The simpler case is the Alloy 600 fusion zone, where the potentia l failure will be a pure shearing of the penetration as the pressurized penetration tube is forced outward from the vessel head, as shown in Figure A-1.

The failure criterion will be that the average shear stress along the fusion line exceeds the limit shear stress. For the critical flaw size, the limiting shear stress is the shear flow stress, which is equal to half the tensile flow stress, according to the Tresca criterion. The tensile flow stress is the average of the yield stress and ultimate tensile stress of the material. The criterion for Alloy 600 at 318°C (604°F) is:

$$\text{Average shear stress} < \text{shear flow stress} = 26.85 \text{ ksi}$$

This value was taken from the ASME Code, Section III, Appendix I, at 600°F.

For each penetration, the axial force which produces this shear stress results from the internal pressure. Since each penetration has the same outer diameter, the axial force is the same. The average shear stress increases as the load carrying area decreases (the area of lack of fusion increases). When this increasing lack of fusion area increases the stress to the point at which it equals the flow stress, failure occurs. This point may be termed the critical flaw size. This criterion is actually somewhat conservative. Alternatively, use of the Von Mises failure criterion would have set the shear flow stress equal to 60 percent of the axial flow stress, and would therefore have resulted in larger critical flaw sizes.

The allowable flaw size, as opposed to the critical flaw size discussed above, was calculated using the allowable limit of Section III of the ASME Code, paragraph NB 3227.2. The criterion for allowable shear stress then becomes:

$$\text{Average shear stress} < 0.6\, S_m = 13.98 \text{ ksi}$$

where S_m = the ASME Code limiting design stress from Section III, Appendix I.

The above approach was used to calculate the allowable flaw size and critical flaw size for the outermost and center penetrations. The results show that a very large area of lack of fusion can be tolerated by the head penetrations, regardless of their orientation. These results can be illustrated for the outermost CEDM penetration.

The total surface contact area for the fusion zone on the outermost head penetration is 17.4 in^2. The calculations above result in a required area to avoid failure of only 1.45 in^2, and using the ASME Code criteria, the area required is 2.79 in^2. These calculations show that as much as 83.9 percent of the weld may be unfused, and the code acceptance criteria can still be met.

To envision the extent of lack of fusion which is allowable, Figure A-2 was prepared. In this figure, the weld fusion region for the outermost penetration has been shown in an unwrapped, or developed view. The figure shows the extent of lack of fusion which is allowed, in terms of limiting lengths for a range of circumferential lack of fusion. This figure shows that the allowable vertical length of lack of fusion for a full circumferential unfused region is 84 percent of the weld length. Conversely, for a region of lack of fusion which extends the full vertical length of the weld, the circumferential extent is limited to 302 degrees. The extent of lack of fusion which would cause failure is labelled "critical" on this figure, and is even larger. The dimensions shown on this figure are based on an assumed rectangular area of lack of fusion.

The full extent of this allowable lack of fusion is shown in Figure A-3, where the axes have been expanded to show the full extent of the tube-weld fusion line. This figure shows that a very large area of lack of fusion is allowable for the outer most penetration. Similar results were found for the center penetration, where the weld fusion area is somewhat smaller at 16.1 in^2.

A similar calculation was also carried out for the fusion zone between the weld and the head, and the result is shown in Figure A-4. The allowable area of unfused weld for this location is 84.8 percent of the total area. This approach to the fusion zone with the carbon steel head is only approximate, but may provide a realistic estimate of the allowable. Note that even a complete lack of fusion in this region would not result in rod ejection, because the weld to the tube would prevent the tube from moving up through the vessel head.

The allowable lack of fusion for the weld fusion zone to the head may be somewhat in doubt, because of the different geometry, where one cannot ensure that the failure would be due to pure shear. To investigate this concern, additional finite element models were constructed with various degrees of lack of fusion discretely modeled, ranging from 30 to 65 percent. The stress intensities around the circumference of the penetration were calculated, to provide for the effects of all stresses, as opposed to the shear stress only, as used above. When the average stress intensity reaches the flow stress (53.7 ksi), failure is expected to occur. The code allowable stress intensity is 1.5 Sm, or 35 ksi, using the lower of the Alloy 600 and ferritic allowables at 316°C (600°F).

The results of this series of analyses are shown in Figure A-5, where it is clear that large areas of lack of fusion are allowable. As the area of lack of fusion increases, the stresses redistribute themselves, and the stress intensity does not increase in proportion to the area lost. These results seem to confirm that the shear stress is the only important stress governing the critical flaw size for the head fusion zone as well.

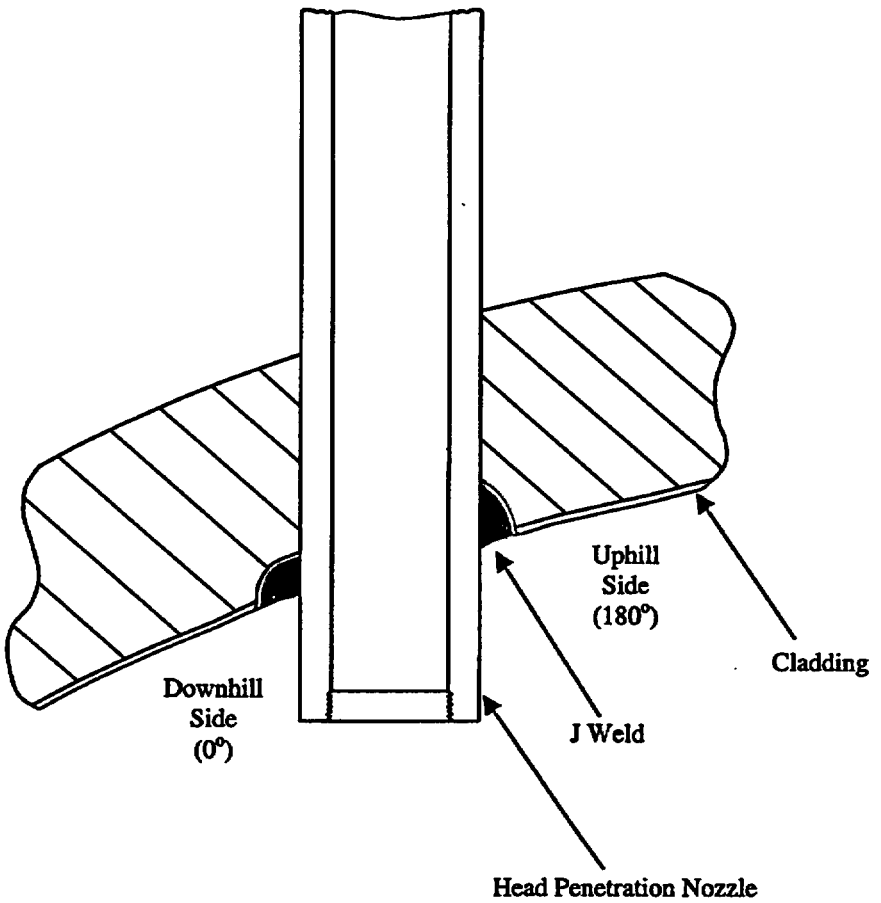

Figure A-1 Typical Head Penetration

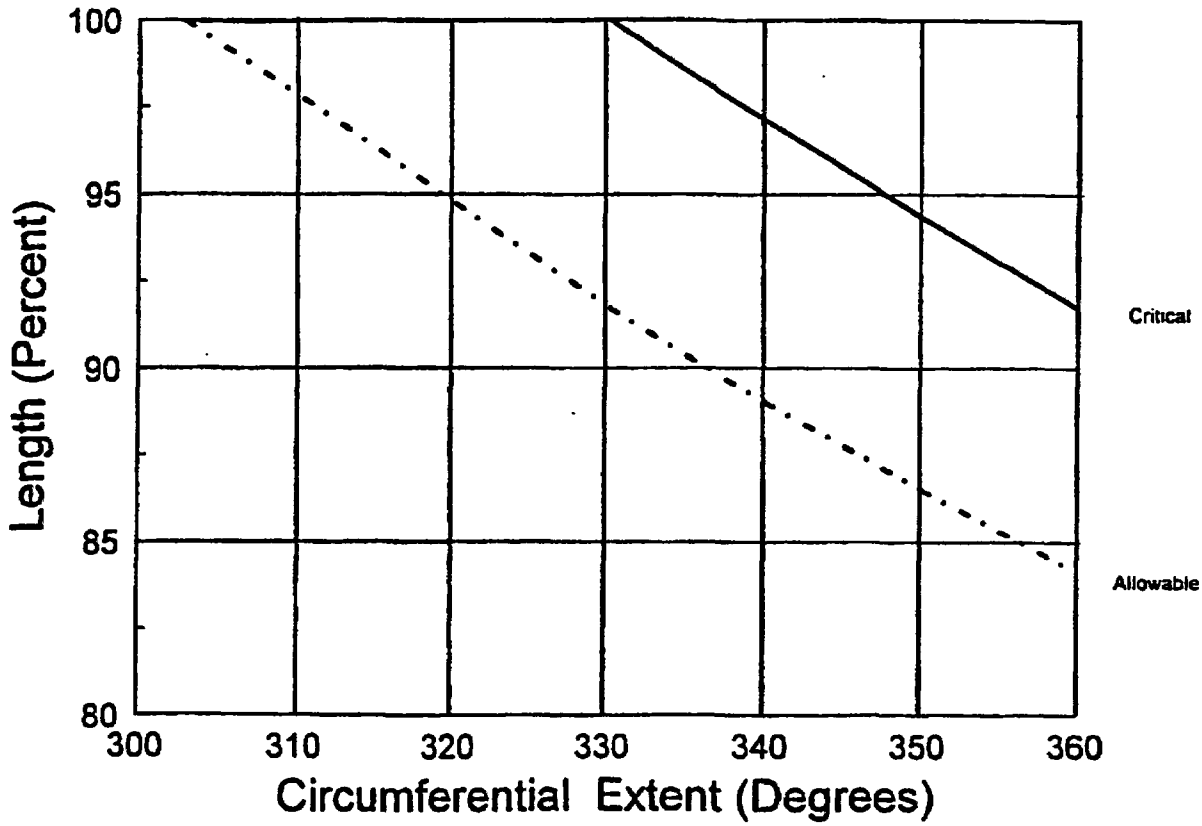

Figure A-2 Allowable Regions of Lack of Fusion for the Outermost Penetration Tube to Weld Fusion Zone: Detailed View

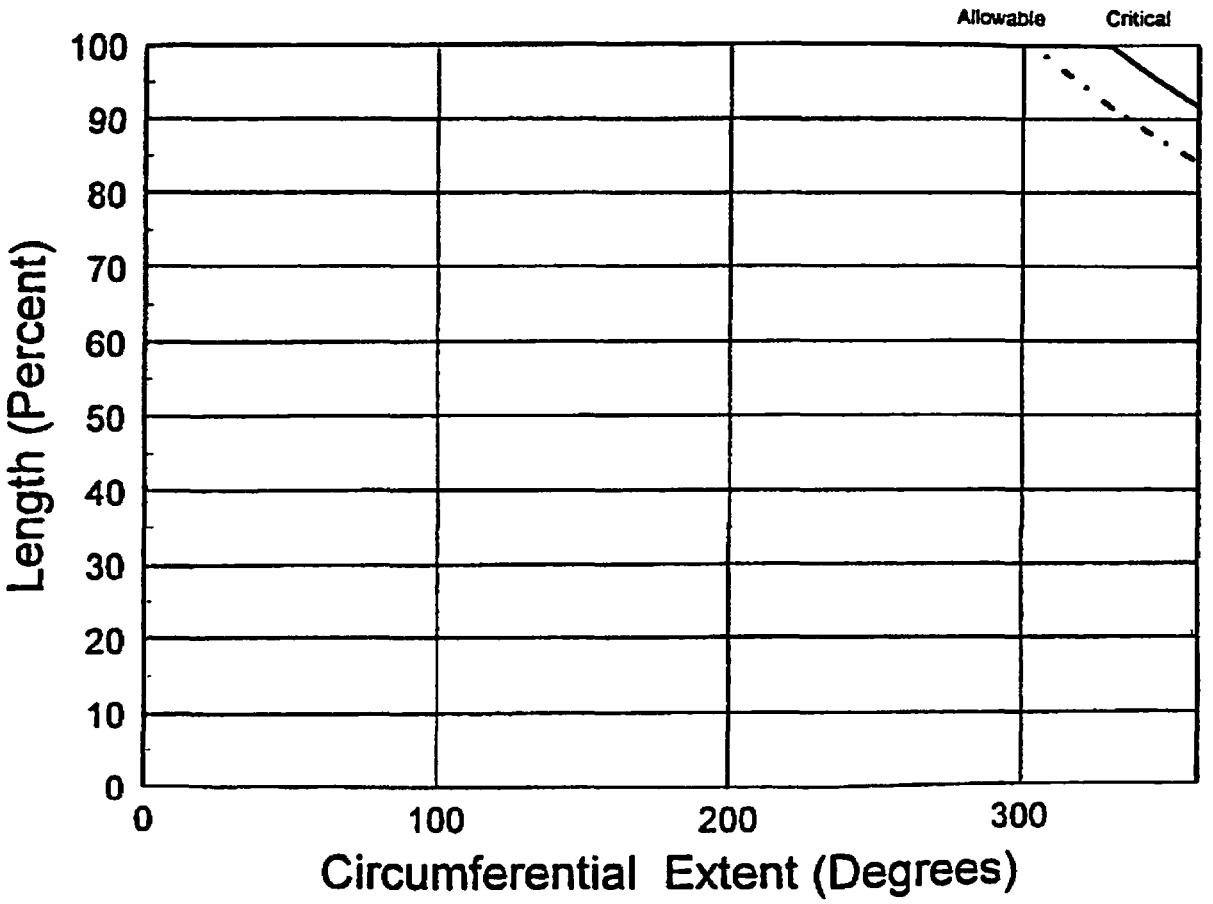

Figure A-3 Allowable Regions of Lack of Fusion for the Outermost Penetration Tube to Weld Fusion Zone

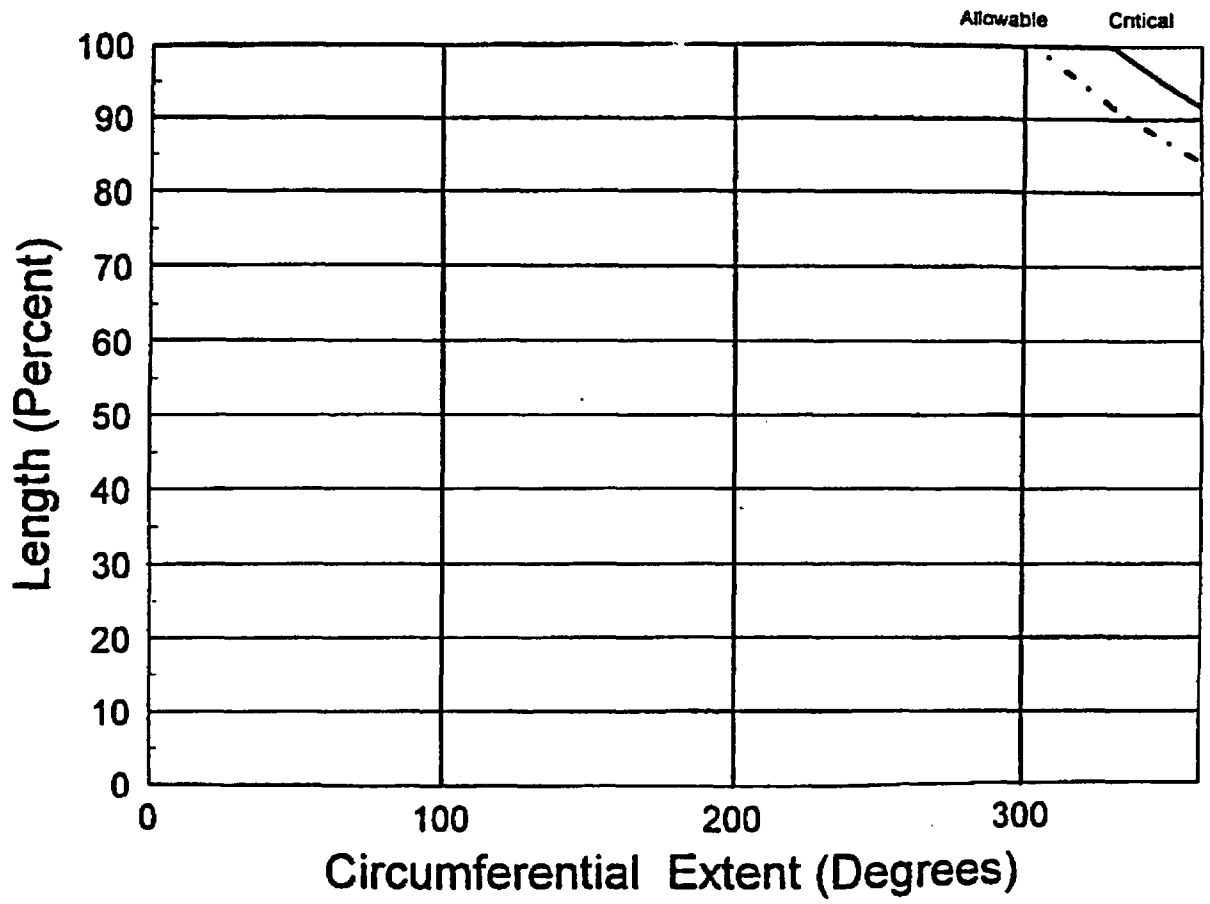

Figure A-4 Allowable Regions of Lack of Fusion for all Penetrations: Weld to Vessel Fusion Zone

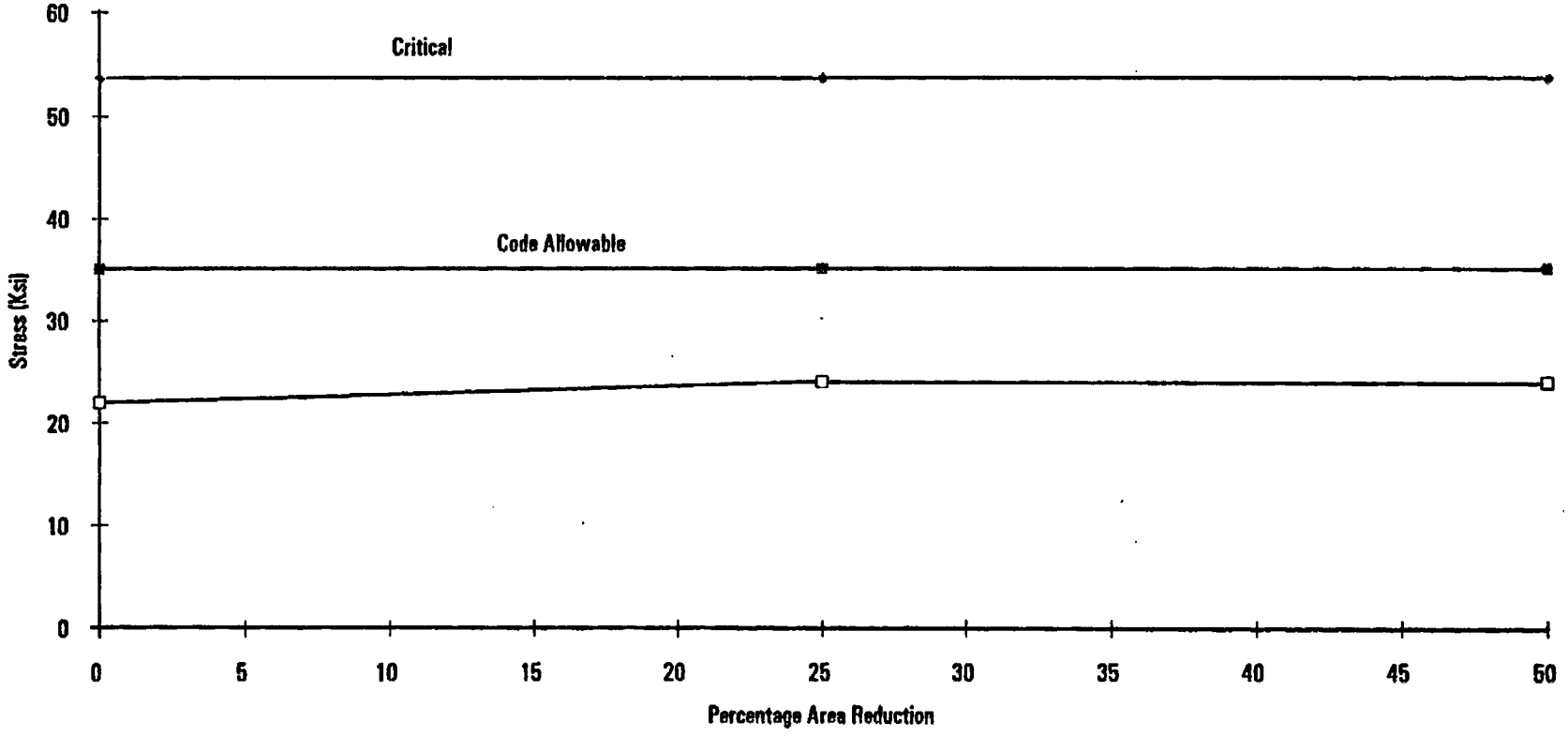

Figure A-5 Allowable Regions of Lack of Fusion for the Weld to Vessel Fusion Zone

Appendix B

CEDM AND ICI NOZZLE HOOP STRESS VS DISTANCE FROM BOTTOM OF WELD PLOTS

Figure B-1

Hoop Stress Distribution Below the Weld Downhill and Uphill Side (0° CEDM Penetration Nozzle)

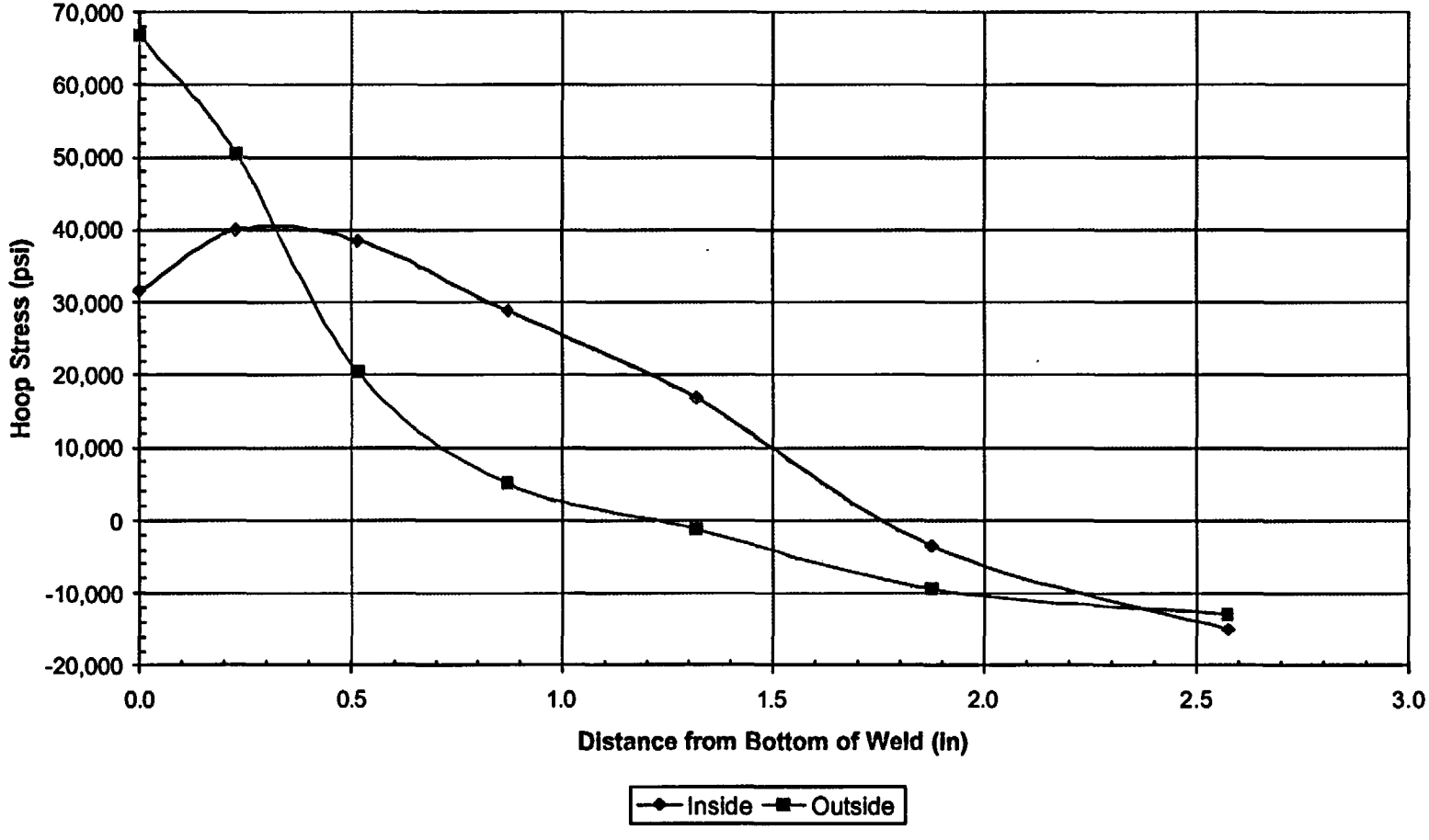

Figure B-2

Hoop Stress Distribution Below the Weld Downhill Side (29.1° CEDM Penetration Nozzle)

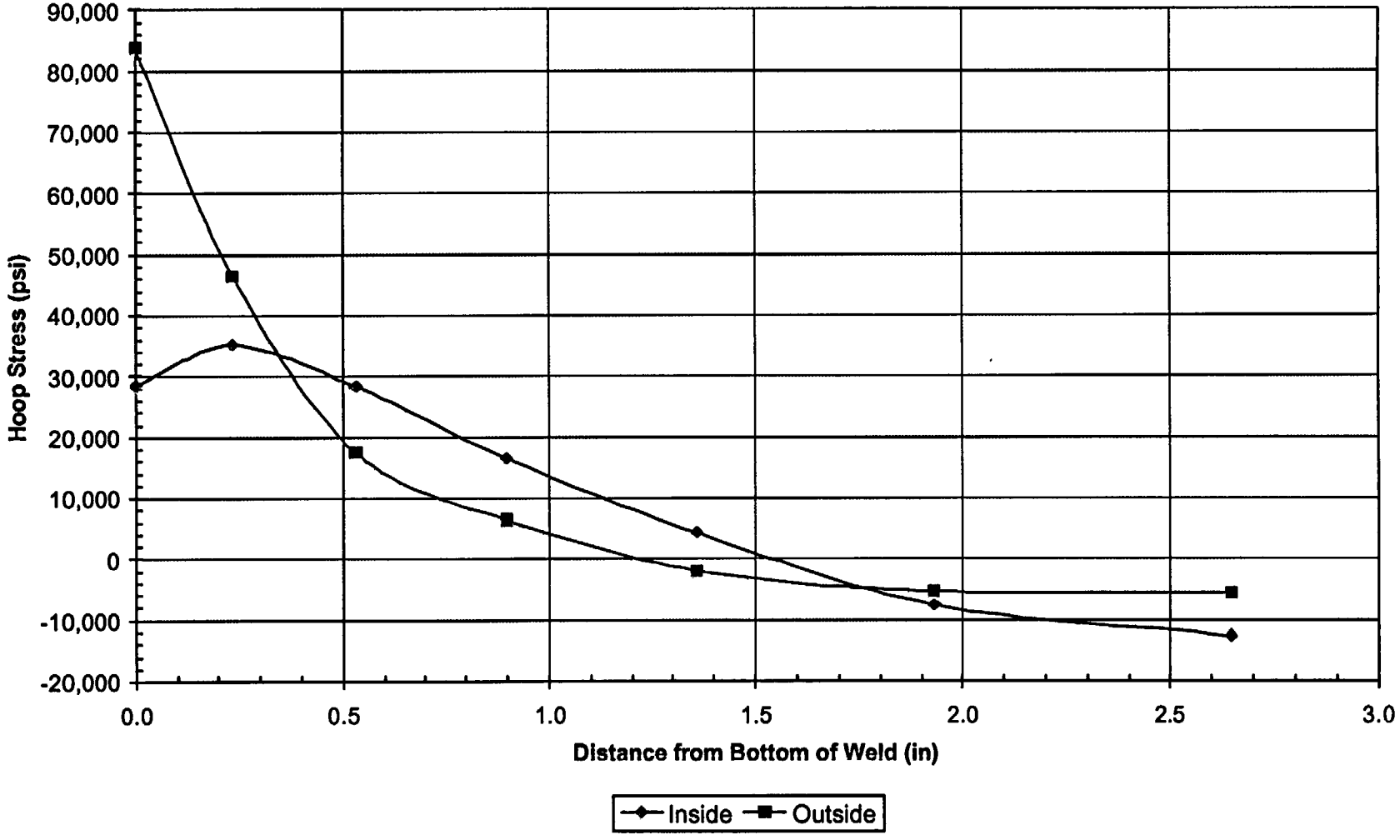

Figure B-3

Hoop Stress Distribution Below the Weld Uphill Side
(29.1° CEDM Penetration Nozzle)

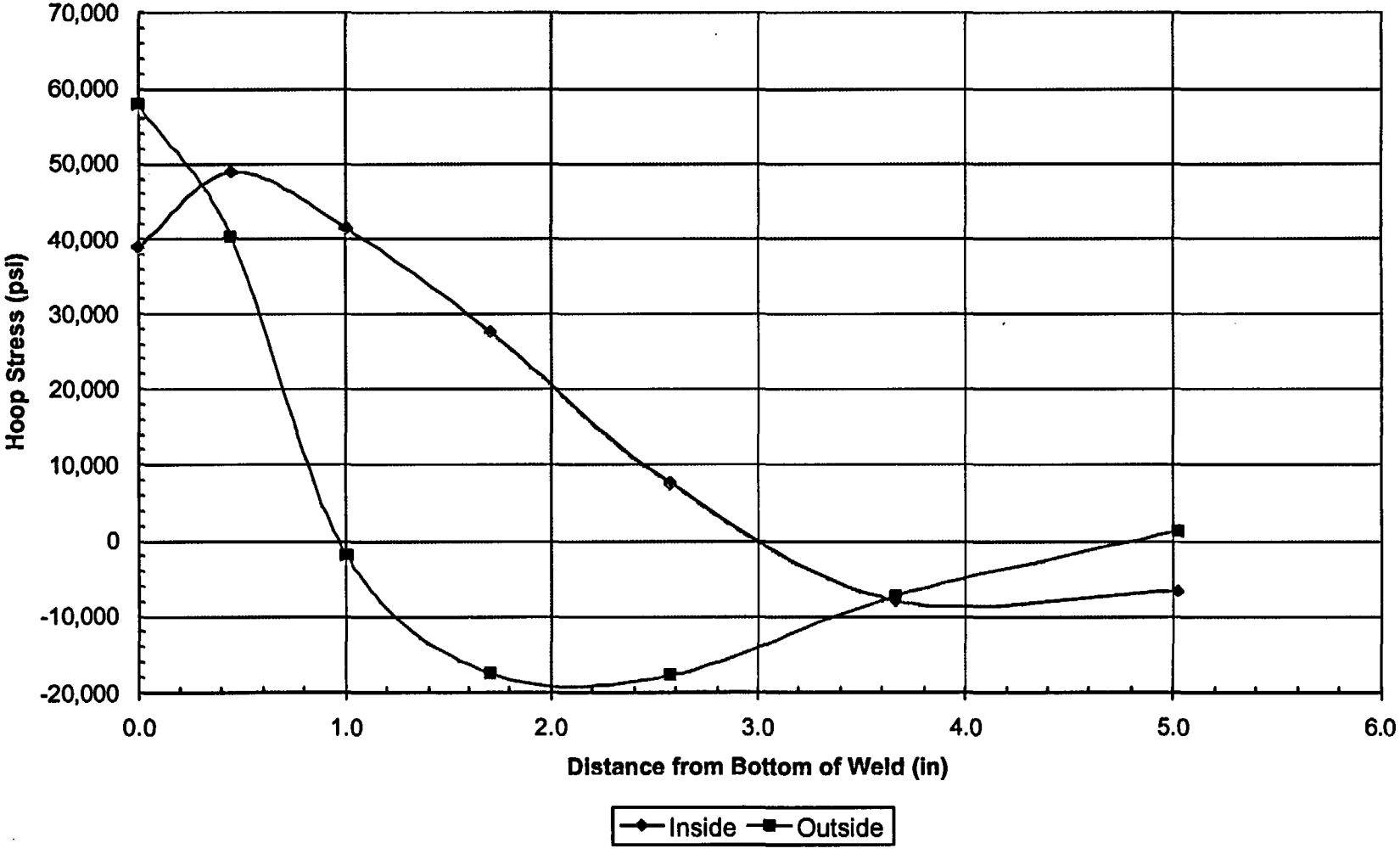

Figure B-4

Hoop Stress Distribution Below the Weld Downhill Side (37.1° CEDM Penetration Nozzle)

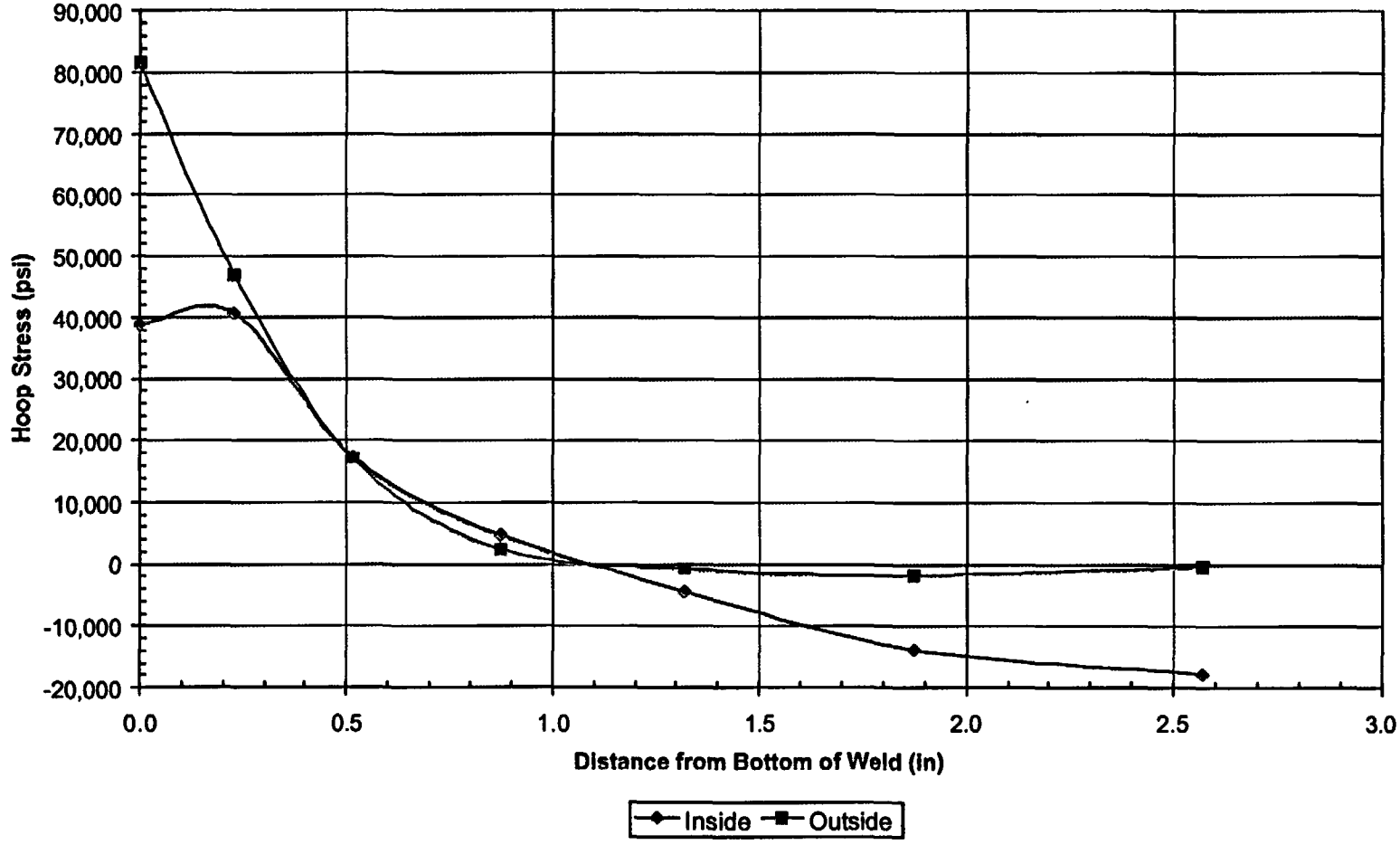

Figure B-5

Hoop Stress Distribution Below the Weld Uphill Side (37.1° CEDM Penetration Nozzle)

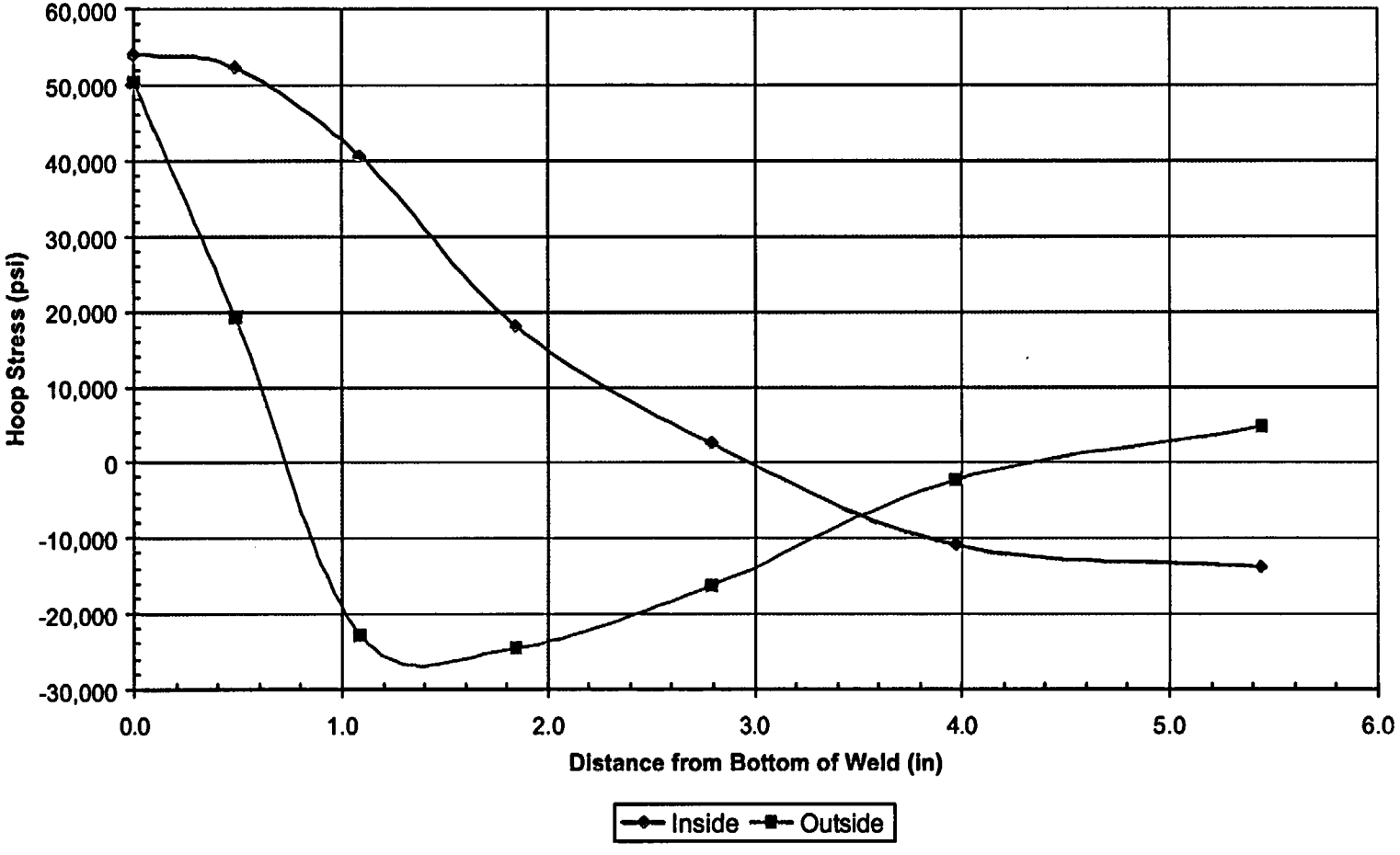

Figure B-6

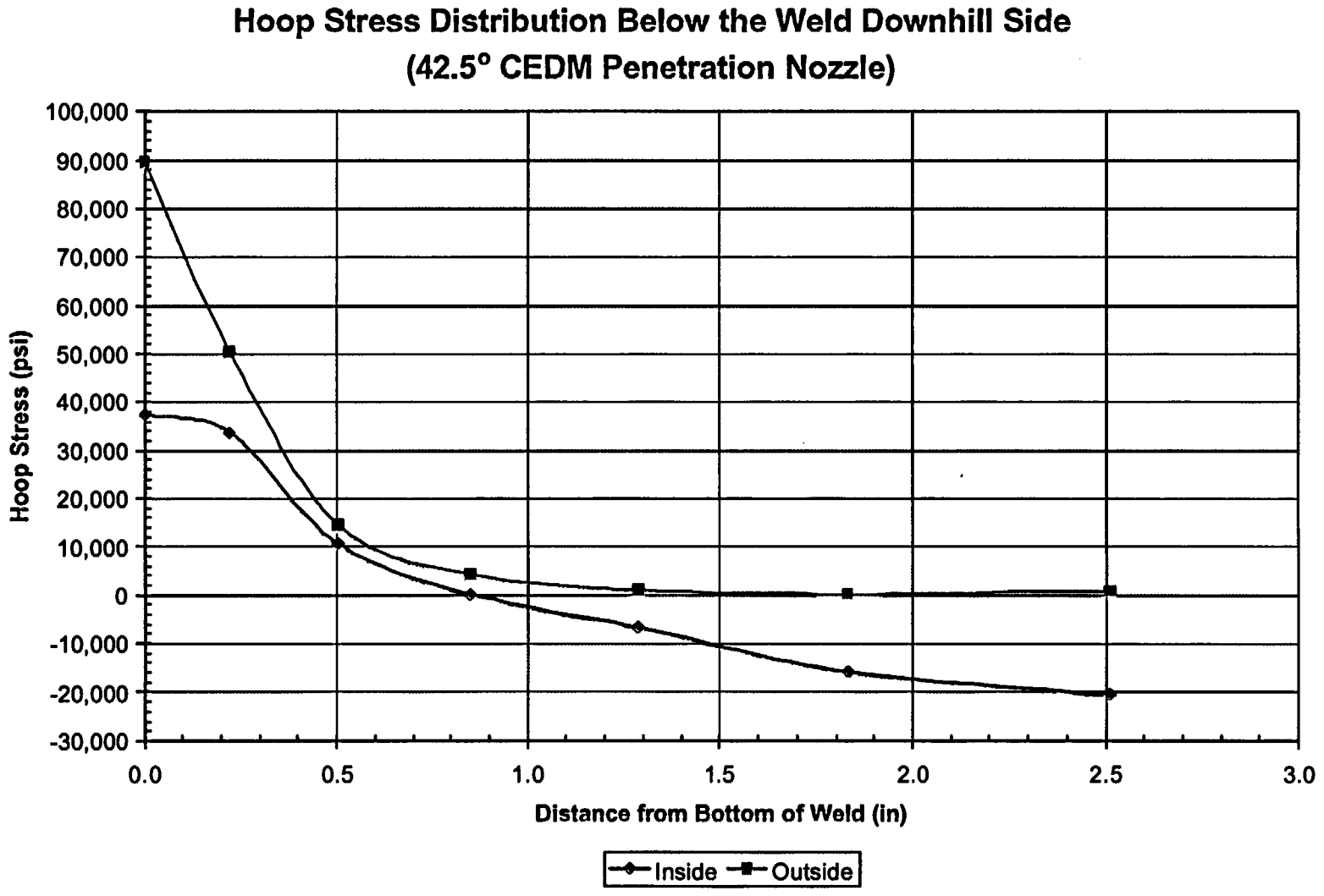
Hoop Stress Distribution Below the Weld Downhill Side
(42.5° CEDM Penetration Nozzle)
Hoop Stress (psi)
100,000
90,000
80,000
70,000
60,000
50,000
40,000
30,000
20,000
10,000
0
-10,000
-20,000
-30,000
0.0
0.5
1.0
1.5
2.0
2.5
3.0
Distance from Bottom of Weld (in)
Inside
Outside

Figure B-7

Hoop Stress Distribution Below the Weld Uphill Side (42.5° CEDM Penetration Nozzle)

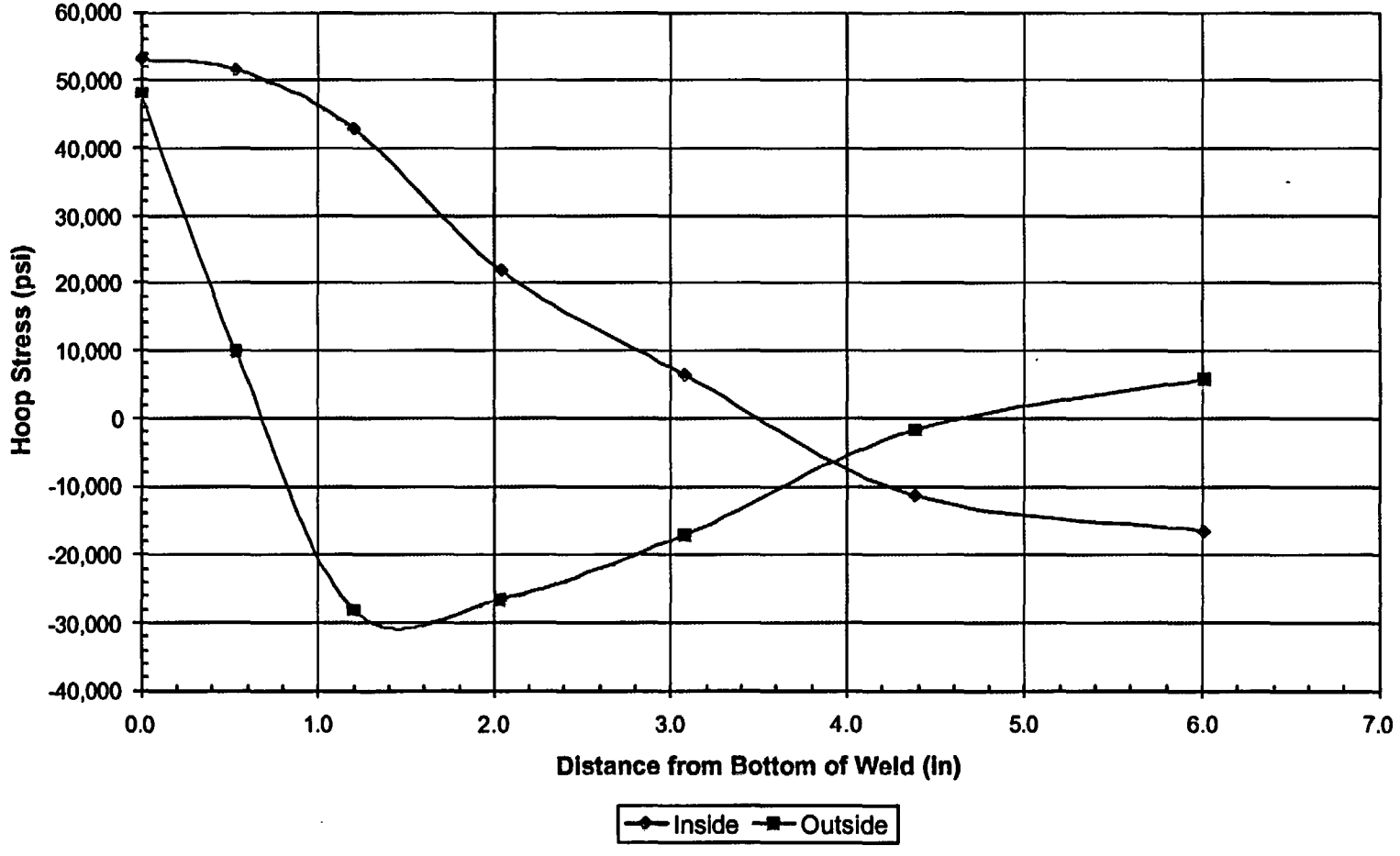

Figure B-8

Hoop Stress Distribution Below the Weld Downhill Side (54.8° ICI Penetration Nozzle)

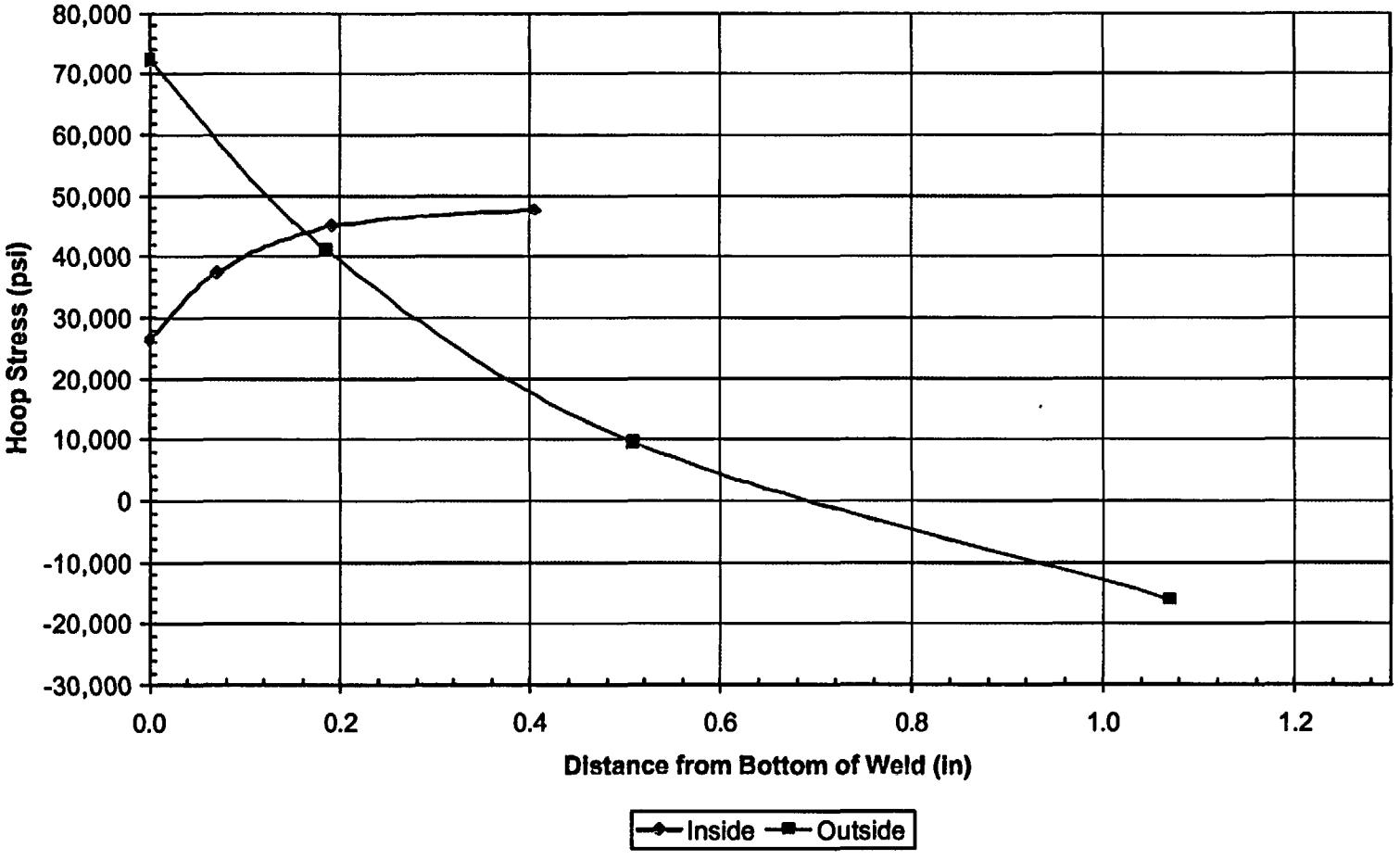

Figure B-9

Hoop Stress Distribution Below the Weld Uphill Side (54.8° ICI Penetration Nozzle)